RESEARCH ON ENERGY ABSORBING STRUCTURES

FINAL REPORT

Contract Number: AF 49(638)-1144

Prepared for

Air Force Office of Scientific Research

Washington 25, D.C.

ARA, inc.

AEROSPACE RESEARCH ASSOCIATES

2017 WEST GARVEY AVENUE • WEST COVINA, CALIFORNIA • TEL. 962-1045

FEBRUARY 1963

Research on Energy Absorbing Structures

Final Report

Contract Number: AF 49(638)-1144 New

Prepared for

Air Force Office of Scientific Research
Washington 25, D.C.

February 1963

FOREWORD

The research work in this report was performed by ARA, Inc., West Covina, California, for the Mechanics Division, Directorate of Engineering Sciences, Air Force Office of Scientific Research, Washington 25, D.C., under Contract No. AF 49(638)-1144. This research is part of a continuing effort in the study of variable geometry energy absorbing structures. The Project No. is 9782 and the Task No. is 37718. The project engineers were Mr. Howard S. Wolko and Dr. Jacob Pomerantz. The studies presented began in February 1962 and were concluded in February 1963. Mr. Bernard Mazelsky, president of ARA, Inc., was the principal investigator.

Although the studies were a group effort, the chief contributors were Dr. D. L. Platus, Mr. P. J. Cunningham, Mr. F. A. Marovich, and Mr. Bernard Mazelsky.

The authors are indebted to Mr. Howard S. Wolko, who stimulated and encouraged the investigation, and to Dr. Jacob Pomerantz, whose invaluable guidance and assistance helped to make this program a success.

TABLE OF CONTENTS

TABLE OF CONTENTS (cont'd)

LIST OF FIGURES AND TABLES

LIST OF FIGURES AND TABLES (cont'd)

LIST OF FIGURES AND TABLES (cont'd)

NOMENCLATURE

a	dimension of U-shaped configuration defined in Figure 8
a_1, b_1	constants defined by Equation (97)
a_2, b_2	constants defined by Equation (101)
A	material parameter of Equation (48)
B_n, C_n	constants defined by Equations (67)
c	half-thickness of elastic zone in plastic bending analysis
D	flexural rigidity
D'	effective flexural rigidity for plastic behavior
D'_i	value of D' at end of i-th element
$\overline{D}'$	average value of D' during application of load increment
$\overline{D}'_i$	value of $\overline{D}'$ at end of i-th element
E	modulus of elasticity
E_e	effective elastic modulus defined by Equation (42)
f	functional relation of Equation (45)
G	shear modulus
GJ	torsional rigidity per unit length of cross section of axial strip in convoluted cylindrical structure
h	thickness
i	index
k	effective elastic constant for idealized convoluted cylinder, defined by Equation (80)
k_1	constant defined by Equation (92)

NOMENCLATURE (cont'd)

ℓ	length of cantilever beam of Figure 1; width of axial strip defined in Figure 25
ℓ_i	length of i-th elemental cantilever beam
L	height of convoluted cylindrical structure
M	moment per unit length
M_o	reference moment per unit length, $T_o h$
$\overline{\Delta M}$	average value of ΔM during application of load increment
$\overline{\Delta M}_i$	value of $\overline{\Delta M}$ at end of i-th element
$\Delta M'$	effective incremental moment defined by Equation (9)
$\overline{\Delta M}'$	average value of $\Delta M'$ during application of load increment
$\overline{\Delta M}'_i$	value of $\overline{\Delta M}'$ at end of i-th element
M_m	maximum bending moment, Tz_o
M_{PL}	value of M at proportional limit
M_y	value of M corresponding to σ_y
n	index; material parameter defined by Equation (48)
N	number of axial strips in convoluted cylindrical structure
p	differential pressure across convoluted cylindrical structure
h	initial radius of convolute
R	radius of cone
R_1	average radius of convoluted cylindrical structure
s	coordinate of length along convoluted curve

NOMENCLATURE (cont'd)

T	load per unit length
T_o	reference load per unit length, D/λ^2
$\bar{T}$	average value of T during application of load increment
T_n	value of T after application of n-th load increment
ΔT_n	n-th load increment
U	elastic strain energy of bending per unit width of cantilever beam of Figure 1
U_n	value of U after application of n-th load increment
U_B	bending energy in convoluted cylindrical structure
U_F	bending energy required to form convoluted cylindrical structure from straight convoluted strip
U_T	twisting energy in convoluted cylindrical structure
W	total energy in convoluted cylindrical structure
x	axial coordinate of convoluted cylindrical structure
x,y	Cartesian coordinates with x-axis tangent to convoluted curve for given load; coordinates of Figure 4 used in plastic bending analysis
x_o,y_o	values of x,y corresponding to initial undeformed structure
x',y'	values of x,y after application of load increment (Figure 2)
z	moment arm in two-dimensional structure
z_i	value of z at end of i-th element
$\bar{z}_i$	average value of z_i during application of load increment
z_o	maximum value of z for a given load
z_{on}	value of z_o after application of n-th load increment

NOMENCLATURE (cont'd)

α	cone half-angle
α_i	parameter defined by Equations (19) or (26)
β_i	parameter defined by Equation (27)
β_n, γ_n	constants defined by Equations (70)
δ	end deflection of elemental cantilever beam
δ'	end slope of elemental cantilever beam
δ_i	deflection of end of i-th element relative to (i - 1)th element
δ_i'	slope of end of i-th element relative to (i - 1)th element
ϵ_p	plastic bending strain
ϵ_{PL}	"plastic strain" at proportional limit defined by Equations (48) and (49)
θ	slope of tangent to two-dimensional structure
θ_o	initial value of θ corresponding to unloaded structure
θ_i	value of θ at end of i-th element
$\bar{\theta}_i$	average value of θ_i during application of load increment
$\Delta\theta$	change in slope, $\theta - \theta_o$
λ	parameter defined by Equation (41)
ν	Poisson's ratio
ξ, η	horizontal and vertical deflections, respectively, of end of cantilever beam of Figure 1
ξ_i, η_i	horizontal and vertical deflections, respectively, of end of i-th element of Figure 1c, relative to (i - 1)th element
$\Delta\xi_n$	incremental change in ξ during application of n-th load increment

NOMENCLATURE (cont'd)

σ	bending stress
σ_m	maximum bending stress
σ_{PL}	proportional limit stress
σ_y	yield strength
φ	angle defined in Figure 25; change in slope of S-shaped strip of convoluted cylindrical structure
φ_m	maximum value of φ for S-shaped strip of convoluted cylindrical structure
φ_1, φ_2	minimum and maximum values of φ, respectively, defined in Figure 25
ψ	material efficiency factor defined by Equation (56)
ψ_n	value of ψ after application of n-th load increment

FINAL REPORT ON "RESEARCH ON ENERGY ABSORBING STRUCTURES"

I. SUMMARY

Theoretical and experimental studies of convoluted type structures are described. An incremental method for predicting the nonlinear large-deformation behavior of two-dimensional convoluted strips is shown. The method is applicable for elastic as well as plastic stress-strain behavior of the material. The results of the two-dimensional analysis are extended to an analysis of a circumferentially-convoluted cylinder which deforms into a conical shape. Tests on typical two- and three-dimensional convoluted metal specimens are described and correlations of theoretical predictions with experimental results are shown.

II. INTRODUCTION

Flexible metal structures which can grossly change their shape by the absorption or release of energy to their environment offer an attractive potential for aerospace applications. In particular, it would be desirable to be able to utilize a passive metal structure of preset convoluted geometry which, when acted upon by external environmental forces, would vary its geometry in a predetermined manner. These forces can arise from numerous sources; e.g., aerodynamic pressures, thermal stresses, variations in material properties due to temperature changes, etc. In view of the limited knowledge available on this type of structure a theoretical and experimental program is being carried out to develop methods suitable for their analysis.

III. SCOPE OF WORK

The scope of the work performed under this study is summarized as follows:

(1) An incremental technique was developed for predicting the large-deflection load-deformation behavior of two-dimensional convoluted metal strips of arbitrary shape which exhibit elastic and plastic material behavior.

(2) The load-deformation behavior of two-dimensional convoluted strips loaded within the elastic range was computed for several typical configurations and is presented in nondimensional form.

(3) The load-deformation behavior of two-dimensional convoluted strips of semi-circular-arc configuration was computed for several conditions of yielding and plastic stress-strain behavior and is presented in nondimensional form.

(4) The results of the two-dimensional analyses were extended to an analysis of a three-dimensional circumferentially-convoluted cylindrical structure which deforms into a conical shape.

(5) Tests were performed on typical two- and three-dimensional structures and the results were correlated with the theoretical predictions.

IV. TWO-DIMENSIONAL ANALYSIS

The large-deflection analysis of convoluted metal structures is severely complicated by the fact that the large deflections give rise to nonlinearities in the load-deflection behavior. Even when the material stress-strain behavior is elastic, geometrical nonlinearities are present. If, in addition, the material is deformed into the plastic range, nonlinearities result in the stress-strain behavior and the

problem is further complicated. Because of these complications, analytical closed-form solutions can only be obtained for the simplest cases, and severe assumptions and approximations are usually required.

In order to arrive at more general and useful results, an incremental approach has been taken in the analysis of two-dimensional convoluted strips. Solutions are developed in increments of load, and the incremental deformations resulting in each load increment are determined by dividing the structure into incremental segments. This technique is described in detail in the following sections.

A. Development of Incremental Method

Consider the simple two-dimensional strip shown in Figure 1a, which is deformed by loads applied to its ends. As the load increases, deformation results from changes in the bending moment distribution and, if the material is loaded into the plastic range, changes in the effective flexural rigidity of the structure. Since large deformations are being considered, changes in the bending moment at any point are due to changes in the load as well as changes in the effective-moment arm. Because of symmetry it is necessary to analyze only one typical section of the strip, such as the curved cantilevered beam of Figure 1b. At a point "a" the change in slope is zero and at point "b" the moment is zero since the moment arm vanishes. As the structure deforms, the edge load T (load/unit length) remains horizontal so that the bending moment at any point is the product of T and the moment arm, z.

The basic problem is to describe the deformation of a convoluted strip of arbitrary shape as the load increases from zero to some arbitrary value. For

FIG. 1 GEOMETRIC PARAMETERS AND COORDINATES USED IN THE ANALYSIS OF TWO-DIMENSIONAL STRIPS

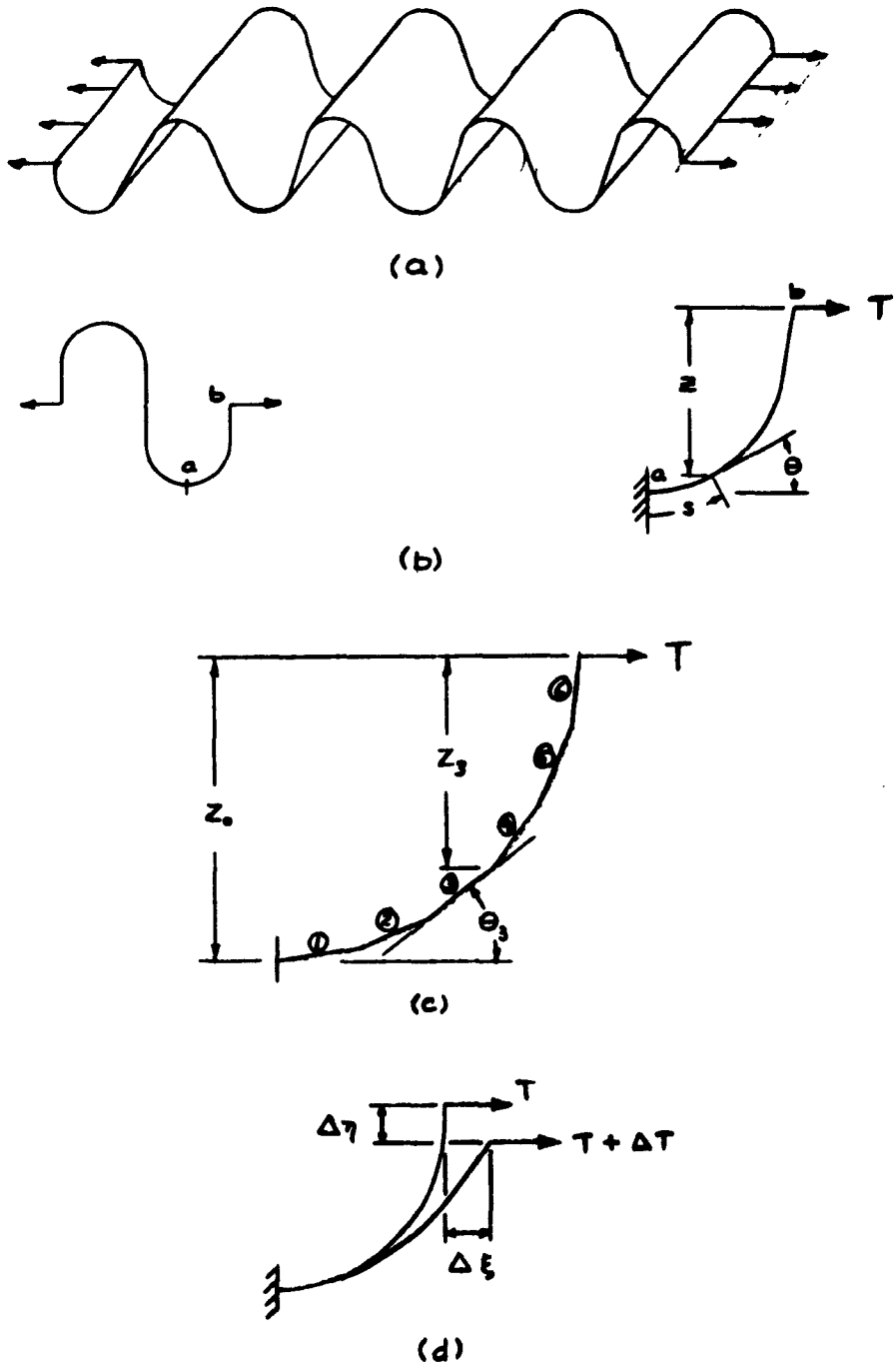

this purpose the following assumptions are made:

1. The thickness of the material is small enough in relation to the other dimensions that classical bending theory can be used to relate change in curvature to bending moment.

2. The effects of normal forces acting in the tangent plane at any point can be ignored.

3. Material stress-strain behavior in both the elastic and plastic range occurs.

4. The structure is deformed in a state of plane strain bending and end effects can be ignored.

With the above assumptions the deformation behavior is determined by a step-by-step procedure in which an incremental load is applied and the incremental deformation is estimated from the inital shape and the applied load. Since the moments and (in the plastic range) the effective flexural rigidity change during application of the load, average values are used which can be determined by trial and error. In order to determine the incremental deformations a second incremental procedure is utilized in which the curved cantilever beam of Figure 1b is approximated by straight segments, as shown in Figure 1c. The analytical development of both incremental procedures is given below.

The bending equation can be expressed by

$$\frac{d\theta}{ds} - \frac{d\theta_0}{ds} = -\frac{M}{D'} \quad , \tag{1}$$

where θ is the slope, θ_o is the slope for the initial undeformed shape, s is the coordinate of length along the curved section, and D' is an effective flexural rigidity.

The moment M is given by

$$M = T z \quad . \tag{2}$$

For elastic material behavior,

$$D' = D = \frac{E h^3}{12(1-\nu^2)} \quad , \tag{3}$$

where E is Young's modulus, h is the material thickness, and ν is Poisson's ratio.

Equation (1) expresses the change in curvature due to the moment M. The curvature $d\theta/ds$ can also be expressed in terms of Cartesian coordinates x,y by the relation*

$$\frac{d\theta}{ds} = - \frac{\frac{d^2y}{dx^2}}{\left[1+\left(\frac{dy}{dx}\right)^2\right]^{3/2}} \quad . \tag{4}$$

Since the location of the x,y-axes is arbitrary, it is useful to consider a "moving" set of coordinate axes with the origin on the curved beam and the x-axis tangent

* It is convenient to select the coordinate axes so that a positive change of curvature in the x,y coordinates corresponds to a decrease in the original curvature of the convoluted shape.

to the beam at the point s. The first derivative term in Equation (4) is then zero and Equations (1) and (2) may be written

$$\frac{d^2y}{dx^2} - \frac{d^2y_o}{dx_o^2} = \frac{Tz}{D'} \quad , \tag{5}$$

where the subscript o denotes the initial undeformed shape. Equation (5) expresses the curvature relation at a particular point s since the coordinate axes of x,y are now functions of s and T, and those of x_o, y_o correspond to T = 0. However, if Equation (5) is extended to a small finite range of x about x = 0 for fixed coordinate axes of x,y and x_o, y_o, the error will be small since the first derivative term in Equation (4) will be small compared with unity. This is the basis for the present incremental procedure.

Consider, first, an incremental change in the load ΔT and express the resulting change in curvature from Equation (5). This result can be written

$$\Delta \frac{d^2y}{dx^2} = \frac{d}{dT}\left(\frac{Tz}{D'}\right)\Delta T = \frac{1}{D'}\left(z + T\frac{dz}{dT} - \frac{Tz}{D'}\frac{dD'}{dT}\right)\Delta T \quad , \tag{6}$$

provided the load increment is sufficiently small. The term on the left of Equation (6) can be interpreted, with the aid of Figure 2, as follows: Let x,y represent the coordinates at point s which correspond to the load T, and let x',y' correspond to $T + \Delta T$, as shown in Figure 2a. By superposing the coordinate axes, as indicated in Figure 2b, the incremental change in curvature is seen to be

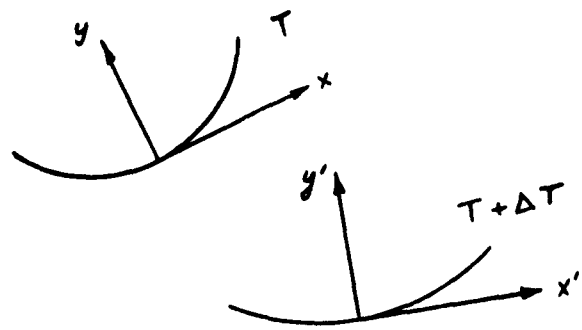

(a)

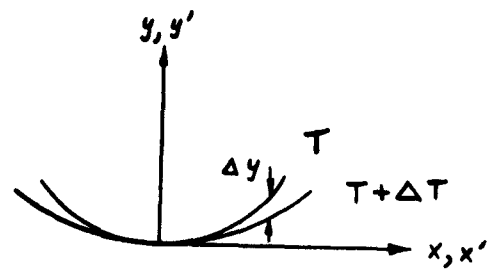

(b)

FIG. 2 GEOMETRIC INTERPRETATION OF LEFT SIDE OF EQUATION (6)

$$\Delta \frac{d^2y}{dx^2} = \frac{d^2y'}{dx^2} - \frac{d^2y}{dx^2} = \frac{d^2(y-y')}{dx^2} = \frac{d^2\Delta y}{dx^2} \quad , \tag{7}$$

where Δy is the incremental deflection normal to the tangent at the point s. Equations (6) and (7) can be written

$$\frac{d^2\Delta y}{dx^2} = \frac{\Delta M'}{D'} \quad , \tag{8}$$

where

$$\Delta M' = \left(z + T \frac{dz}{dT} - \frac{Tz}{D'} \frac{dD'}{dT} \right) \Delta T \quad . \tag{9}$$

The quantity $\Delta M'$ is an effective incremental moment which also takes into account variations in D' which result if the material is in the plastic range.

Equations (8) and (9) form the basis for the incremental technique by which the incremental deformation is determined for each load increment. As mentioned earlier, the cantilever beam of Figure 1b is approximated by a series of straight elements, shown in Figure 1c. If the increments of length and load are small enough, each element can be treated as a cantilever beam with linearly varying moment and, in the plastic range, linearly varying flexural rigidity. The incremental changes in lateral deflection and slope of the end of each element relative to its

base are determined from Equations (8) and (9). The gross deflections are then determined by accumulating rotations and deflections of each element starting from the base of the original cantilever beam.

Let the relative incremental slope and bending deflection for the i-th element of Figure 1c be denoted by δ_i' and δ_i, respectively.* Positive values for δ_i' and δ_i correspond to a clockwise rotation of the element, as shown in Figure 3. The total lateral deflection of the end of the i-th element relative to the end of the (i - 1)th element results from δ_i and the rigid body rotation $\sum_{k=1}^{i-1} \delta_k'$ produced by the bending of all the preceding elements, and is given by

$$\text{total lateral deflection of end of i-th element relative to end of (i - 1)th element} = \delta_i + \ell_i \sum_{k=1}^{i-1} \delta_k' \qquad (10)$$

where ℓ_i is the length of the i-th element. The average slope of the i-th element $\bar{\theta}_i$ during application of the load increment can be approximated by

$$\bar{\theta}_i = \theta_i - \frac{1}{2} \sum_{k=1}^{i-1} \delta_k' \qquad (11)$$

where θ_i is the slope before application of the load increment.

The horizontal and vertical incremental defections of the end of the i-th element relative to the (i - 1)th element are, from Equations (10) and (11),

$$\left.\begin{aligned} \Delta\xi_i - \Delta\xi_{i-1} &= \left(\delta_i + \ell_i \sum_{k=1}^{i-1} \delta_k'\right) \sin\left(\theta_i - \frac{1}{2} \sum_{k=1}^{i-1} \delta_k'\right) \\ \Delta\eta_i - \Delta\eta_{i-1} &= \left(\delta_i + \ell_i \sum_{k=1}^{i-1} \delta_k'\right) \cos\left(\theta_i - \frac{1}{2} \sum_{k=1}^{i-1} \delta_k'\right) \end{aligned}\right\} . \qquad (12)$$

* In terms of the previous notation, $\delta_i' \equiv \left.\frac{d\Delta\gamma}{dx}\right|_{x=\ell_i}$ and $\delta_i \equiv \left.\Delta\gamma\right|_{x=\ell_i}$.

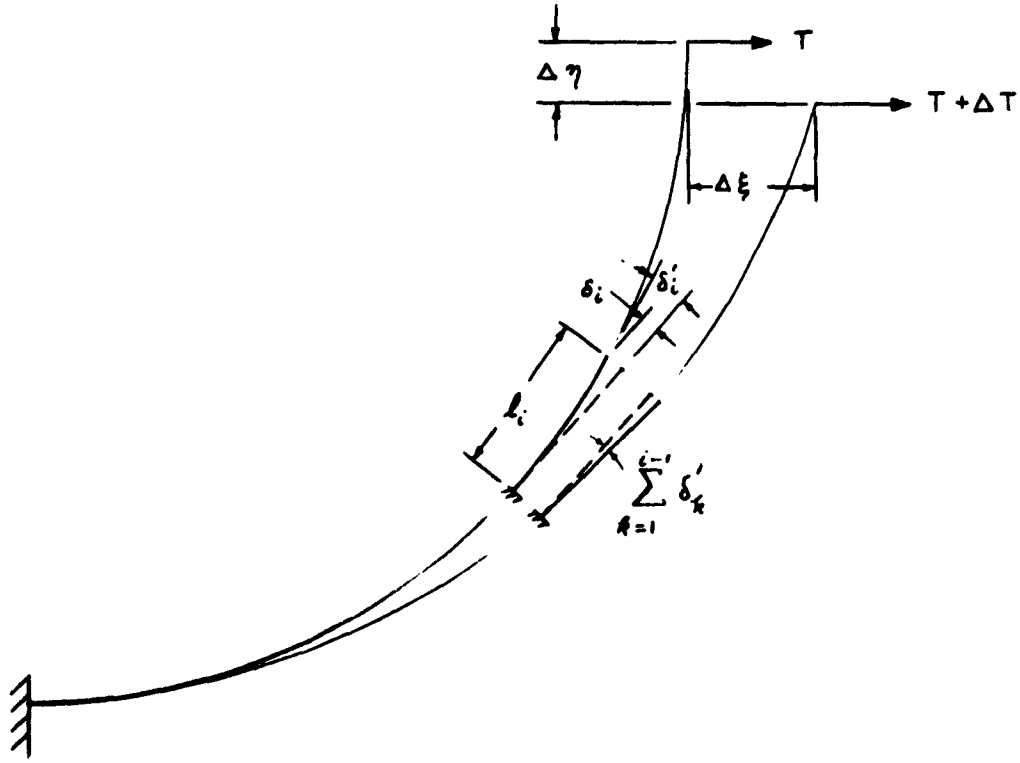

FIG. 3 INCREMENTAL ROTATIONS AND DEFLECTIONS FOR iTH ELEMENT

With the fixed end boundary conditions for the original cantilever beam denoted by

$$\Delta\xi_0 = \Delta\eta_0 = \delta_0' = 0, \tag{13}$$

the incremental deflections of the end of the i-th element can be written

$$\left.\begin{aligned} \Delta\xi_i &= \sum_{k=1}^{i} (\Delta\xi_k - \Delta\xi_{k-1}) \\ \Delta\eta_i &= \sum_{k=1}^{i-1} (\Delta\eta_k - \Delta\eta_{k-1}) \end{aligned}\right\} . \tag{14}$$

Equations (12) - (14) constitute the relations from which the gross deflections of the original cantilever beam can be computed for each load increment, provided the quantities δ_i and δ_i' are known. The determination of δ_i and δ_i' for elastic and plastic material behavior is described in the following sections.

B. Incremental Slopes and Deflections for Elastic Material Behavior

For elastic behavior Equation (3) applies so that dD'/dT is zero and Equations (8) and (9) become

$$\frac{d^2\Delta y}{dx^2} = \frac{\Delta M}{D} , \tag{15}$$

where

$$\Delta M = \left(z + T\frac{dz}{dT}\right) . \tag{16}$$

The quantities δ_i and δ_i' can be determined from these two equations. Since

finite variations occur in z, T, and dz/dT during application of the load increment, average values of these quantities are used to compute ΔM.

As was mentioned earlier, if the increments of length are small enough the variation in ΔM over each elemental beam can be assumed linear. Thus, let

$$\overline{\Delta M}(x) = \overline{\Delta M}_{i-1} \left(1 - \alpha_i \frac{x}{\ell_i} \right), \qquad 0 \le x \le \ell_i, \tag{17}$$

where

$$\overline{\Delta M}_i = \left[\bar{z}_i + \bar{T} \left(\frac{dz}{dT} \right)_i \right] \Delta T, \tag{18}$$

and the bars denote average quantities during application of the load increment. The subscript i on M and z denotes a quantity evaluated at the end of the i-th element, and α_i is defined by

$$\alpha_i \equiv \frac{\overline{\Delta M}_{i-1} - \overline{\Delta M}_i}{\overline{\Delta M}_{i-1}} . \tag{19}$$

Substitution of Equation (17) into Equation (15), and integration of the result with the boundary conditions,

$$\Delta y(0) = \frac{d\Delta y}{dx}(0) = 0, \tag{20}$$

yields

$$\delta_i' = \frac{d\Delta y}{dx}(\ell_i) = \frac{\overline{\Delta M}_{i-1}\, \ell_i}{D} \left(1 - \frac{\alpha_i}{2} \right), \tag{21}$$

and

$$\delta_i = \Delta y(l_i) = \frac{\overline{\Delta M}_{i-1}\, l_i^2}{2D}\left(1 - \frac{\alpha_i}{3}\right) . \tag{22}$$

Equations (21) and (22) with Equations (18) and (19) constitute the required relations.

For computational purposes it is convenient to introduce the reference load and moment,

$$T_0 \equiv \frac{D}{h^2} \quad , \quad M_0 \equiv T_0 h = \frac{D}{h} , \tag{23}$$

and to express the above equations in nondimensional form. Here h, is a typical dimension of the convolute, such as an initial radius of curvature. Equations (21) and (22) become

$$\delta_i' = \frac{\overline{\Delta M}_{i-1}}{M_0}\,\frac{l_i}{h}\left(1 - \frac{\alpha_i}{2}\right) , \tag{24}$$

and

$$\frac{\delta_i}{h} = \frac{1}{2}\,\frac{\overline{\Delta M}_{i-1}}{M_0}\left(\frac{l_i}{h}\right)^2\left(1 - \frac{\alpha_i}{3}\right) . \tag{25}$$

C. Incremental Slopes and Deflections for Plastic Material Behavior

In the plastic case both $\Delta M'$ and D' vary over the length of the element. As before, if the element length is sufficiently small, both of these quantities can be assumed to vary linearly. Thus, let

$$\alpha_i \equiv \frac{\overline{\Delta M'_{i-1}} - \overline{\Delta M'_i}}{\overline{\Delta M'_{i-1}}} \quad , \tag{26}$$

and

$$\beta_i \equiv \frac{\overline{D'_i} - \overline{D'_{i-1}}}{\overline{D'_{i-1}}} \quad , \tag{27}$$

so that

$$\overline{\Delta M'(x)} = \overline{\Delta M'_{i-1}} \left(1 - \alpha_i \frac{x}{l_i} \right) \quad , \tag{28}$$

and

$$\overline{D'(x)} = \overline{D'_{i-1}} \left(1 + \beta_i \frac{x}{l_i} \right) \quad . \tag{29}$$

Substitution of Equations (28) and (29) into Equation (8), and integration of the result with the boundary conditions of Equations (20), gives

$$\delta'_i = \frac{\overline{\Delta M'_{i-1}}\, l_i}{\overline{D'_{i-1}}} \left[\frac{1}{\beta_i} \left(1 + \frac{\alpha_i}{\beta_i} \right) \ln (1+\beta_i) - \frac{\alpha_i}{\beta_i} \right] \quad , \tag{30}$$

and

$$\delta_i = \frac{\overline{\Delta M'_{i-1}}\, l_i^2}{\overline{D'_{i-1}}} \left\{ \frac{1}{\beta_i} \left(1 + \frac{\alpha_i}{\beta_i} \right) \left[\frac{1}{\beta_i} (1+\beta_i) \ln (1+\beta_i) - 1 \right] - \frac{\alpha_i}{2\beta_i} \right\} . \tag{31}$$

As before, it is convenient to use Equation (23) and to write Equations (30) and (31) in the nondimensional form,

$$\delta_i' = \frac{(\overline{\Delta M_{i-1}'}/M_o)(l_i/h)}{\overline{D_{i-1}'}/D}\left[\frac{1}{\beta_i}\left(1+\frac{\alpha_i'}{\beta_i'}\right)\ln(1+\beta_i') - \frac{\alpha_i'}{\beta_i'}\right], \tag{32}$$

$$\frac{\delta_i}{h} = \frac{(\overline{\Delta M_{i-1}'}/M_o)(l_i/h)^2}{\overline{D_{i-1}'}/D}\left\{\frac{1}{\beta_i'}\left(1+\frac{\alpha_i'}{\beta_i'}\right)\left[\frac{1}{\beta_i'}(1+\beta_i')\ln(1+\beta_i')-1\right] - \frac{\alpha_i'}{2\beta_i'}\right\}. \tag{33}$$

If the value of β_i is small these equations are difficult to evaluate due to small differences between large numbers. For this case the following series expansions are useful:

$$\delta_i' = \frac{(\overline{\Delta M_{i-1}'}/M_o)(l_i/h)}{\overline{D_{i-1}'}/D}\left[1-(\alpha_i'+\beta_i')\left(\frac{1}{2}-\frac{\beta_i'}{3}+\frac{\beta_i'^2}{4}-\cdots\right)\right], \tag{34}$$

$$\frac{\delta_i}{h} = \frac{(\overline{\Delta M_{i-1}'}/M_o)(l_i/h)^2}{2\,\overline{D_{i-1}'}/D}\left[1-(\alpha_i'+\beta_i')\left(\frac{1}{3}-\frac{\beta_i'}{6}+\frac{\beta_i'^2}{10}-\cdots\right)\right]. \tag{35}$$

D. Plastic Bending Relations

In the plastic analysis described above a knowledge of the moment-curvature relation is required in order to calculate the effective flexural rigidity

and the parameter β_1. Because of the numerical procedure involved this relation can be determined from the actual stress-strain behavior of the material and utilized in graphical or tabular form. However, in order to illustrate the method, an ideal elastic-plastic material behavior is first assumed, for which an analytical solution can be obtained in closed form. The following analysis is based on that described in Reference A.

1. Ideal Elastic-Plastic Behavior

Consider the bending of a uniform sheet of nonhardening material under conditions of plane strain. The material is assumed to have the stress-strain behavior of Figure 4a in both tension and compression and is assumed to yield in accordance with the Tresca law. It is further assumed that the radius of curvature is so large in relation to the thickness that the induced transverse stresses in the direction normal to the sheet can be neglected.

The coordinate axes are chosen as shown in Figure 4b with the z-axis in the direction in which strain is prevented. When the moment per unit width is greater than the yield value,

$$M_y = \frac{h^2 \sigma_y}{6} , \tag{36}$$

elastic and plastic zones are produced, as shown in Figure 4b. The moment is expressed by

$$M = \frac{2E}{(1-\nu^2)} \frac{d(\theta-\theta_0)}{ds} \int_0^c y^2 dy + 2\sigma_y \int_c^{h/2} y\, dy$$

$$= \frac{2Ec^3}{3(1-\nu^2)} \frac{d(\theta-\theta_0)}{ds} + \sigma_y \left(\frac{h^2}{4} - c^2\right) , \tag{37}$$

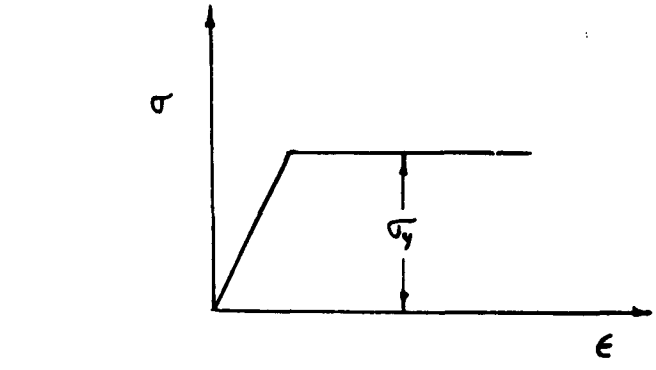

(a)

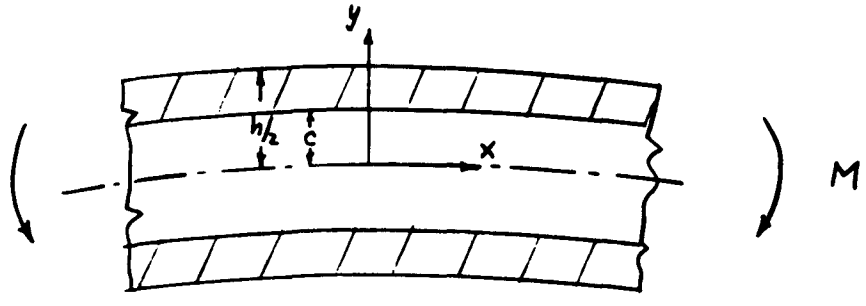

(b)

Figure 4. Parameters and Coordinates Used in Idealized Plastic Bending Analysis

and the parameter c is given by

$$c = \frac{(1-\nu^2)\sigma_y}{E\,\frac{d(\theta-\theta_o)}{ds}} \quad . \tag{38}$$

Solution of $d(\theta - \theta_o)/ds$ from Equations (37) and (38) gives the result,

$$\frac{d(\theta-\theta_o)}{ds} = \frac{2(1-\nu^2)\frac{\sigma_y}{Eh}}{\sqrt{3}\sqrt{1-\frac{4M_y}{h^2\sigma_y}}} \quad . \tag{39}$$

This result with Equations (1), (3), and (36) gives for the effective flexural rigidity,

$$\frac{D'}{D} = \sqrt{3}\,\frac{M}{M_y}\sqrt{1-\frac{2}{3}\frac{M}{M_y}} \quad , \qquad M_y \le M \le \frac{3}{2}M_y \quad . \tag{40}$$

With this material behavior one additional structural parameter is required in order to describe the load or deflection value at which the material first yields. For this purpose it is convenient to introduce the parameter λ, defined by

$$\lambda \equiv \frac{h/a}{\sigma_{PL}/E_\nu} \quad , \tag{41}$$

where σ_{PL} is the proportional limit, equal to σ_y for this case, and E_ν is defined by

$$E_\nu \equiv \frac{E}{1-\nu^2} \quad . \tag{42}$$

Equation (40) with Equations (3) and (23) can then be written,

$$\frac{D'}{D} = \frac{\sqrt{3}}{2}\left(\frac{\lambda M}{M_o}\right)\sqrt{1-\frac{1}{3}\left(\frac{\lambda M}{M_o}\right)}, \qquad 2 \leq \frac{\lambda M}{M_o} \leq 3 . \tag{43}$$

Equations (40), or (41) and (43), constitute the required relations. A treatment of the problem for more general stress-strain behavior is given in the following section.

2. Arbitrary Stress-Strain Behavior

In the previous section relations were derived for plane strain bending of a wide sheet of ideal nonhardening elastic-plastic material. The present analysis, based on that of Reference B, extends the treatment to arbitrary stress-strain behavior. As in the former analysis, the following assumptions are made:

(i) The material has the same stress-strain behavior in tension and compression.

(ii) Transverse stresses in the direction normal to the sheet can be neglected.

(iii) The neutral axis remains coincident with the midplane of the sheet.

(iv) The total strain component in the restrained direction is zero.

In addition to the above, the usual laws of plasticity are imposed, which include the constancy of volume condition, the von Mises condition, and a criterion of plastic flow. For the latter the "maximum shear stress vs.

numerically largest principal strain" criterion is used.* With these conditions the result of Reference B may be written as

$$y \frac{d\Delta\theta}{ds} = (1-\nu)\epsilon_p + \frac{\sigma}{2E}(2-2\nu-\nu^2) + \frac{\nu}{2E}\left\{\left[2E\epsilon_p + (2-\nu)\sigma\right]^2 - 4(1-2\nu)E\sigma\epsilon_p\right\}^{\frac{1}{2}} , \quad (44)$$

where σ is the bending stress and ϵ_p is the plastic bending strain.

In addition to Equation (44) there exists a stress-strain relation between ϵ_p and σ,

$$\epsilon_p = f(\sigma) , \quad (45)$$

which can be determined from a tensile test. The present flow criterion is such that the functional relation of Equation (45) is the same as that between axial stress and plastic strain in a tensile test.

Equations (44) and (45), with the expression for moment per unit width,

$$M = 2\int_0^{h/2} \sigma y\, dy , \quad (46)$$

can be used to compute the moment-curvature relation. For a particular value of $d\Delta\theta/ds$, values of σ can be selected for which the corresponding values of y can be determined from Equations (44) and (45). Equation (46) can then be used to compute the corresponding moment.

* Although the von Mises-Hencky criterion is generally considered to be slightly better, the added complexity is not warranted in this analysis.

If, instead of Assumption (iv), which is the usual condition for plane strain, it is assumed that both the elastic and plastic components of strain are zero, the result is

$$\gamma \frac{d\Delta\theta}{ds} = (1-\gamma^2)\frac{\sigma}{E} + \epsilon_p \quad , \tag{47}$$

which is considerably simpler than Equation (44). A comparison of Equations (44) and (47) is given below.

For many structural metals the stress-strain relation of Equation (45) can be expressed in the form

$$\epsilon_p = A\,\sigma^n \quad . \tag{48}$$

With the addition of the elastic strain, σ/E, the expression for total strain becomes identical to the well-known Ramberg-Osgood relation (Reference C) by proper definition of the constant A. It is convenient to express Equation (48) in terms of the proportional limit stress σ_{PL} and some corresponding plastic strain ϵ_{PL}. This result can be written as

$$\frac{\epsilon_p}{\epsilon_{PL}} = \left(\frac{\sigma}{\sigma_{PL}}\right)^n \quad . \tag{49}$$

Although, strictly speaking, there is no plastic strain at the proportional limit, Lubahn and Felgar* have suggested 20×10^{-6} as a suitable value since this is close to the minimum value that can be detected experimentally.

* Reference B, p. 111

In Reference B a comparison of Equations (44) and (47) is given for a particular case of bending, using the expression of Equation (48) with n = 5. Further comparisons are shown in Figure 5 for n = 3, 5, and 10. For each of these cases the maximum plastic bending strain is half of the total strain. From these results it appears that Equation (47) provides a good approximation to Equation (44).

With the stress-strain relation of Equation (49) analytical expressions can be determined from Equations (46) and (47) which relate $d\Delta\theta/ds$ and M. Substitution of Equation (49) in Equation (47) gives

$$y \frac{d\Delta\theta}{ds} = \frac{\sigma_{PL}}{E_y}\left(\frac{\sigma}{\sigma_{PL}}\right) + \epsilon_{PL}\left(\frac{\sigma}{\sigma_{PL}}\right)^n , \tag{50}$$

where $E_y \equiv E/(1-\nu^2)$. Substitution of y and dy from Equation (50) into Equation (46), and integration over the half-thickness of the sheet, gives the result

$$\frac{h^2}{12}\left(\frac{d\Delta\theta}{ds}\right)^2 \frac{M}{M_{PL}} = \frac{\sigma_{PL}^2}{3E_y^2}\left(\frac{\sigma_m}{\sigma_{PL}}\right)^2 + \left(\frac{n+1}{n+2}\right)\frac{\epsilon_{PL}\sigma_{PL}}{E_y}\left(\frac{\sigma_m}{\sigma_{PL}}\right)^{n+2} + \frac{n\epsilon_{PL}^2}{(2n+1)}\left(\frac{\sigma_m}{\sigma_{PL}}\right)^{2n+1} , \quad \frac{\sigma_m}{\sigma_{PL}} \geq 1 , \tag{51}$$

where M_{PL} is the moment at which the maximum bending stress is σ_{PL}, given by

$$M_{PL} = \frac{h^2\sigma_{PL}}{6} , \tag{52}$$

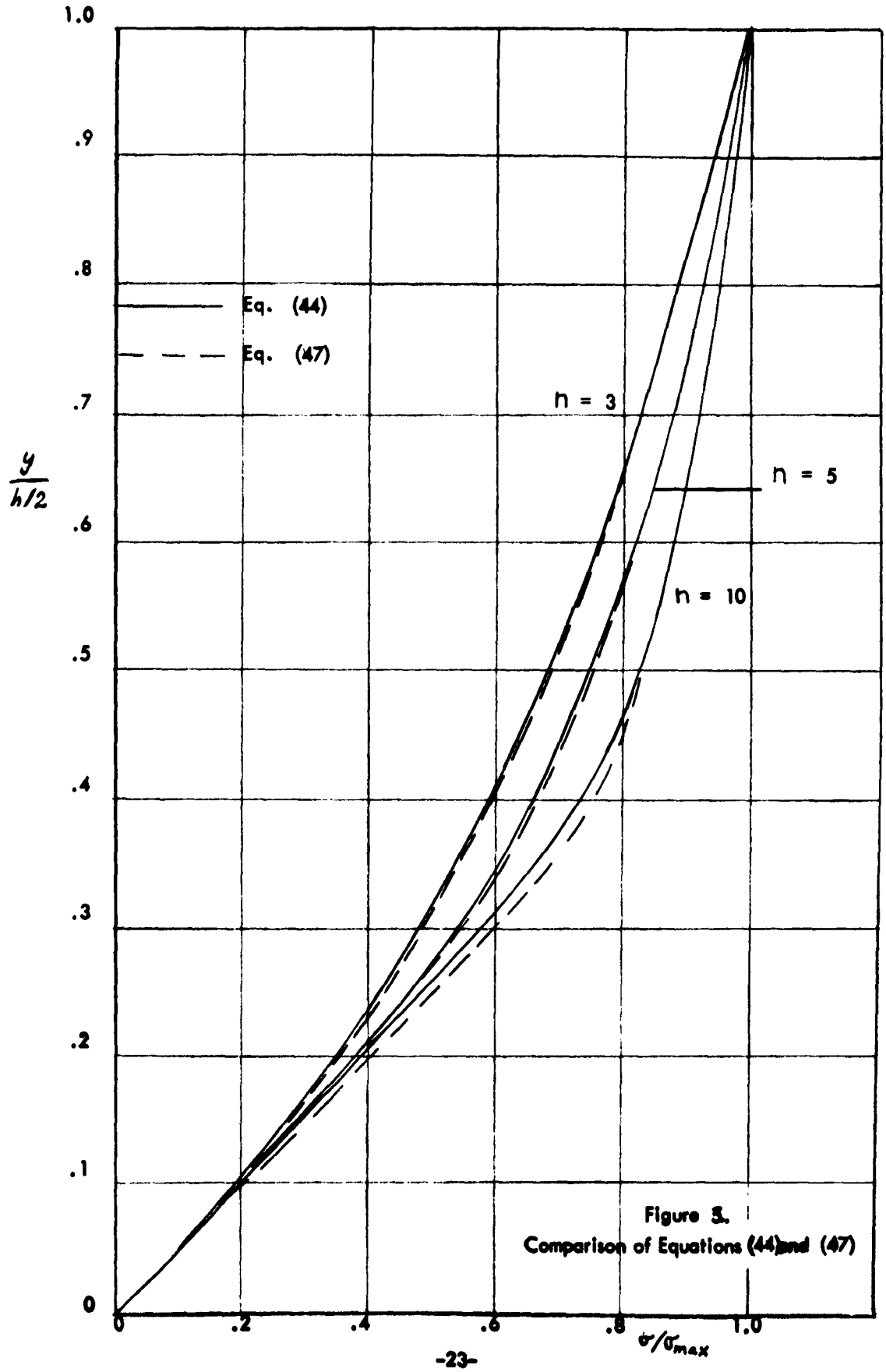

Figure 3.
Comparison of Equations (44) and (47)

and σ_m is the maximum bending stress corresponding to the moment M.

Equations (47) and (49) evaluated at $y = h/2$ give the relation

$$\frac{d\Delta\theta}{ds} = \frac{2}{h}\left[\frac{\sigma_{PL}}{E_v}\left(\frac{\sigma_m}{\sigma_{PL}}\right) + \epsilon_{PL}\left(\frac{\sigma_m}{\sigma_{PL}}\right)^n\right], \quad \frac{\sigma_m}{\sigma_{PL}} \geq 1. \tag{53}$$

The required moment-curvature relations, from which the effective flexural rigidity can be determined, are expressed by Equations (51) to (53).

It is convenient to introduce again the parameter λ, defined by Equation (41). With this relation and that of Equations (23), Equations (51) to (53) give for the effective flexural rigidity,

$$\frac{D'}{D} = \frac{1}{2}\frac{\left(\frac{\lambda M}{M_o}\right)\left(\frac{\sigma_{PL}}{E_v}\right)}{\left[\left(\frac{\sigma_{PL}}{E_v}\right)\left(\frac{\sigma_m}{\sigma_{PL}}\right) + \epsilon_{PL}\left(\frac{\sigma_m}{\sigma_{PL}}\right)^n\right]}, \quad \frac{\sigma_m}{\sigma_{PL}} \geq 1, \tag{54}$$

where

$$\frac{\lambda M}{M_o} = 6\frac{\left[\frac{1}{3}\left(\frac{\sigma_{PL}}{E_v}\right)^2\left(\frac{\sigma_m}{\sigma_{PL}}\right)^3 + \frac{(n+1)\epsilon_{PL}}{(n+2)}\left(\frac{\sigma_{PL}}{E_v}\right)\left(\frac{\sigma_m}{\sigma_{PL}}\right)^{n+2} + \frac{n\epsilon_{PL}^2}{(2n+1)}\left(\frac{\sigma_m}{\sigma_{PL}}\right)^{2n+1}\right]}{\left[\left(\frac{\sigma_{PL}}{E_v}\right)\left(\frac{\sigma_m}{\sigma_{PL}}\right) + \epsilon_{PL}\left(\frac{\sigma_m}{\sigma_{PL}}\right)^n\right]^2}, \quad \frac{\sigma_m}{\sigma_{PL}} \geq 1 \tag{55}$$

By substituting values of σ_m / σ_{PL} into Equations (54) and (55) a curve of D'/D vs $\lambda M/M_o$ can be constructued for use with the incremental procedure. This result may be compared with that of Equation (43) for the ideal nonhardening material. It should be noted that the ideal nonhardening material can be considered as a limiting case of Equation (48) as n approaches infinity.

For the analysis of two-dimensional convoluted structures in nondimensional form with the material behavior of Equation (48) only four of the parameters introduced need be specified. These are, for example, σ_{PL}/E_ν, ϵ_{PL}, n, and λ. For most cases of interest the value 20×10^{-6} for ϵ_{PL} will probably suffice, so that only three parameters may be required. Moreover, for the case of Equation (43) only one parameter is required.

Examples of stress-strain curves, based on the material behavior of Equation (48), are shown in Figure 6 for cases of strain-hardening exponents corresponding to $n = 5$, $n = 10$, and the nonhardening case, $n = \infty$. The other material parameters assumed are $\epsilon_{PL} = 20 \times 10^{-6}$ and $\sigma_{PL}/E_\nu = 10^{-3}$. The corresponding flexural rigidity-moment curves are shown in Figure 7.

E. Computational Procedure

The procedure by which the incremental technique is used to compute the deformation behavior of a convoluted strip is described in the following steps:

1. The typical cantilever section is divided into suitable increments of length and the initial values of z_i and θ_i are determined, as shown in Figure 1c.

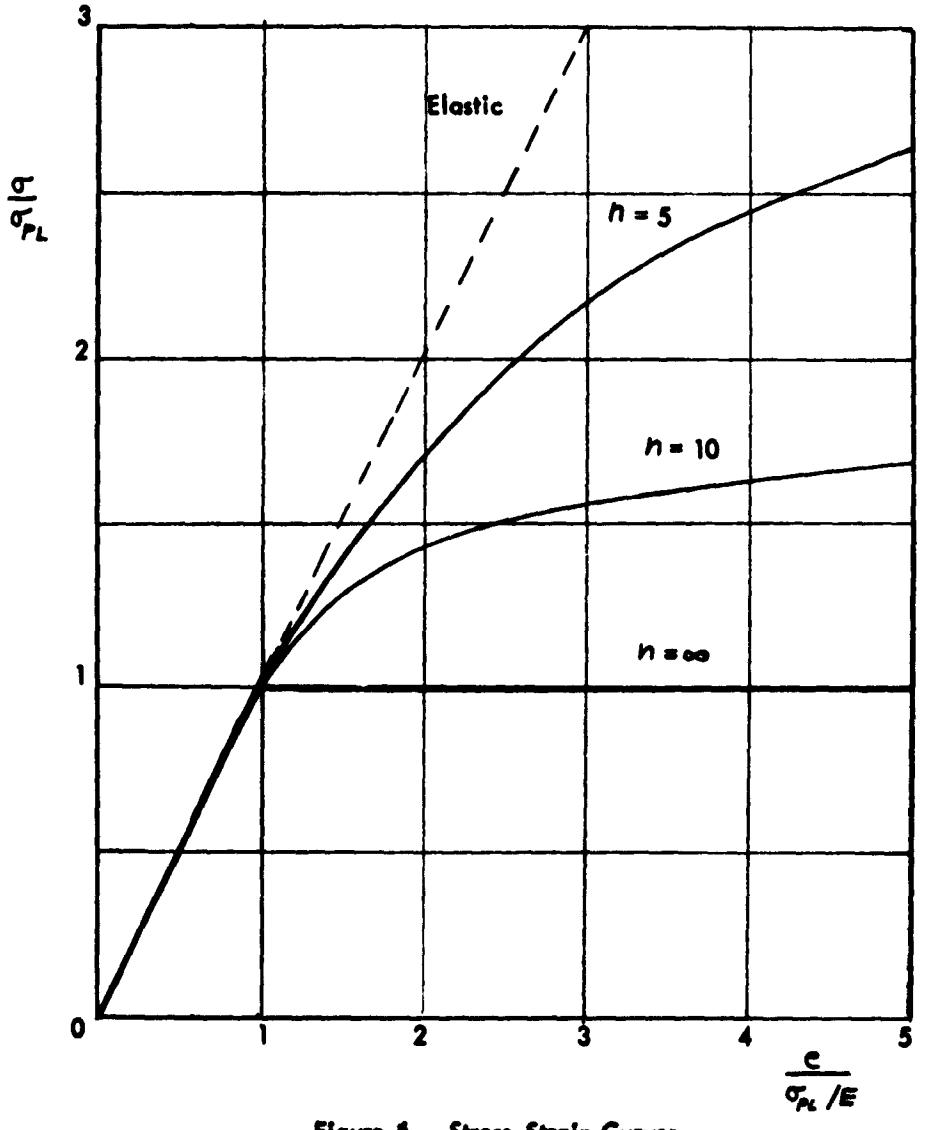

Figure 8. Stress-Strain Curves

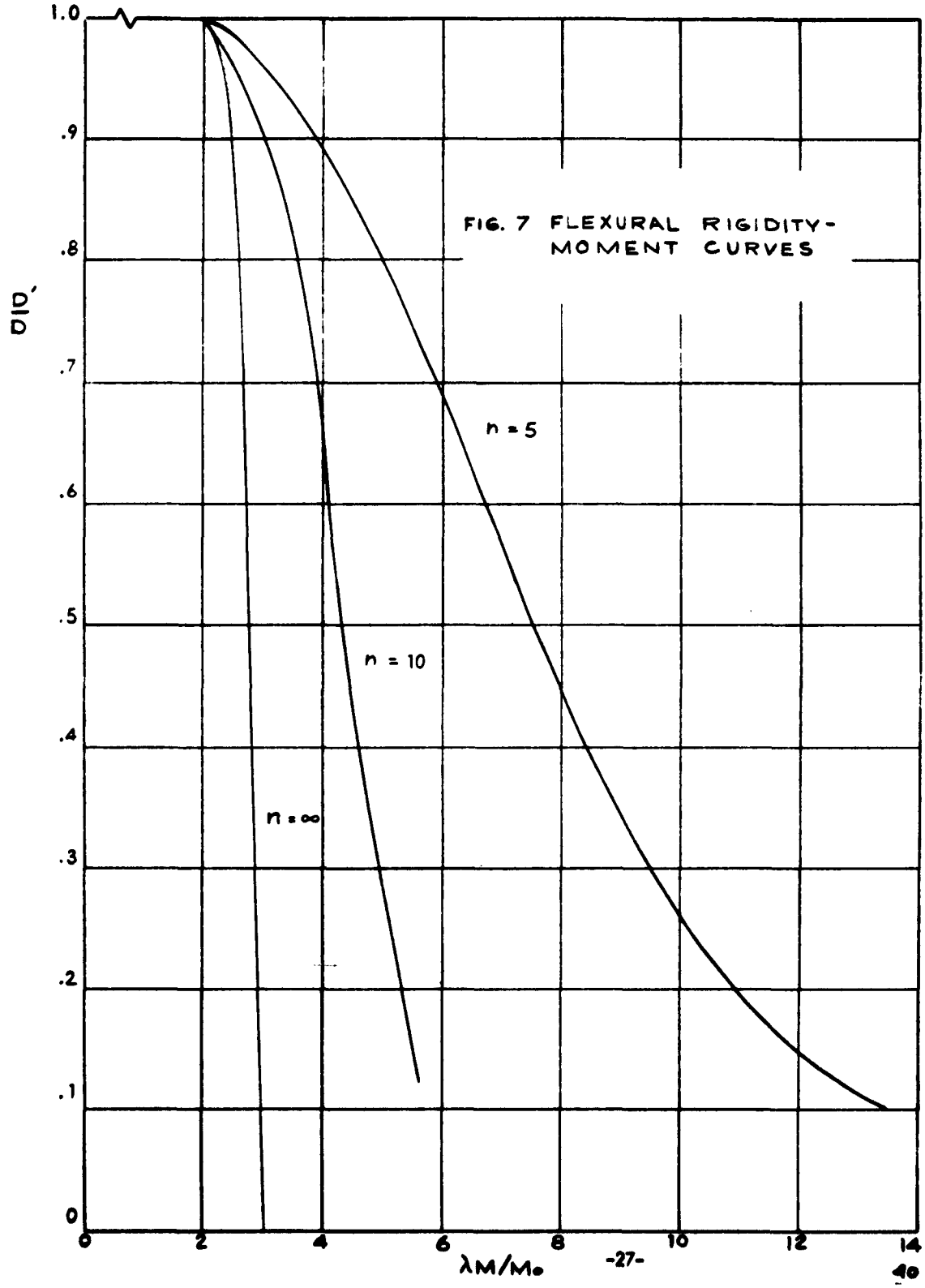

FIG. 7 FLEXURAL RIGIDITY-MOMENT CURVES

40

2. A small increment of load is applied and the corresponding deformations are computed from small-deflection elastic theory. For simple shapes classical analytical methods can be used. However, if the shapes are more complicated the present increment technique can be used. For this purpose the values of $\overline{\Delta M_i}$ are computed from Equation (18), taking $\bar{T} = 0$ and using the initial values of z_i for $\bar{z}_i$. The incremental cantilever slopes and deflections are then computed from Equations (19), (24), and (25), and the resulting deflections $\Delta\xi_i$ and $\Delta\eta_i$ are determined from Equations (12) to (14).

3. The deformations corresponding to the first load increment are recomputed using the results of Step (2) to determine better values for the effective incremental moments, $\overline{\Delta M_i'}$. The values of $\bar{T}$, $\bar{z}_i$, and $\overline{(dz/dT)_i}$ are computed using one-half the values of ΔT and $\Delta\eta_i$. If the material is in the plastic range values of the effective flexural rigidity $\overline{D_i'}$ are computed from the average moment $\bar{T}\bar{z}_i$ and the appropriate relations of Section IV-D. The values of $\overline{\Delta M_i'}$ are computed from Equations (18) or (9), depending on whether the material is in the elastic or plastic range. The deformations are then computed using Equations (24) and (25) or Equations (32) and (33) for the incremental cantilever relations.

4. The values of $\overline{(dz/dT)_i}$ are computed from the results of Step (3) and compared with the initial values used in Step (3). If the agreement is unsatisfactory, Step (3) is repeated using the final values of $\overline{(dz/dT)_i}$ until agreement between two successive values is attained.

5. Subsequent load increments are applied and the procedure of Step (4) is used to obtain the incremental deformations.

Although an iterative technique is used for each load increment, convergence appears to be sufficiently rapid in most cases that the method can be used with a desk calculator. In the case of a plastic analysis with the nonhardening material behavior some difficulty was experienced due to the severe variation of effective flexural rigidity with moment, as illustrated in Figure 7. However, if the load increment is sufficiently small it is expected that this difficulty can be avoided. Moreover, with the present incremental technique it is just as easy to use a more realistic material behavior, such as illustrated in the other curves of Figures 6 and 7, which converge more readily. A more complete discussion of the computations is given in the following section.

If the material behavior is limited to the elastic range, it is possible to use a direct procedure for each load increment and to correct the value of the load increment on the basis of energy considerations. For this purpose it is convenient to introduce a material efficiency factor defined by

$$\psi \equiv \frac{\text{elastic strain energy in structure}}{\text{elastic strain energy capacity corresponding to maximum stress}} = \frac{U}{\frac{\sigma_m^2 h \ell}{2E_y}}, \qquad (56)$$

where U is the elastic strain energy per unit width of the cantilever beam of Figure 1, ℓ is the total length of the beam, and σ_m is the maximum bending stress. With the expression for U in terms of bending moment, given by

$$U = \int_0^{\ell} \frac{M^2 ds}{2D} = \frac{6}{E_v h^3} \int_0^{\ell} M^2 ds \quad , \tag{57}$$

and the maximum stress, given by

$$\sigma_m = \frac{6 M_m}{h^2} \quad , \tag{58}$$

where M_m is the maximum bending moment, ψ may be written

$$\psi = \frac{1}{3\ell} \int_0^{\ell} \left(\frac{M}{M_m}\right)^2 ds \quad . \tag{59}$$

Since the elastic strain energy in the structure is equal to the work done during deformation,

$$U = \int_0^{\xi} T(\xi') d\xi' \quad , \tag{60}$$

where ξ is the total horizontal deflection, as indicated in Figure 1d.

Equations (56), (58), and (60) yield the relation

$$\psi = \frac{E_v h^3}{18 \ell M_m^2} \int_0^{\xi} T(\xi') d\xi' \quad . \tag{61}$$

The maximum bending moment is

$$M_m = T z_0 \quad , \tag{62}$$

where z_o is the maximum moment arm, as indicated in Figure 1c. With this result Equations (56) and (59) can be written

$$\psi = \frac{1}{3\ell} \int_0^{\ell} \left(\frac{z}{z_o}\right)^2 d\xi \ , \tag{63}$$

and

$$\psi = \frac{E_y h^3}{18 \ell T^2 z_o^2} \int_0^{\xi} T(\xi') d\xi' \ . \tag{64}$$

It will be shown in the numerical examples that ψ is a slowly varying function of the load and deflection. Therefore, by determining the value of a given load increment so that the expressions of Equations (63) and (64) are equal, a more accurate result can be obtained on the basis of total energy absorbed. In addition, it is useful to evaluate ψ as a function of load and deflection, since this quantity is a measure of the effectiveness with which the available material is being utilized. The procedure by which the corrected load increment is determined is described below.

After application of a particular load increment ψ is determined From Equation (63) by numerical integration. This value of ψ is then used in Equation (64) to determine the corrected load increment. Let ΔT_n denote the n-th corrected load increment, and let the subscript n denote values of the parameters of Equations (60), (63), and (64) after application of the n-th load

increment. Then, assuming a linear load-deflection relation for each load increment, Equation (64) can be expressed in the form

$$(T_{n-1} + \Delta T_n)^2 = \frac{E_v h^3}{18 \ell \psi_n z_{on}^2} \left[U_{n-1} + (T_{n-1} + \tfrac{1}{2} \Delta T_n) \Delta \xi_n \right] . \tag{65}$$

The solution for ΔT_n from Equation (65) is

$$\Delta T_n = - \frac{B_n}{2} + \sqrt{\left(\frac{B_n}{2}\right)^2 + C_n} , \tag{66}$$

where

$$\left.\begin{aligned} B_n &\equiv 2 T_{n-1} - \frac{E_v h^3}{36 \ell} \frac{\Delta \xi_n}{\psi_n z_{on}^2} \\ C_n &\equiv \frac{E_v h^3}{18 \ell} \frac{(U_{n-1} + T_{n-1} \Delta \xi_n)}{\psi_n z_{on}^2} - T_{n-1}^2 \end{aligned}\right\} . \tag{67}$$

For the first load increment corresponding to n = 1, the solution is

$$\Delta T_1 = \frac{E_v h^3}{36 \ell} \frac{\Delta \xi_1}{\psi_1 z_{o1}^2} . \tag{68}$$

Equations (66) and (67) may be written in the nondimensional form,

$$\frac{\Delta T_n}{T_o} = - \frac{\beta_n}{2} + \sqrt{\left(\frac{\beta_n}{2}\right)^2 + \gamma_n} , \tag{69}$$

where

$$\left.\begin{aligned} \beta_n \equiv \frac{B_n}{T_o} &= 2\left(\frac{T_{n-1}}{T_o}\right) - \frac{1}{3}\,\frac{\Delta\xi_n/h}{\left(\frac{l}{h}\right)\psi_n\left(\frac{z_{on}}{h}\right)^2} \\ \gamma_n \equiv \frac{C_n}{T_o^2} &= \frac{2}{3}\,\frac{\left[\frac{U_{n-1}}{T_o h} + \left(\frac{T_{n-1}}{T_o}\right)\left(\frac{\Delta\xi_n}{h}\right)\right]}{\left(\frac{l}{h}\right)\psi_n\left(\frac{z_{on}}{h}\right)^2} - \left(\frac{T_{n-1}}{T_o}\right)^2 \end{aligned}\right\} . \qquad (70)$$

F. Computational Results

The accuracy of the elemental beam approach was investigated by the application of this part of the method to the small-deflection analysis of a semi-circular-arc convolute for which the true solution is known. The quarter circle corresponding to the cantilever beam of Figure 1 was divided into three, four, and five increments, and the resulting load-deflection relations are compared with the known solutions. The results are summarized in Table I, in which ξ and η represent the horizontal and vertical deflections, respectively, and h is the initial radius of curvature. The true solutions are,

$$\frac{\xi/h}{T/T_o} = 0.785, \qquad \frac{\eta/h}{T/T_o} = 0.500 \qquad (71)$$

Table I. Small-Deflection Solution for 3, 4, and 5 Beam Increments

No. of Increments	$\frac{\xi/h}{T/T_o}$	$\frac{\eta/h}{T/T_o}$	% error in ξ	% error in η
3	.757	.505	3.6	1.0
4	.770	.504	1.9	0.8
5	.775	.501	1.3	0.2

It is seen that the incremental beam technique gives rather accurate results for relatively few increments. For example, according to Table I the use of four beam elements for the large-deflection analysis should introduce less than 2% error in ξ and less than 1% in η, particularly since the straight beam approximation improves as the curvature decreases.

Large-deflection elastic cases were carried out for the semi-circular-arc configuration and two U-shaped configurations, illustrated in Figure 8. The principal results for the semi-circular-arc are shown in Figures 9 to 12, and those for the two U-shapes, in Figures 13 to 20. The results include the load-deflection curve; a curve of η/r vs. ξ/r which indicates the "flattening" of the convolute; a curve of the yield parameter $(h/r) / (\sigma_{PL}/E_y)$ which indicates the deflection at which the proportional limit is reached; and the variation of the material efficiency factor Ψ with ξ/r.

For comparison, the small-deflection solutions for the U-shaped convolute are given by

$$\left.\begin{aligned} \frac{\xi/h}{T/T_o} &= \frac{\pi}{4} + 2\frac{a}{h} + \frac{\pi}{2}\left(\frac{a}{h}\right)^2 + \frac{1}{3}\left(\frac{a}{h}\right)^3 \\ \frac{\eta/h}{T/T_o} &= \frac{1}{2} + 0.5708\,\frac{a}{h} \end{aligned}\right\} . \qquad (72)$$

Plastic cases were run for the semi-circular-arc configuration with the material behavior of Figures 6 and 7, and two values of the yield parameter λ. The resulting load-deflection curves are shown in Figures 21 and 22. As mentioned

FIG. 8 U-SHAPED CONFIGURATION

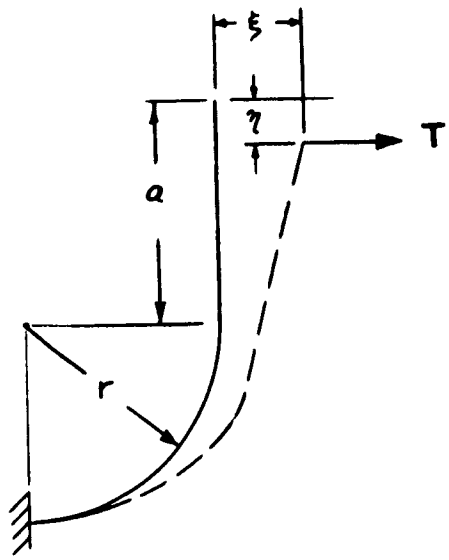

LOAD - DEFLECTION CURVE

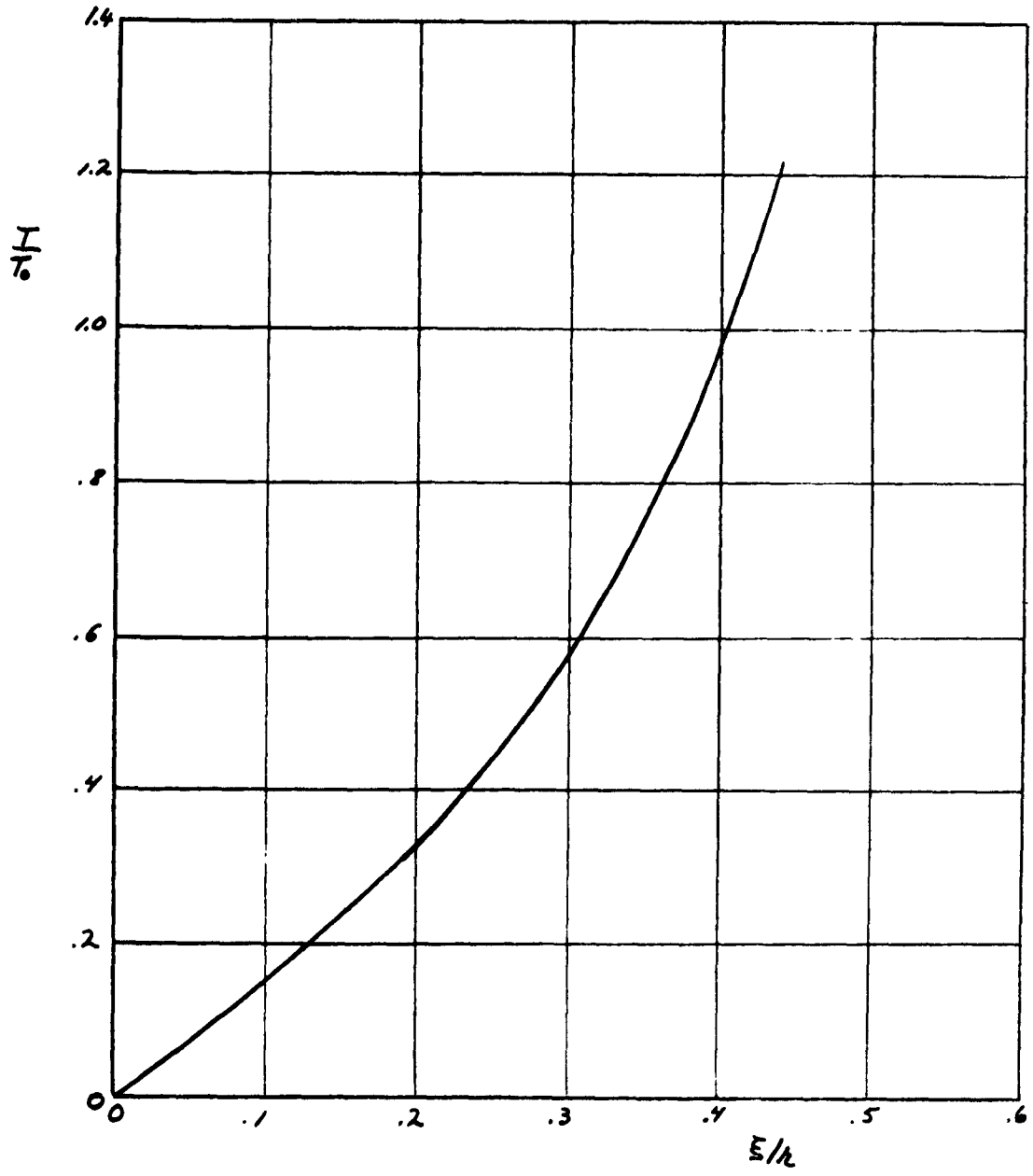

Figure 9. Elastic Semi-Circular Arc

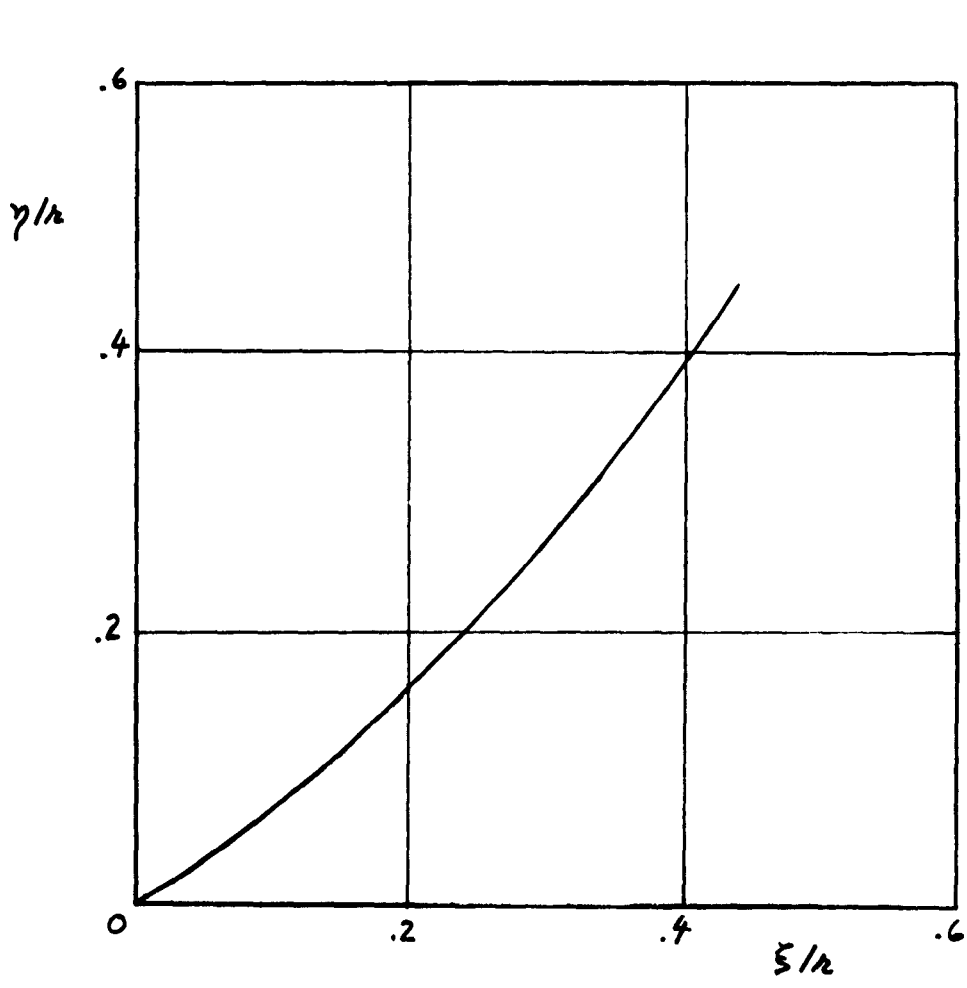

Figure 10. Elastic Semi-Circular Arc

YIELD PARAMETER vs. ξ/r

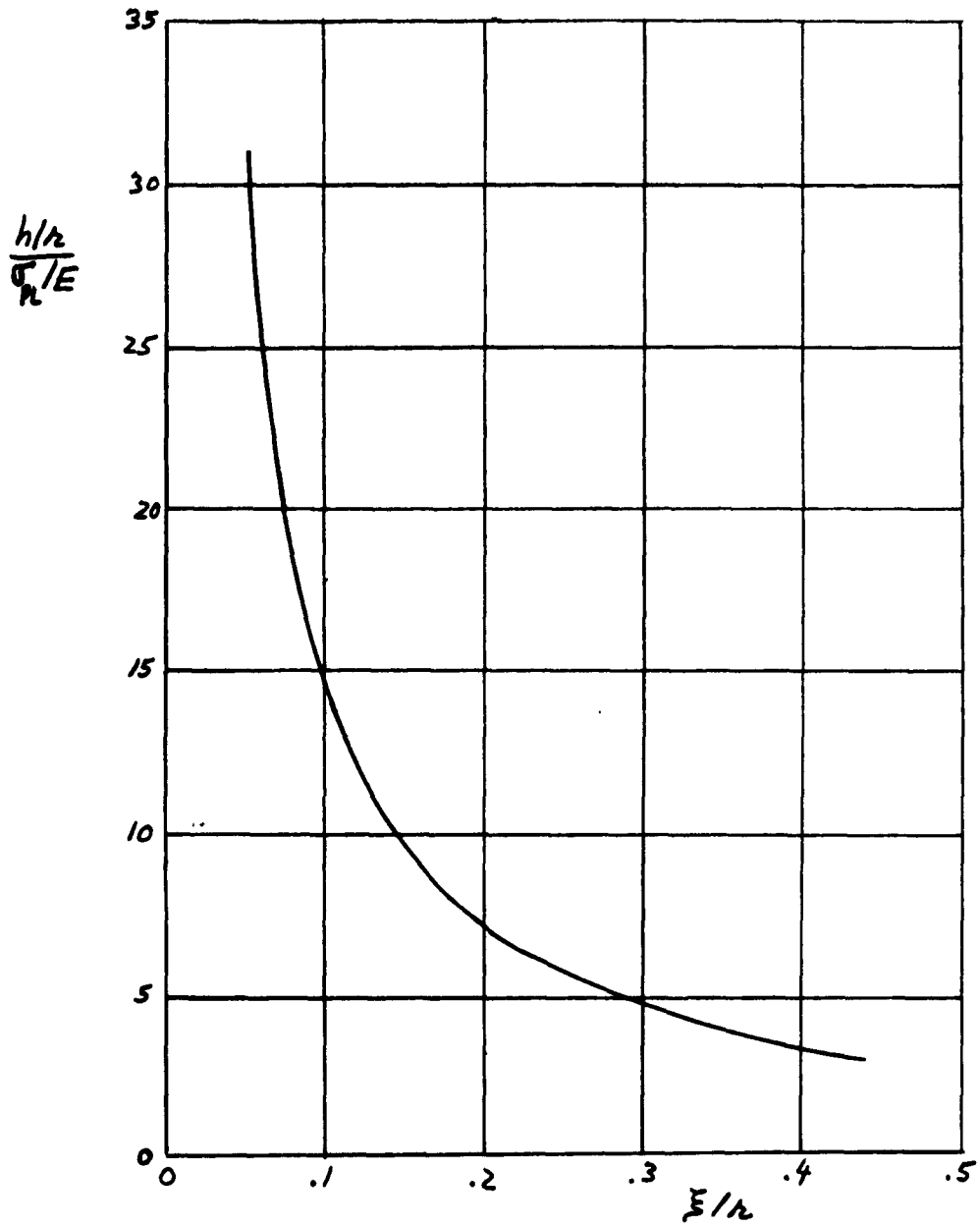

Figure 11. Elastic Semi-Circular Arc

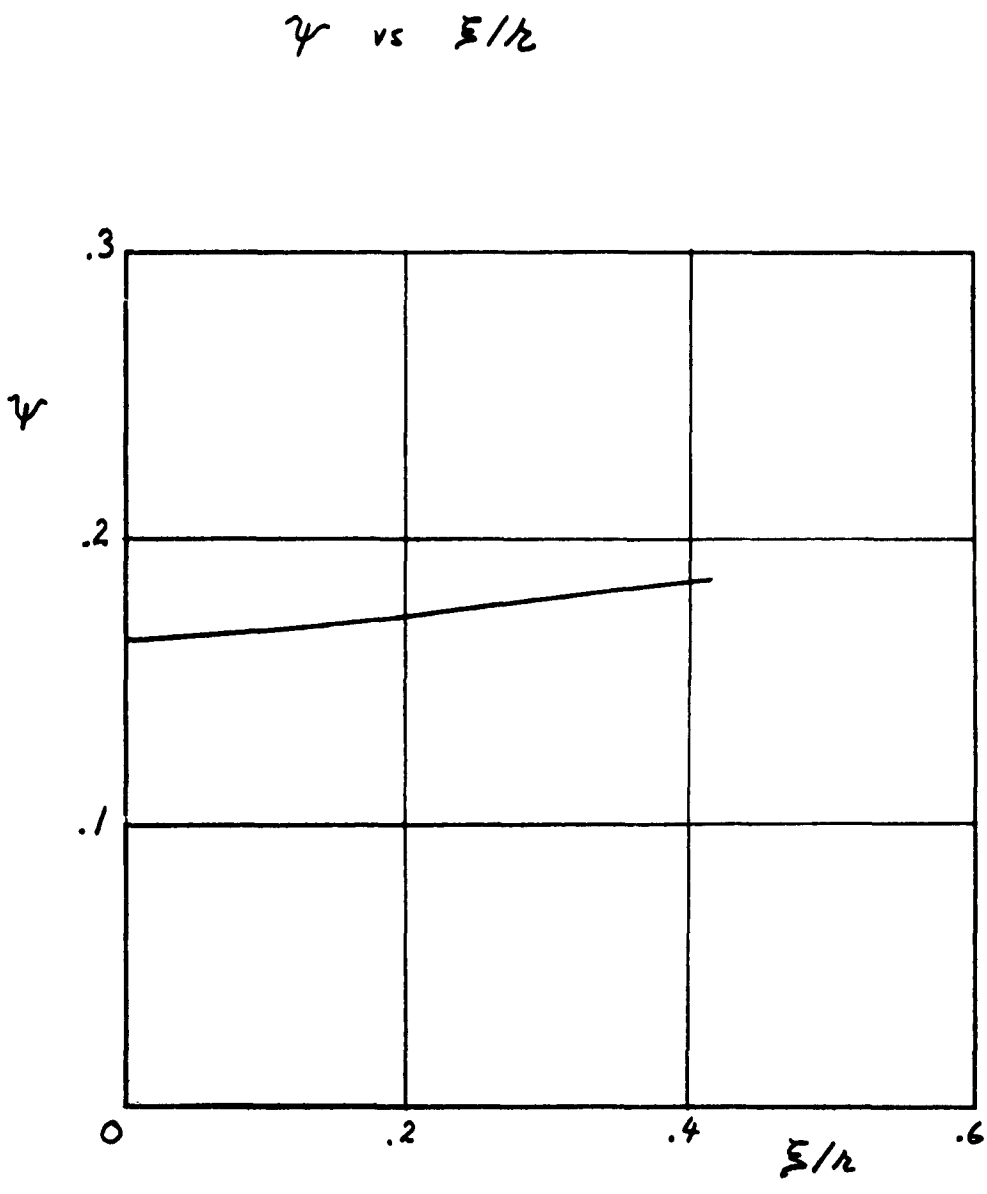

Figure 12. Elastic Semi-Circular Arc

LOAD - DEFLECTION CURVE

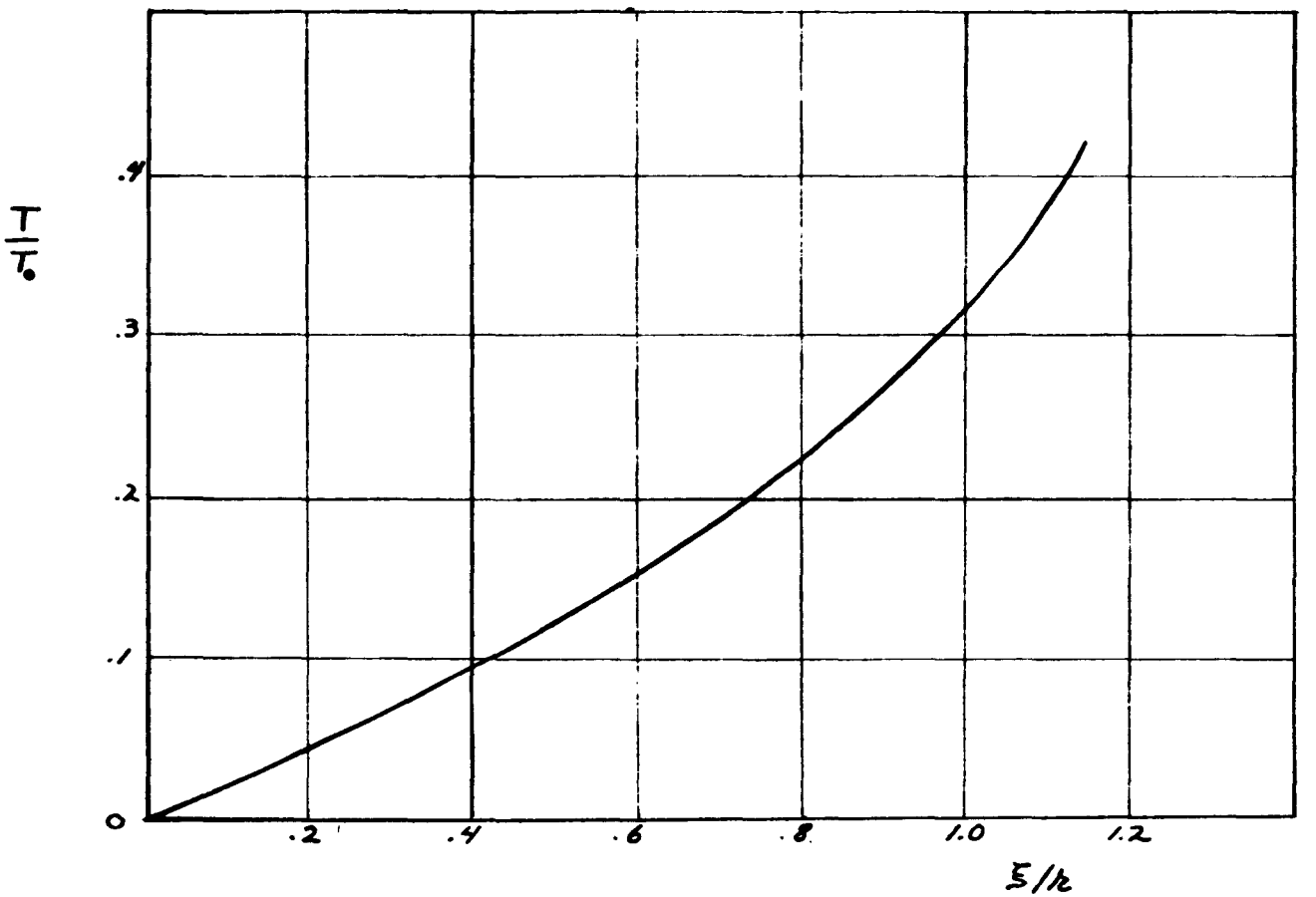

Figure 13. Elastic U-shaped Configuration, a/r = 1

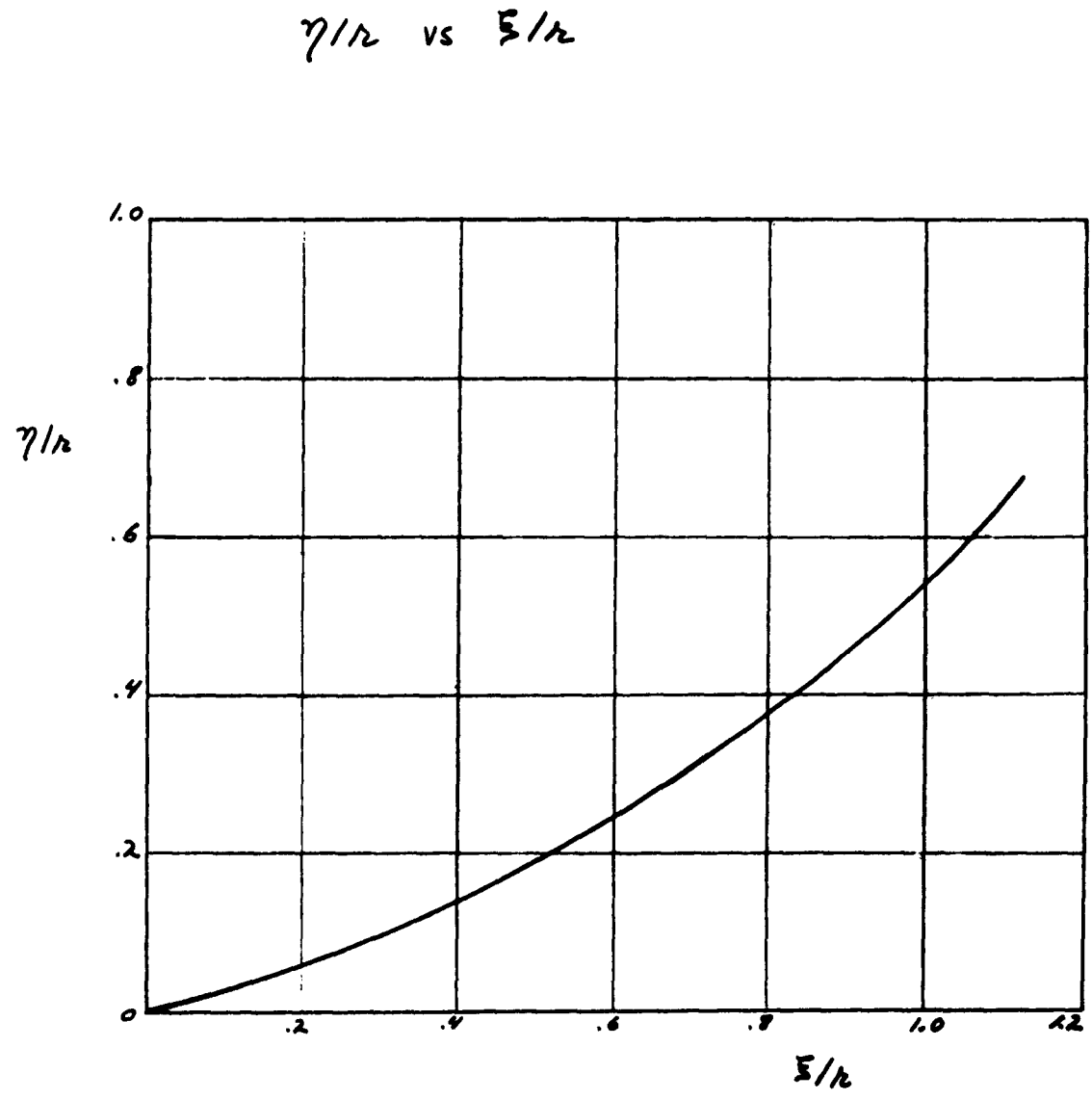

Figure 14. Elastic U-shaped Configuration, a/r = 1

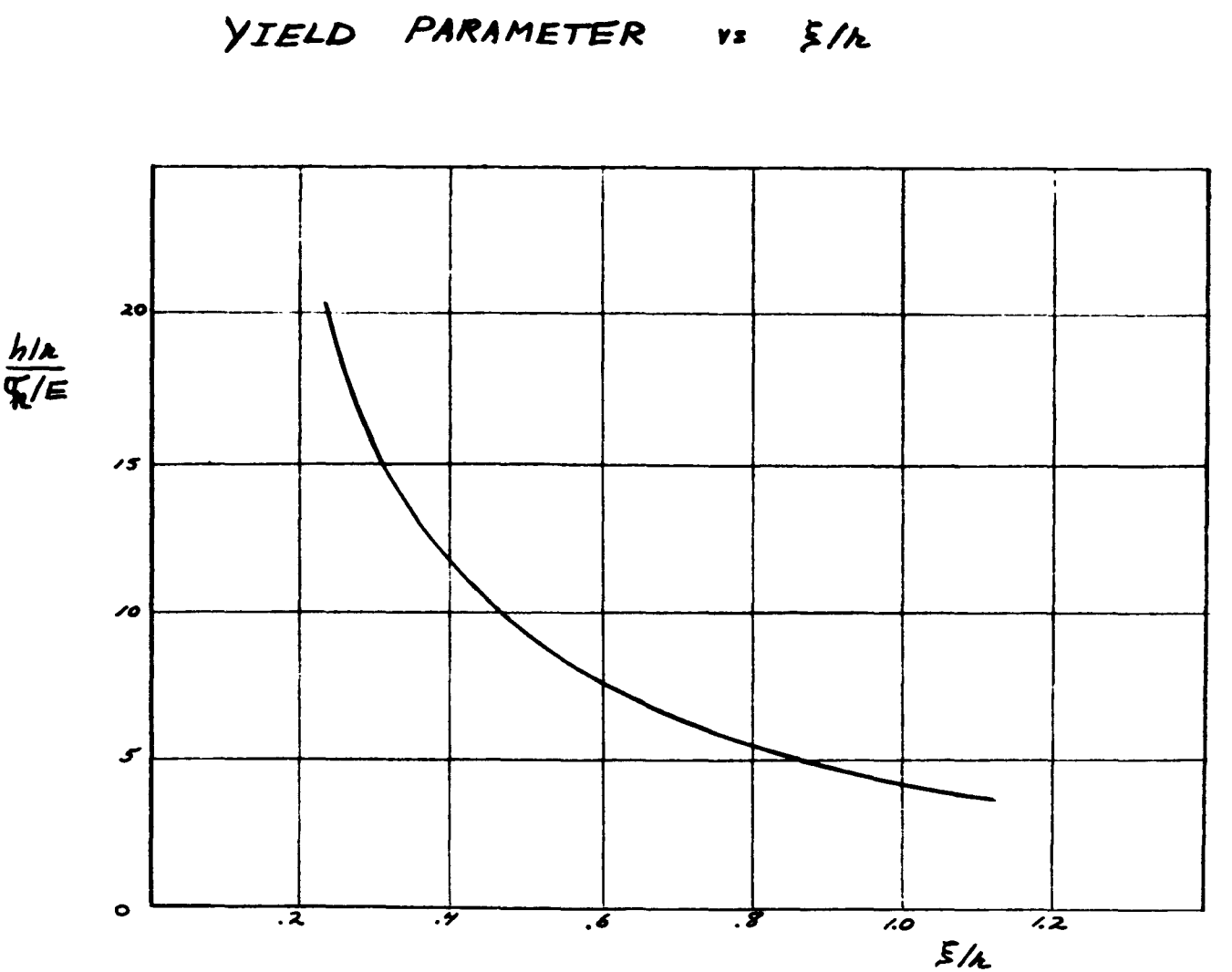

Figure 15. Elastic U-shaped Configuration, a/r = 1

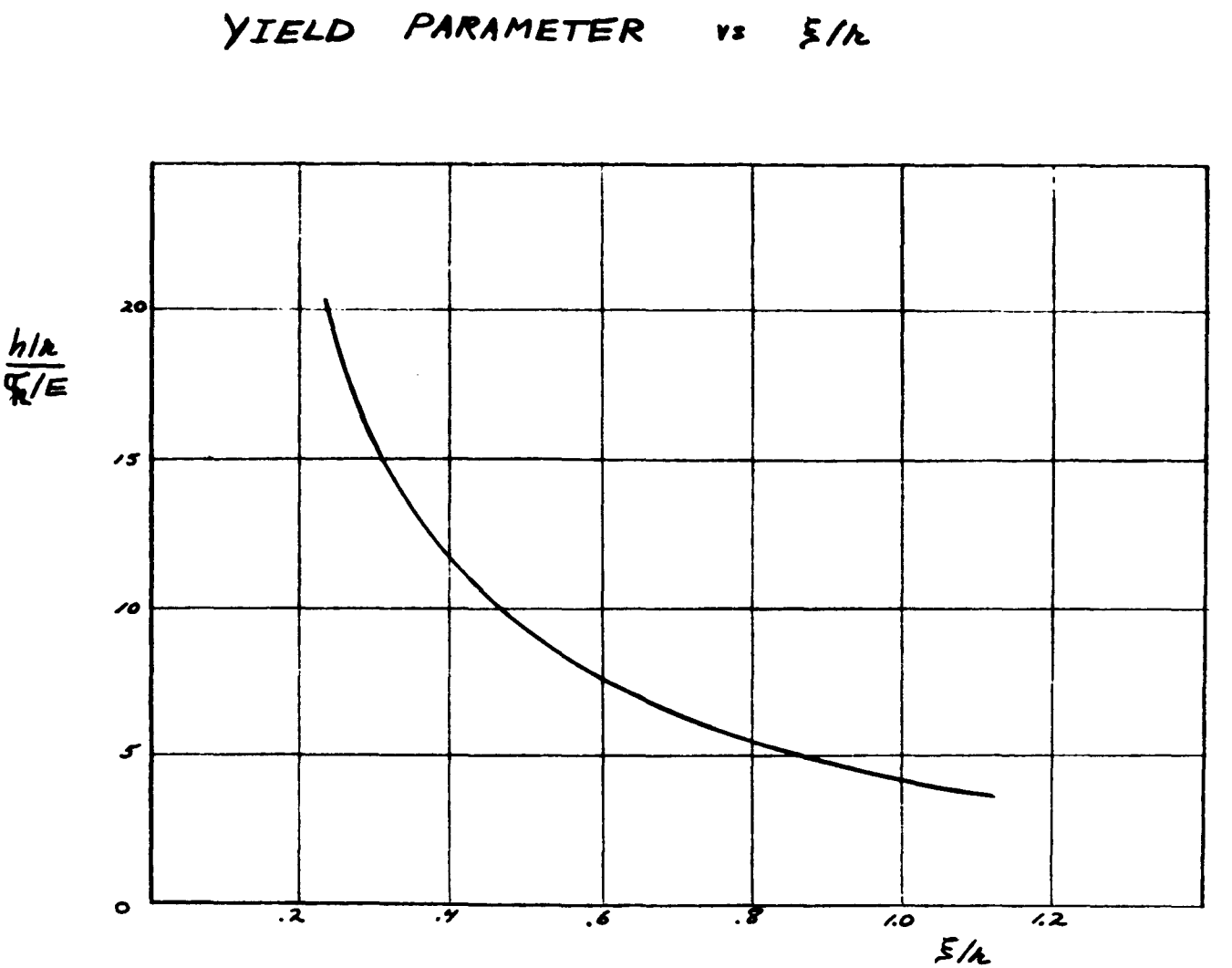

Figure 15. Elastic U-shaped Configuration, a/r = 1

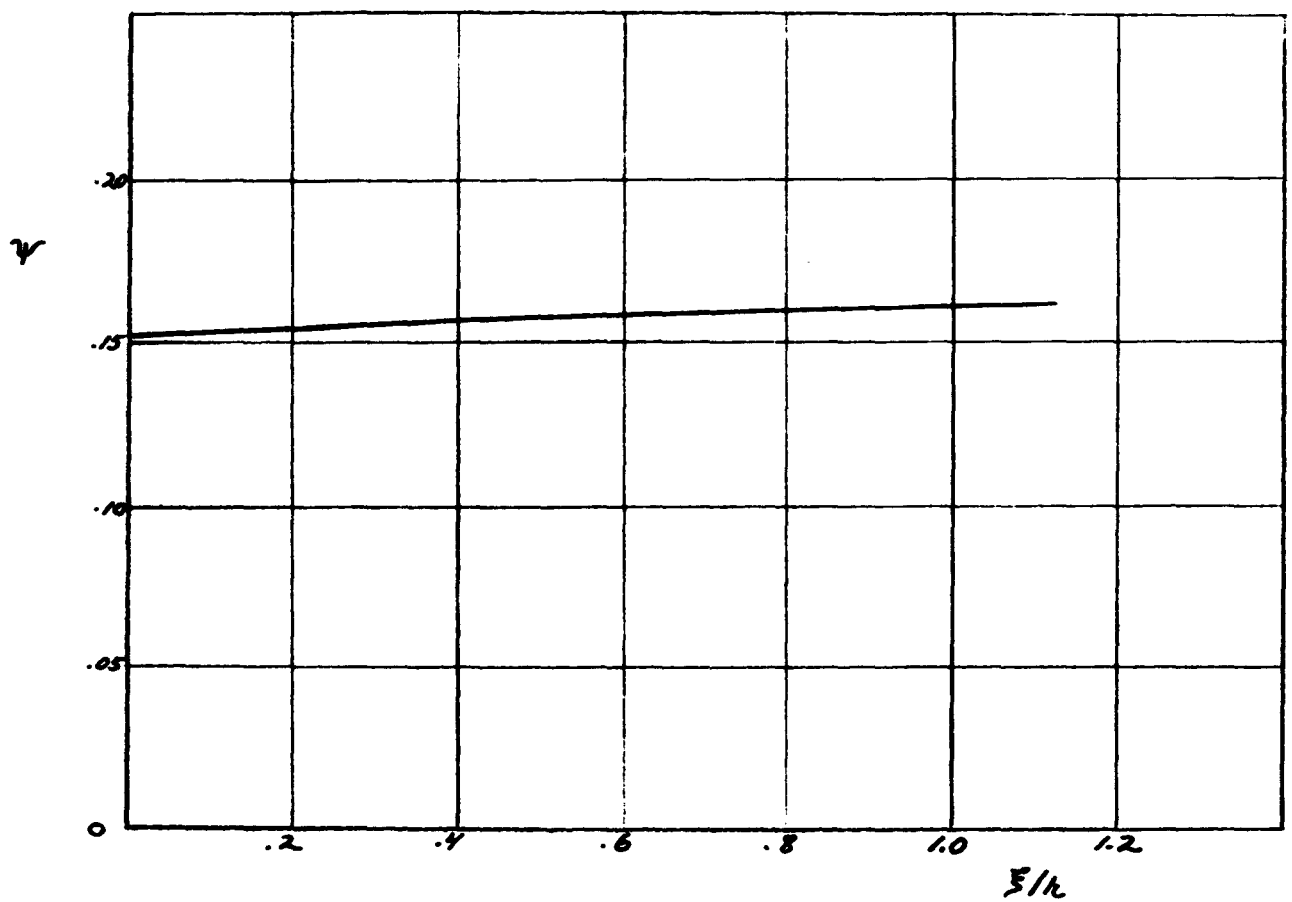

Figure 16. Elastic U-shaped Configuration, a/r = 1

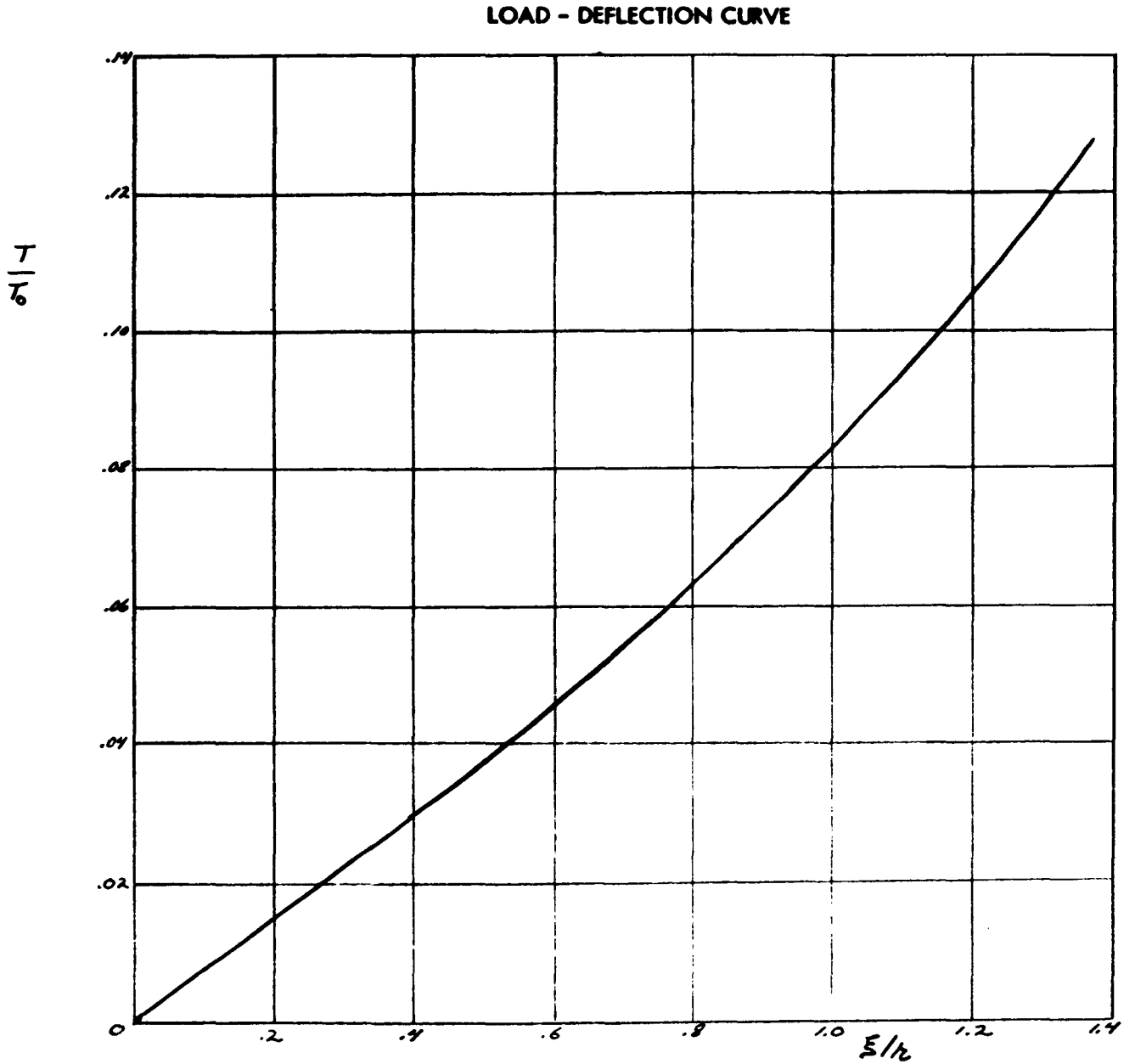

Figure 17. Elastic U-shaped Configuration, a/r = 2

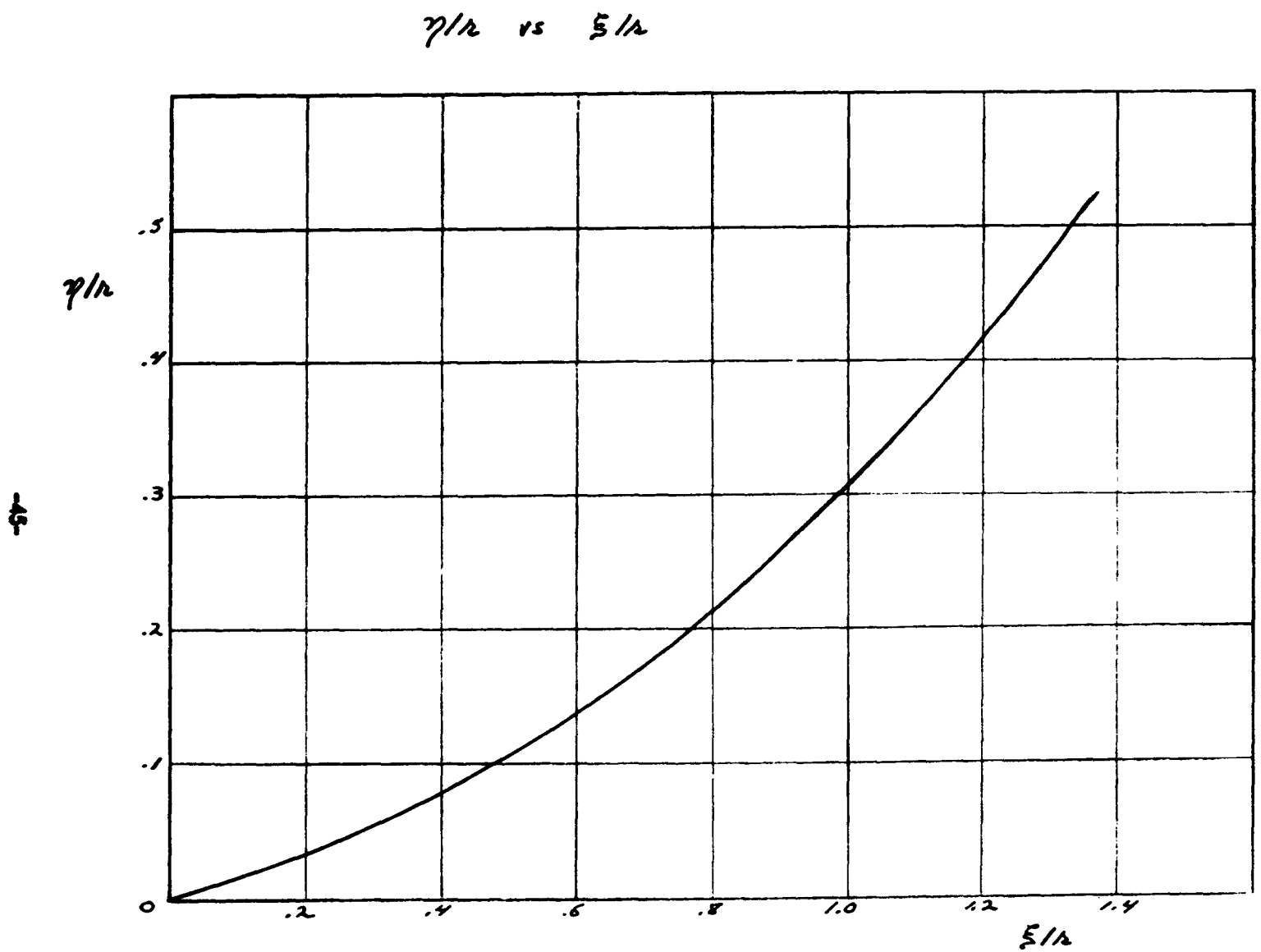

Figure 18. Elastic U-shaped Configuration, a/r = 2

YIELD PARAMETER vs. ξ/ℓ

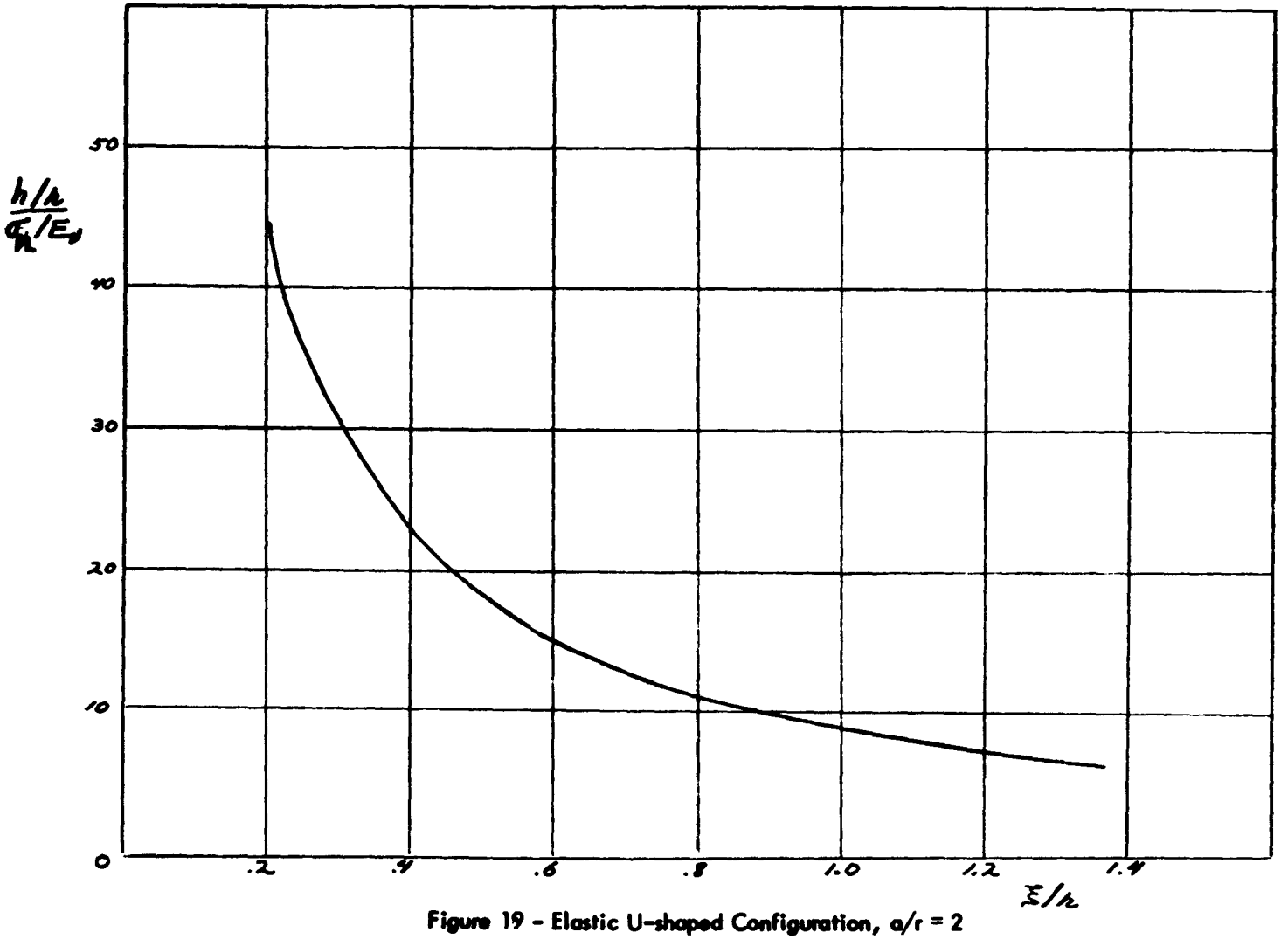

Figure 19 - Elastic U-shaped Configuration, a/r = 2

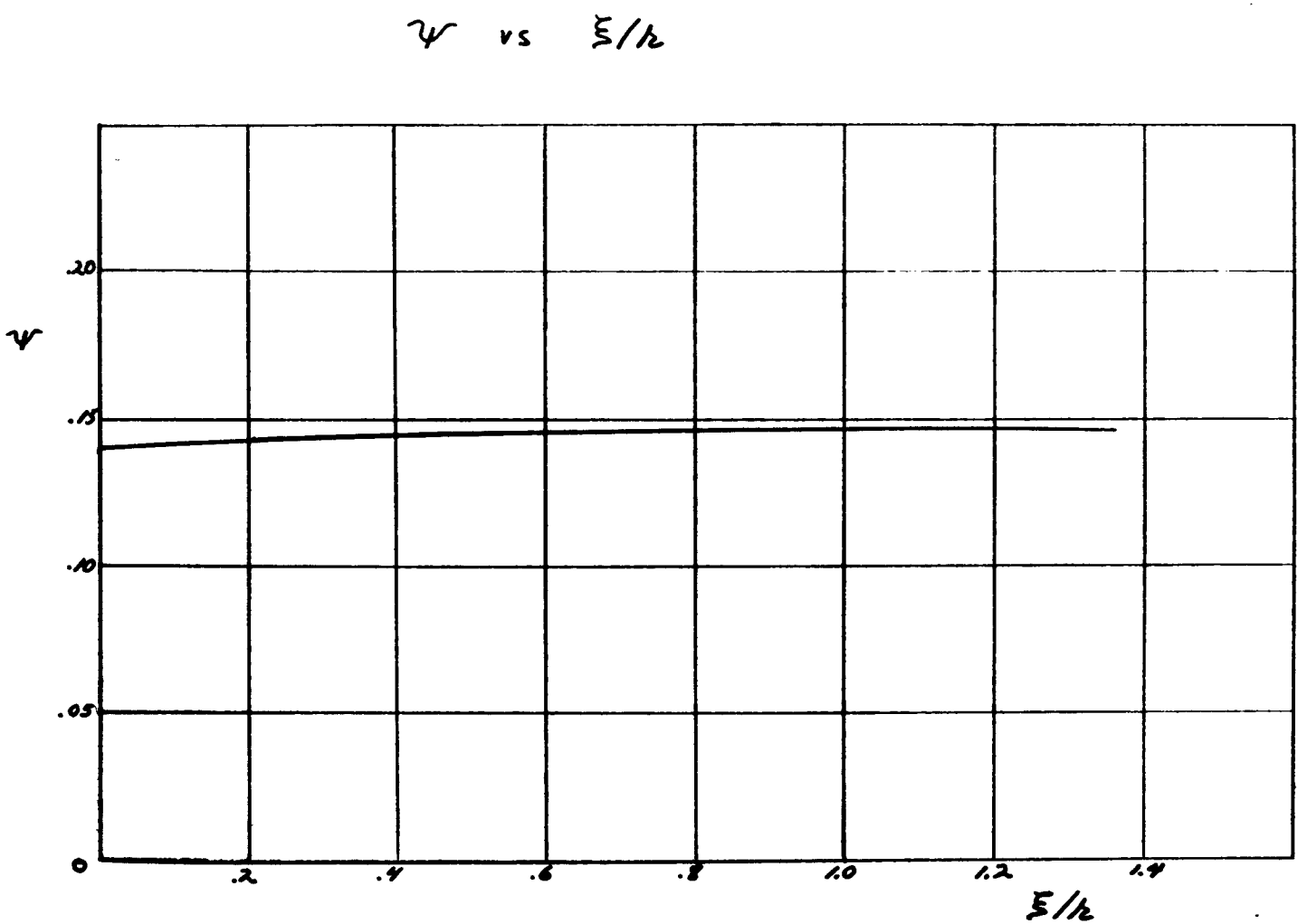

Figure 20 – Elastic U-shaped Configuration, a/r = 2

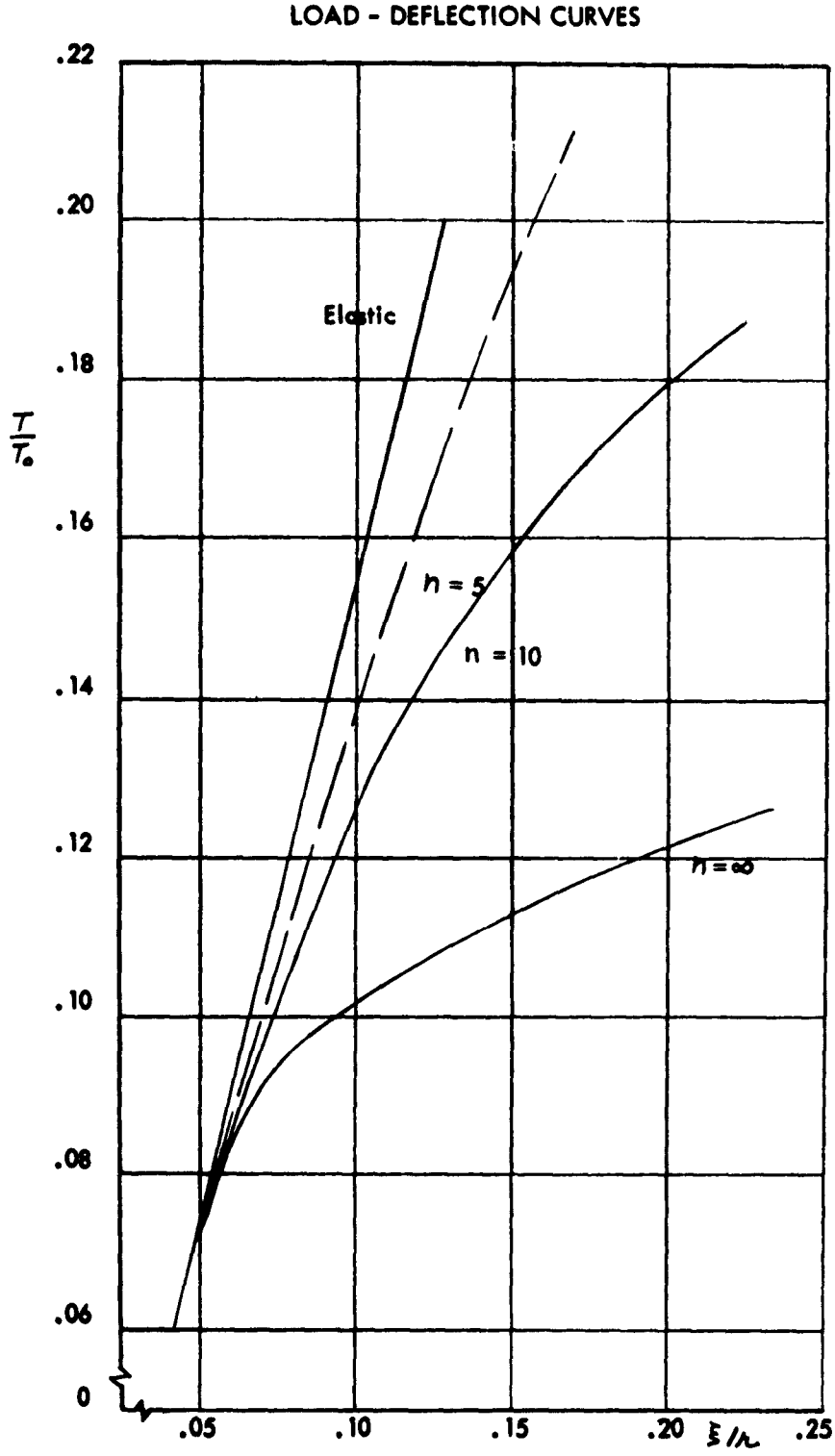

Figure 21. Plastic Semi-Circular Arc, $\lambda = 31$

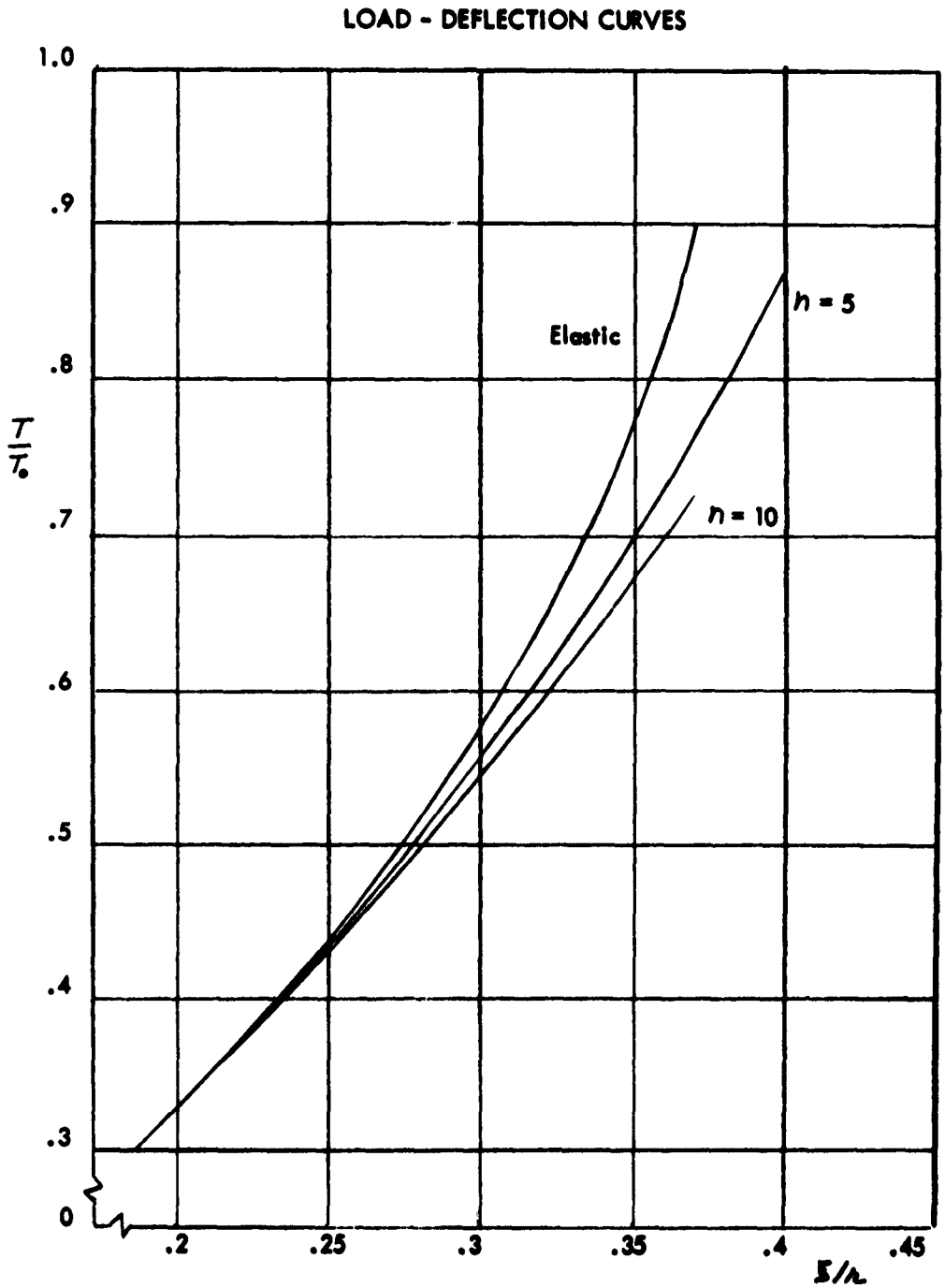

Figure 22. Plastic Semi-Circular Arc, $\lambda = 7.25$

earlier, some difficulty was encountered with convergence of the nonhardening material case due to the sensitivity of effective flexural rigidity with bending moment. The curve of Figure 21 corresponding to $n = \infty$ was computed with only three load increments, although as many as six iterations were required for a particular load increment. In order to test the accuracy of these calculations, the same case was repeated using load increments of half the magnitude, and six instead of four length increments. These results are shown in Figure 23 and indicate only small deviations from the original solution. The curves corresponding to the other cases of strain hardening were computed with considerably more ease, with only one or two iterations being adequate for some of the load increments.

V. THREE-DIMENSIONAL CONVOLUTED STRUCTURES

In a two-dimensional convoluted structure, such as the strip of the previous analyses, deformation arises from bending in the plane of the convolute which is essentially constant over the width of the strip. In the usual three-dimensional convoluted structure, however, additional restraints are present so that the structure is not free to deform by a uniform bending in the convoluted plane. For example, in the common bellows of Figure 24a, extension or contraction of the bellows is accompanied by changes in the diameter which produce lateral "hoop" stresses. These stresses impose severe restrictions on the flexibility of the bellows, particularly in the case of large deflections. Similarly, in the deformation of a convoluted structure from a cylindrical to a conical shape, as shown in Figure 24b, the non-uniform circumferential expansion is accompanied by twisting of the longitudinal

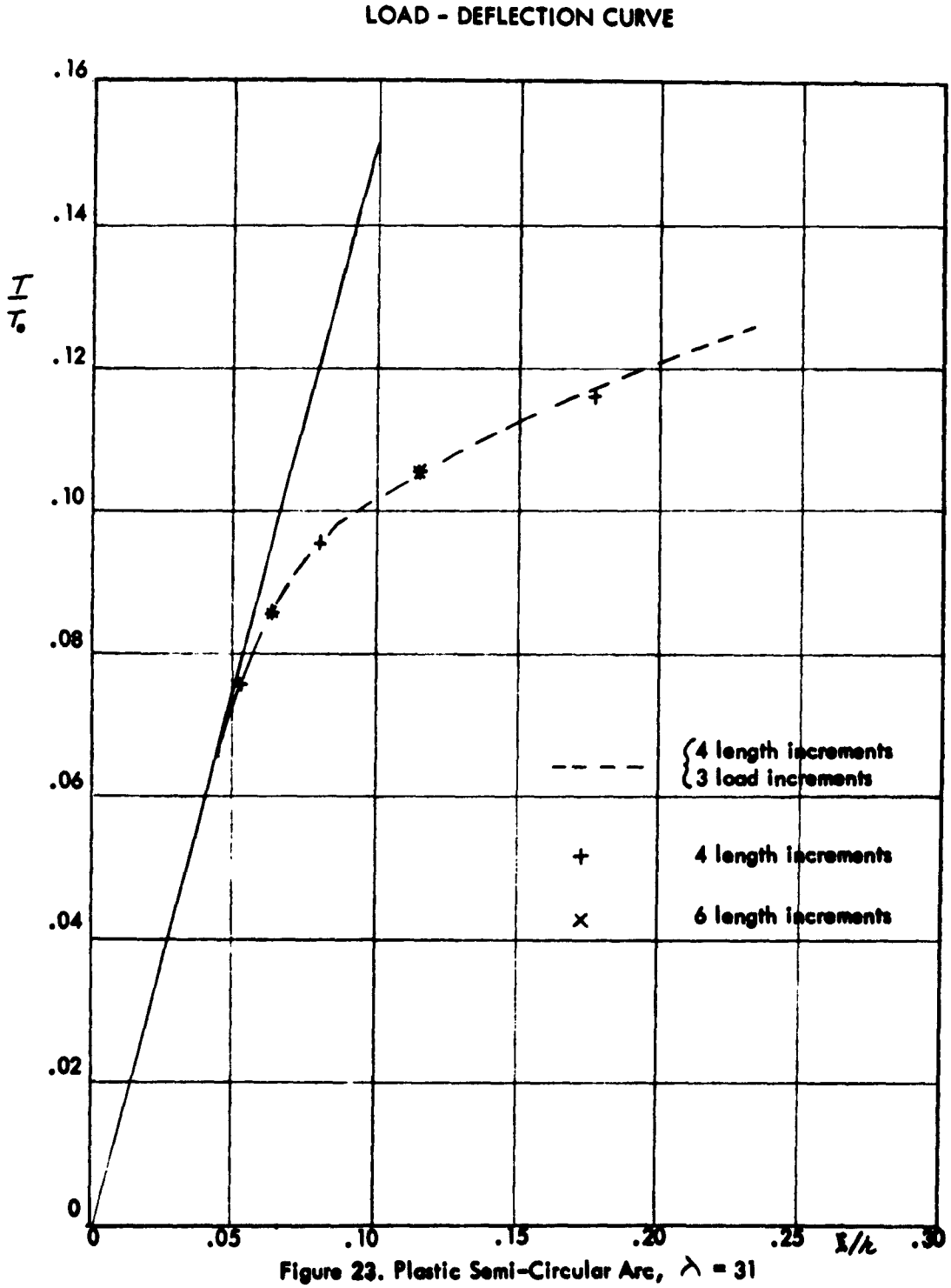

Figure 23. Plastic Semi-Circular Arc, $\lambda = 31$

FIG. 24 EXAMPLES OF THREE-DIMENSIONAL CONVOLUTED STRUCTURES

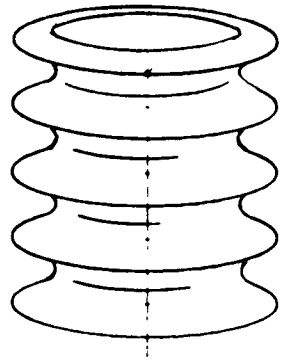

(a) BELLOWS

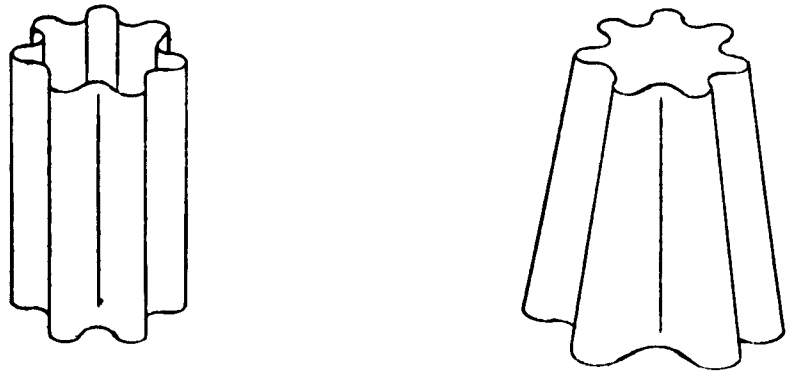

(b) CYLINDER - CONE

elements. This produces restraints which, although not generally as severe as in the bellows, can significantly affect the behavior of the structure.

For the present analysis, two cases of the circumferentially-convoluted cylinder of Figure 24b are treated. The first case represents an idealized structure of saw-tooth configuration which expands into a conical shape, and illustrates in a simplified manner the three-dimensional restraining effects. The second case deals with a more realistic structure in which the convolute has one of the U-shapes considered earlier. These analyses are described in the following sections.

A. Circumferentially-Convoluted Cylinder with Idealized Saw-Tooth Configuration

In the present example the idealized cylindrical structure is restrained at one end and is expanded into a conical shape by a uniform pressure differential across the walls. The following assumptions are used in the analysis:

1. The convolute span height is small compared with the radius of the cylinder.

2. All of the deformation in the plane of the convolute occurs at the bends so that only the angle of the saw-tooth is changed.

3. A linear relation exists between bending moment and convolute (saw-tooth) angle.

4. The centerline of each longitudinal strip remains straight so that twisting but no bending occurs in the longitudinal direction.

5. Small-deflection torsion theory applies to the twisting of the strips.

6. The material behavior is elastic.

With the above assumptions expressions can be derived for the elastic energy of bending and twisting of the longitudinal strips and the work done on the structure during expansion. By equating the work done with the total elastic energy the relation between differential pressure and cone angle can be determined.

The coordinates and some of the geometric parameters are shown in Figure 25. Because of symmetry it is necessary to treat only one of the longitudinal strips.

The twisting energy for a structure componed of N strips is given by

$$U_T = \frac{NGJ}{2} \int_0^L \left(\frac{d\varphi}{dx}\right)^2 dx \,, \tag{73}$$

where GJ is the torsional rigidity of the strip. From Figure 25 we have the geometric relations

$$2\pi R = N\ell \sin\varphi \tag{74}$$

and

$$\sin\varphi = \left(1 + \frac{x}{R_1}\sin\alpha\right)\sin\varphi_1 \,. \tag{75}$$

Equation (75) and its derivative with respect to x give the result

$$\left(\frac{d\varphi}{dx}\right)^2 = \frac{\sin^2\alpha}{R_1^2 \operatorname{ctn}^2\varphi_1 - 2R_1 x \sin\alpha - x^2\sin^2\alpha} \,. \tag{76}$$

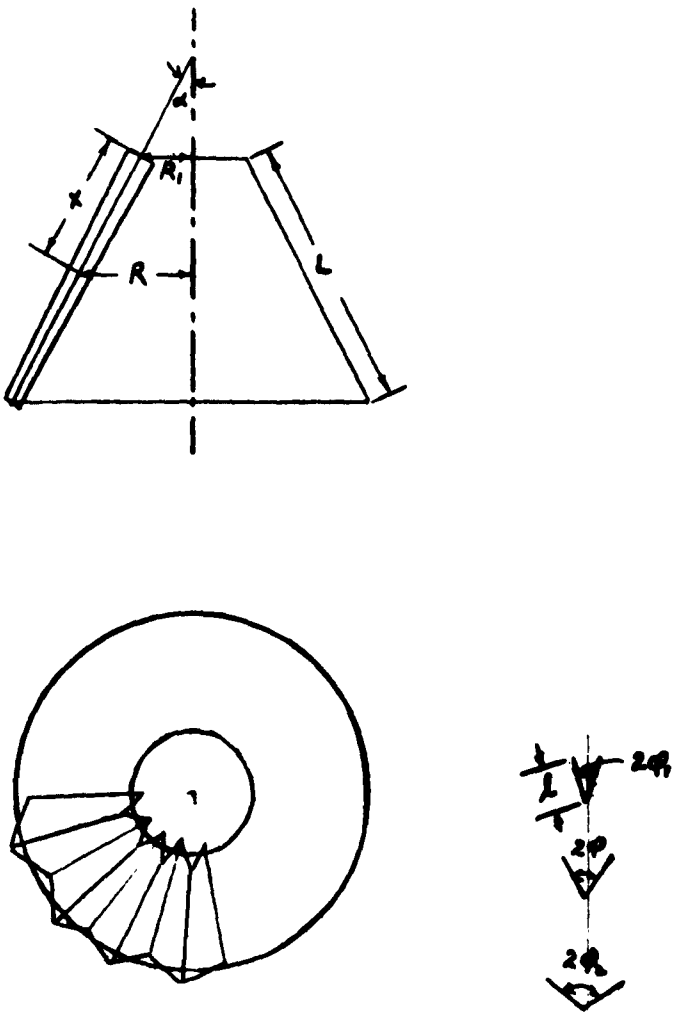

Figure 25. Coordinates and Geometric Parameters for Convoluted Cylindrical Structure

Substitution of Equation (76) into Equation (73) and integration gives the result

$$U_T = \frac{NGJ}{2R_1} \sin\varphi_1 \sin\alpha \left\{ \tanh^{-1}\left[\left(1+\frac{L}{R_1}\sin\alpha\right)\sin\varphi_1\right] - \tanh^{-1}(\sin\varphi_1)\right\} . \quad (77)$$

The change in U_T due to the change $d\alpha$ in the cone half-angle is, by differentiation of Equation (77),

$$dU_T = \frac{NGJ}{2R_1} \sin\varphi_1 \cos\alpha \left[\tanh^{-1}(\sin\varphi_2) - \tanh^{-1}(\sin\varphi_1) + \frac{L}{R_1}\frac{\sin\varphi_1 \sin\alpha}{\cos^2\varphi_2}\right] d\alpha , \quad (78)$$

where

$$\varphi_2 = \sin^{-1}\left[\left(1+\frac{L}{R_1}\sin\alpha\right)\sin\varphi_1\right] . \quad (79)$$

The bending energy for the strip can be expressed by

$$U_{B/N} = k \int_0^L (\varphi-\varphi_1)^2 dx \quad (80)$$

where k is an effective elastic constant for the joint. With the substitution of φ from Equation (75) into Equation (80), the result of the integration can be expressed by

$$U_B = \frac{NkR_1}{\sin\varphi_1 \sin\alpha}\left[u(\sin^{-1}u)^2 - 2u + 2\sqrt{1-u^2}\sin^{-1}u - 2\varphi_1(u\sin^{-1}u + \sqrt{1-u^2})\right]_{\sin\varphi_1}^{\sin\varphi_2} + NkL\varphi_1^2 . \quad (81)$$

The change in U_B due to the change in the cone half-angle can be written as

$$\frac{dU_B}{d\alpha} = \frac{dU_B}{d\sin\varphi_2} \frac{d\sin\varphi_2}{d\alpha} \quad . \tag{82}$$

Differentiation of Equation (81) with Equations (79) and (82) gives the result

$$dU_B = \frac{NkR_1\cot\alpha}{\sin\alpha}\left[2\frac{L}{R_1}\sin\alpha - (\varphi_2-\varphi_1)^2 - 2(\varphi_2-\varphi_1)\frac{\cos\varphi_2}{\sin\varphi_1}\right] d\alpha \quad . \tag{83}$$

The work done on the structure by the differential pressure p during the expansion $d\alpha$ is, from Figure 26,

$$dW = p\int_{x=0}^{L}(2\pi R\,dx)\,x\,d\alpha \quad . \tag{84}$$

Integration of Equation (84) with the relation,

$$R = R_1 + x\sin\alpha \quad , \tag{85}$$

gives the result

$$dW = \pi R_1 L^2 p\left(1 + \frac{2}{3}\frac{L}{R_1}\sin\alpha\right) d\alpha \quad . \tag{86}$$

The work done on the structure can be equated with the total energy absorbed in the structure, to give

$$dW = dU_T + dU_B \quad . \tag{87}$$

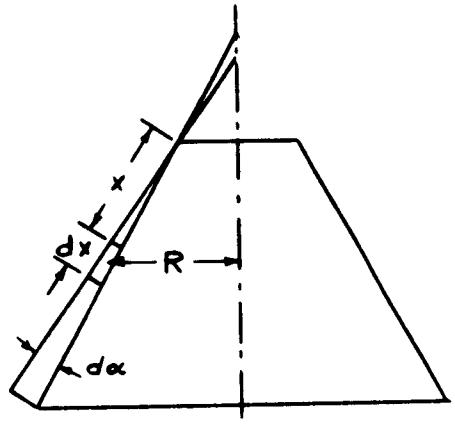

FIG. 26 Coordinates Used to Express Incremental Work

Substitution of Equations (78), (83) and (86) into Equation (87) gives the required pressure relation,

$$\frac{\pi R_1^2 L^2 P}{NGJ} = \frac{\sin\varphi_1 \cos\alpha}{2\left(1+\frac{2}{3}\frac{L}{R_1}\sin\alpha\right)}\left[\tanh^{-1}(\sin\varphi_2) - \tanh^{-1}(\sin\varphi_1) + \frac{L}{R_1}\frac{\sin\varphi_1 \sin\alpha}{\cos^2\varphi_2}\right] \tag{88}$$

$$+ \frac{k R_1^2}{GJ}\frac{\cot\alpha \csc\alpha}{\left(1+\frac{2}{3}\frac{L}{R_1}\sin\alpha\right)}\left[2\frac{L}{R_1}\sin\alpha - (\varphi_2-\varphi_1)^2 - 2(\varphi_2-\varphi_1)\frac{\cos\varphi_2}{\sin\varphi_1}\right].$$

This example illustrates the manner in which three-dimensional restraints can give rise to twisting as well as bending energy absorption by the structure, and might provide a first-approximation solution for certain convoluted configurations. However, a more realistic analysis is presented in the following section.

B. Circumferentially-Convoluted Cylinder with U-Shaped Configuration

The present analysis is similar to the preceding one except that lateral bending of the longitudinal strips is treated more properly, and the resulting effects on the twisting of the strips is taken into account. A typical strip of the present structure has an S-shaped cross section which deforms as shown in Figure 27. The lateral deformation of the strip at a particular axial location is determined from the two-dimensional analysis. It is seen from the sketch of Figure 27 that the angle of twist φ varies over the cross section of the strip, as compared with the uniform twisting in the previous analysis. This variable twisting is taken into account by

FIG. 27 CROSS-SECTION OF TYPICAL LONGITUDINAL STRIP

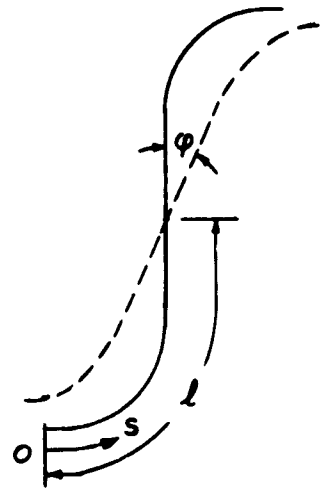

treating the strip as though it were made up of many smaller strips, each of which twists a different amount. From symmetry it is necessary to treat only half of the S-shaped strip, as in the two-dimensional analysis.

The following assumptions are made:

1. The convolute span height is small compared with the radius of the cylinder.

2. The center line of each longitudinal S-shaped strip remains straight as the cylinder deforms into a conical shape.

3. The load-deformation behavior due to lateral bending at any axial location is the same as that determined in the two-dimensional analysis.

4. Small-deflection torsion theory applies to the twisting of each element of the S-shaped strip, and a constant torsional rigidity relates twisting moment per unit length of cross section with the local angle of twist.

5. The material behavior is elastic.

With the above assumptions the twisting energy of the structure per unit length in the axial direction can be written

$$\frac{dU_T}{dx} = NGJ \int_0^l \left[\frac{d\varphi}{dx}(x,s) \right]^2 ds \ , \tag{89}$$

where N is the number of S-shaped strips and GJ is the torsional rigidity of the strip per unit length of cross section. The angle of twist $\varphi(x,s)$ is a function of both the axial coordinate x and the cross section coordinate s. For a strip of narrow cross section the torsional rigidity per unit length is, from Reference D,

$$GJ = \frac{Gh^2}{3} \ . \tag{90}$$

If it is assumed that the functional form of $\varphi(x,s)$ with s is the same for all values of x, Equations (89) and (90) can be written

$$\frac{dU_T}{dx} = \frac{NGh^3 k_1 \ell}{3}\left[\frac{d\varphi_m}{dx}(x)\right]^2 , \tag{91}$$

where k_1 is independent of x and is defined by

$$k_1 \equiv \frac{1}{\ell\left[\frac{d\varphi_m}{dx}(x)\right]^2}\int_0^{\ell}\left[\frac{d\varphi}{dx}(x,s)\right]^2 ds \tag{92}$$

and φ_m is the maximum angle of twist, corresponding to $s = \ell$. Although k_1 appears to be a function of x by Equation (92), it will be shown in the example that it is nearly invariant in x.

Integration of Equation (91) from 0 to L gives for the total twisting energy,

$$U_T = \frac{NGh^3 k_1 \ell}{3L}\int_{\frac{x}{L}=0}^{1}\left[\frac{d\varphi_m}{d(x/L)}\right]^2 d\left(\frac{x}{L}\right) . \tag{93}$$

For the U-shaped configuration discussed earlier, the fractional expansion ξ/λ is related to the present structural parameters by

$$\xi/\lambda = \frac{x}{R_1}\sin\alpha , \tag{94}$$

and

$$d\left(\frac{\xi}{\lambda}\right) = \frac{L}{R_1}(\sin\alpha)\, d\left(\frac{x}{L}\right) , \tag{95}$$

so that Equation (93) can be written,

$$U_T = \frac{N G h^3 k_1 \ell}{3 R_1} \sin\alpha \int_{\frac{\xi}{h}=0}^{\frac{L}{R_1}\sin\alpha} \left[\frac{d\varphi_m}{d(\xi/h)}\right]^2 d\left(\frac{\xi}{h}\right) \quad . \tag{96}$$

The functional relation for $d\varphi_m/d(\xi/h)$ vs. ξ/h can be approximated by

$$\frac{d\varphi_m}{d(\xi/h)} = a_1 + b_1 \frac{\xi}{h} \tag{97}$$

where a_1 and b_1 are determined from the two-dimensional analysis. Substitution of Equation (97) into Equation (96) and differentiation with respect to α gives

$$\frac{dU_T}{d\alpha} = \frac{N G h^3 k_1 \ell}{3 R_1}\left[2 a_1^2 \frac{L}{R_1}\sin\alpha + 3 a_1 b_1 \left(\frac{L}{R_1}\right)^2 \sin^2\alpha + \frac{4}{3} b_1^2 \left(\frac{L}{R_1}\right)^3 \sin^3\alpha\right]\cos\alpha \, . \tag{98}$$

This expression can be used with the differential energy relation, as in the preceding analysis, or integrated to give the total twisting energy as a function of α ,

$$U_T = \frac{N G h^3 k_1 \ell}{3 R_1}\left[a_1^2 \frac{L}{R_1}\sin^2\alpha + a_1 b_1 \left(\frac{L}{R_1}\right)^2 \sin^3\alpha + \frac{1}{3} b_1^2 \left(\frac{L}{R_1}\right)^3 \sin^4\alpha\right] \, . \tag{99}$$

The bending energy can be expressed in the form,

$$\frac{dU_B}{dx} = 2 N h T_0 \int_0^{\xi/h(x)} \frac{T}{T_0}\left(\frac{\xi'}{h}\right) d\left(\frac{\xi'}{h}\right) \, , \tag{100}$$

where T is the circumferential load per unit length and T_o is the reference load of Equation (23). The function $T/T_o\,(\xi/\ell)$ can be approximated from the two-dimensional analysis by

$$\frac{T}{T_o}\left(\frac{\xi}{\ell}\right) = a_2\left(\frac{\xi}{\ell}\right) + b_2\left(\frac{\xi}{\ell}\right)^2 \quad . \tag{101}$$

Substitution of Equation (101) into Equation (100) and integration gives the result

$$\frac{dU_B}{dx} = 2N\ell T_o\left[\frac{a_2}{2}\left(\frac{\xi}{\ell}\right)^2 + \frac{b_2}{3}\left(\frac{\xi}{\ell}\right)^3\right] , \tag{102}$$

which, with Equation (94), can be written

$$\frac{dU_B}{d(\xi/\ell)} = 2N\ell T_o R_1 (\csc\alpha)\left[\frac{a_2}{2}\left(\frac{\xi}{\ell}\right)^2 + \frac{b_2}{3}\left(\frac{\xi}{\ell}\right)^3\right] . \tag{103}$$

Integration of this equation from $\xi/\ell = 0$ to $\xi/\ell = (L/R_1)\sin\alpha$ gives the result

$$U_B = \frac{1}{3}N\ell R_1 T_o a_2\left(\frac{L}{R_1}\right)^3\left(1 + \frac{1}{2}\frac{b_2}{a_2}\frac{L}{R_1}\sin\alpha\right)\sin^2\alpha \quad . \tag{104}$$

The differential bending energy expression, analogous to Equation (98), can then be written

$$\frac{dU_B}{d\alpha} = 2N\ell R_1 T_o\left[\frac{a_2}{3}\left(\frac{L}{R_1}\right)^3\sin\alpha + \frac{b_2}{4}\left(\frac{L}{R_1}\right)^4\sin^2\alpha\right]\cos\alpha \quad . \tag{105}$$

With the expression for T_o from Equation (23), and the relations,

$$G = \frac{E}{2(1+\nu)} = \frac{1-\nu}{2} E_\nu \quad , \tag{106}$$

Equations (99) and (100) can be combined to give the total energy input W as a function of α,

$$W = U_T + U_B$$

$$= \frac{1}{36} N E_\nu t^3 a_2 \left(\frac{L}{h}\right)\left(\frac{L}{R_1}\right)^2 \left\{\left(1 + \frac{1}{2}\frac{b_2}{a_2}\frac{L}{R_1}\sin\alpha\right)\right. \tag{107}$$

$$\left. + 6(1-\nu)\frac{t_1 a_1^2}{a_2}\frac{lh}{L^2}\left[1 + \frac{b_1}{a_1}\frac{L}{R_1}\sin\alpha + \frac{1}{3}\left(\frac{b_1}{a_1}\right)^2\left(\frac{L}{R_1}\right)^2\sin^2\alpha\right]\right\}\sin^2\alpha \ .$$

The present method is illustrated with an example based on the U-shaped configuration with $a/h = 1$, used in the two-dimensional analysis. The determination of the constants k_1, a_1, b_1, a_2, and b_2 from the two-dimensional analysis is described in Appendix A. These results are as follows:

$$k_1 = 0.460, \quad a_1 = 0.647, \quad b_1 = 0.121, \quad a_2 = 0.213, \quad b_2 = 0.0612 \tag{108}$$

With these values, and $l/h = 2.571$ for this configuration, Equation (107) can be written

$$W = 0.00592\,N E_v h^3 \frac{L^2}{\pi R_1^2}\left\{\left(1 + 0.1434\,\frac{L}{R_1}\sin\alpha\right)\right.$$

$$\left. + 13.93(1-\nu)\left(\frac{h}{L}\right)^2\left[1 + 0.187\,\frac{L}{R_1}\sin\alpha + 0.0116\left(\frac{L}{R_1}\right)^2\sin^2\alpha\right]\right\}\sin^2\alpha. \quad (109)$$

If the span height of the convoluted structure is not small compared with the radius of the cylinder, as assumed in the foregoing analysis, the resulting equations are not strictly applicable, due to the significant curvature imposed on the (gross) structure. This curvature gives rise to additional twisting deformations as the cylinder is expanded into the conical shape and also affects the bending in the planes of the convolute. However, one simple correction can be applied in order to improve the theory for this case.

Figure 28 illustrates the manner in which a circumferential strip is deformed during forming of the cylinder from a straight convoluted strip. It can be seen that significant bending occurs during the forming operation. Here, "A" represents the undeformed shape and "B" is the shape in the cylindrical structure. If the cylindrical structure is not stress-relieved prior to expansion, as in the experiment described in the following sections, some of the elastic strain energy will be released during expansion. Conversely, if the structure is stress-relieved,

FIG. 28 DEFORMATION OF CONVOLUTE DURING FORMING OF CYLINDER

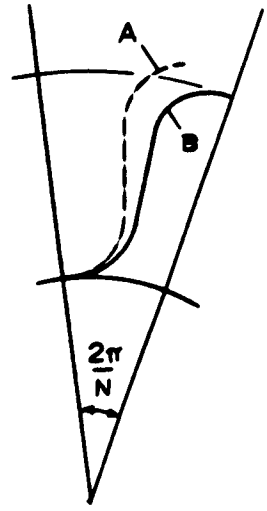

some additional energy will be required to expand it. The energy required to deform the strip of Figure 28 from "A" to "B" is

$$\frac{U_F}{N} = \frac{LD}{2} \int_0^{2\ell} \left(\frac{d\Delta\varphi}{ds} \right)^2 ds \quad , \tag{110}$$

where 2ℓ is the length of the S-shaped strip and U_F is the total energy required to form the cylinder. Since the total angle of rotation of the ends of the strip is $2\pi/N$,

$$\frac{d\Delta\varphi}{ds} = \frac{2\pi}{2N\ell} = \frac{\pi}{N\ell} \quad , \tag{111}$$

and Equation (110) becomes

$$U_F = \frac{\pi^2}{12} \frac{E_y h^3 L}{N\ell} \quad , \tag{112}$$

where the relation of Equation (3) has also been used. During expansion of the cylinder into the cone the angle of rotation of the ends of each S-shaped strip is reduced by the factor $\cos\alpha$, where α is the cone half-angle.* The change in U_F during expansion is, by Equations (110) and (112), proportional to the square of the angle of rotation. Thus, the release in energy for the nonrelieved case is given by

$$\Delta U_F = U_F (1 - \cos^2\alpha) \quad , \tag{113}$$

* Due to the twisting, the strip is not rotated uniformly over its length. However, since this is a second order effect, the average cone angle is taken for simplicity.

or, with Equation (112),

$$\Delta U_F = \frac{\pi^2}{12} \frac{E_\nu h^3}{N} \frac{L}{\ell} \sin^2\alpha \quad . \tag{114}$$

Subtraction of this result from Equation (107) yields

$$W = \frac{1}{36} N E_\nu h^3 a_2 \left(\frac{L}{\ell}\right)\left(\frac{L}{R_1}\right)^2 \left\{ \left(1 + \frac{1}{2}\frac{b_2}{a_2}\frac{L}{R_1}\sin\alpha\right) - \frac{3\pi^2}{a_2 N^2}\frac{\ell}{\ell}\left(\frac{R_1}{L}\right)^2 \right.$$

$$\left. + 6(1-\nu)\frac{k_1 a_1^2}{a_2}\frac{\ell\ell}{L^2}\left[1 + \frac{b_1}{a_1}\frac{L}{R_1}\sin\alpha + \frac{1}{3}\left(\frac{b_1}{a_1}\right)^2\left(\frac{L}{R_1}\right)^2\sin^2\alpha\right]\right\}\sin^2\alpha \quad . \tag{115}$$

For the U-shaped configuration with $a/\ell = 1$ and the parameters of Equations (108), Equation (109) becomes

$$W = 0.00592\, N E_\nu h^3 \frac{L^3}{\ell R_1^2}\left\{ \left(1 + 0.1434\frac{L}{R_1}\sin\alpha\right) - \frac{54.0}{N^2}\left(\frac{R_1}{L}\right)^2 \right.$$

$$+ 13.93(1-\nu)\left(\frac{\ell}{L}\right)^2\left[1 + 0.187\frac{L}{R_1}\sin\alpha \right. \tag{116}$$

$$\left. \left. + 0.0116\left(\frac{L}{R_1}\right)^2\sin^2\alpha\right]\right\}\sin^2\alpha \quad .$$

If there is an appreciable difference between the inner and outer radii of the cylinder, it is expected that Equations (115) and (116) will still be only approximately correct due to the twisting effects mentioned earlier. As the cylinder expands into a conical

shape the nonuniform circumferential elongation produces a nonuniform flattening of the convolute, with the maximum flattening occurring at the expanded end. Consequently, the inside generators of the cylinder rotate through a greater angle than those on the outside, producing additional twisting deformations. Thus, the results of the two-dimensional bending analysis are not directly applicable since some of the circumferential elongation is due to this twisting deformation. A more proper analysis of the problem should treat the bending and twisting deformations simultaneously.

VI. EXPERIMENTS

Tests were conducted with several two-dimensional specimens and a three-dimensional cylindrical structure similar to that described in the preceding section. Descriptions of the test procedures and the experimental results are given in the following sections.

A. Two-Dimensional Strips

Load-deflection tests were conducted on two-dimensional Type 304 stainless steel specimens with semi-circular-arc and U-shaped configurations, as used in the previous numerical examples. Samples of the specimens are shown in Figure 29. The specimens were fabricated from 0.002" and 0.003" annealed sheet material. Some of the specimens were tested in the as-formed state and others were process annealed prior to testing. The radius-to-thickness ratios were selected to give approximately 20 percent expansion prior to yielding for the semi-circular-arc specimens and 63 percent expansion for the U-shaped specimens. A summary of the specimens tested is given in Table II.

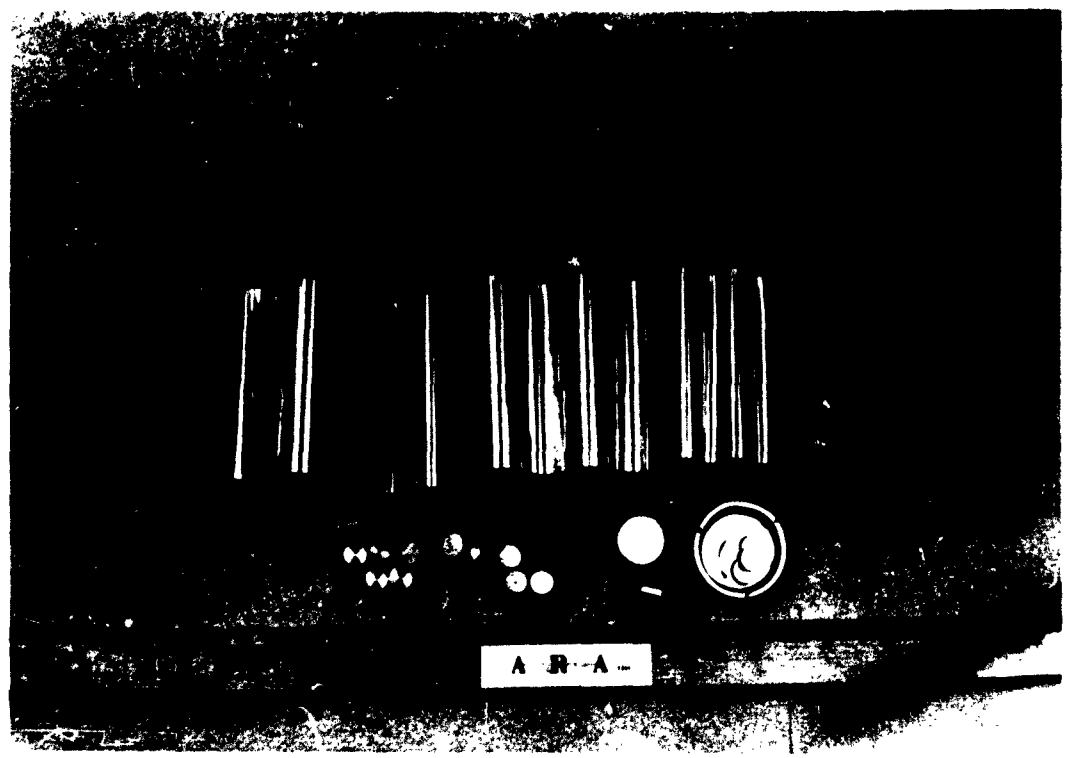

Figure 29. Two-Dimensional Specimens and Small Weights

Table II. Two-Dimensional Specimens

Specimen No.	Type	Nominal Thickness (in.)	Condition	Nominal length/radius
1	U	.003	as formed	4
2	U	.003	as formed	4
3	U	.003	annealed	4
5	semi-circle	.003	as formed	8
6	semi-circle	.003	as formed	8
8	semi-circle	.003	annealed	8
9	U	.002	as formed	4
10	U	.002	as formed	4
12	U	.002	annealed	4
13	semi-circle	.002	as formed	8
14	semi-circle	.002	as formed	8
15	semi-circle	.002	annealed	8

Width = 4.00 inches (all specimens)

Nominal (thickness/radius) = 0.00730 (all specimens)

Estimated variation in thickness = $\pm$ 0.00005 (all specimens)

Estimated variation in radius = $\pm$ 10% (as-formed specimens)

Annealed specimens exhibit considerable distortion.

The specimens were suspended on knife-edges, as shown in Figures 30 and 31, in order to produce zero moment loading conditions at the ends of the active length of the specimens. This was accomplished through the use of fine wires wrapped around thin metal strips and passed through small holes in the ends of the specimens. Loading was accomplished by the addition of calibrated weights to a light pan suspended from the lower end of the specimen. Deflections were measured with a vernier height gage and attaching telescope by sighting on the upper and lower ends of the specimen.

B. Three-Dimensional Cylindrical Structure

A circumferentially-convoluted cylindrical structure was formed by joining the ends of two convoluted strips. The material and dimensions were the same as U-shaped specimens Nos. 1 and 2, and the total length-to-radius of the strips before joining was 40. Manner of loading is illustrated in Figures 32 to 35. The energy required to deform the structure into a conical shape was measured for various cone angles and compared with the theoretical predictions.

Loading was accomplished by the use of ten mass balanced frames secured to the outermost generators of the cylindrical structure and pivoted about the base in radial planes. Fine wires, used to attach the frames to the structure, were passed over slots in the frames and joined to a common point below, from which a light balance pan was suspended. Calibrated weights were added to the pan and the corresponding inner and outer diameters of the upper end of the structure were measured. The changes in diameters were used to compute the cone angle and the movement of the pan, from which the corresponding energy inputs were computed.

Figure 30. Two-Dimensional Load-Deflection Test Setup

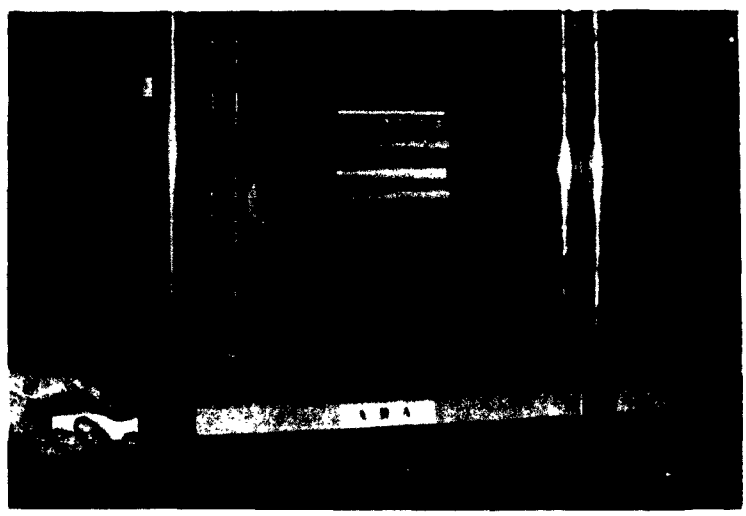

Figure 31. Two-Dimensional Test View Showing Upper Knife Edge

Figure 32. Convoluted Cylindrical Structure Unloaded

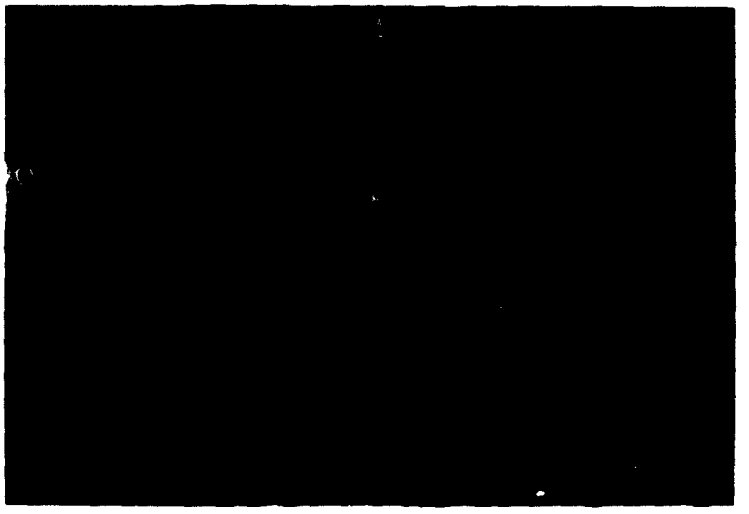

Figure 33. Convoluted Cylindrical Structure Loaded to Partial Expansion

Figure 34. Convoluted Cylindrical Structure View of Loading Segments

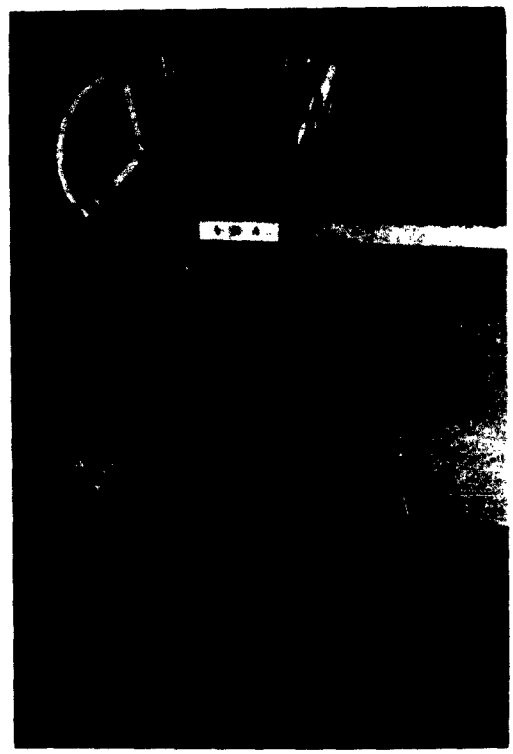

Figure 35. Convoluted Cylindrical Structural Test Setup, Side View

C. Experimental Results

1. Two-Dimensional Specimens

The load-deflection curves for the two-dimensional specimens are shown in Figures 36 to 39. The corresponding theoretical curves are also shown, based on the nominal dimensions and values of 29.4×10^6 psi for E and 0.29 for ν. The considerable scatter in the data can be attributed, in part, to variations in the dimensions of the specimens. This is suggested by the fact that the initial slopes of the curves are also in disagreement with the small-deflection values and, consequently, these curves appear to be rotated about the origin. In order to obtain more valid comparisons with the large-deflection theory, the data have been replotted in nondimensional form by using the initial slopes, with the small-deflection theory solutions, to compute values of the reference load T_o. These curves are shown in Figures 40 to 43.

2. Convoluted Cylindrical Structure

Figure 44 shows the energy-deformation curve for the convoluted cylindrical structure, in which energy input is plotted against cone half-angle. The corresponding theoretical curve, based on Equation (115), is also shown. For these computations the nominal dimensions of the two-dimensional strip were used, with a measured value of 3.142 inches for the average initial cylinder radius, R_1.

VII. CORRELATION OF THEORY AND EXPERIMENT

A. Two-Dimensional Analysis

The scatter in the curves of Figures 36 to 39 can be attributed, in part, to the variation in specimen dimensions, as noted above. For example, the 10%

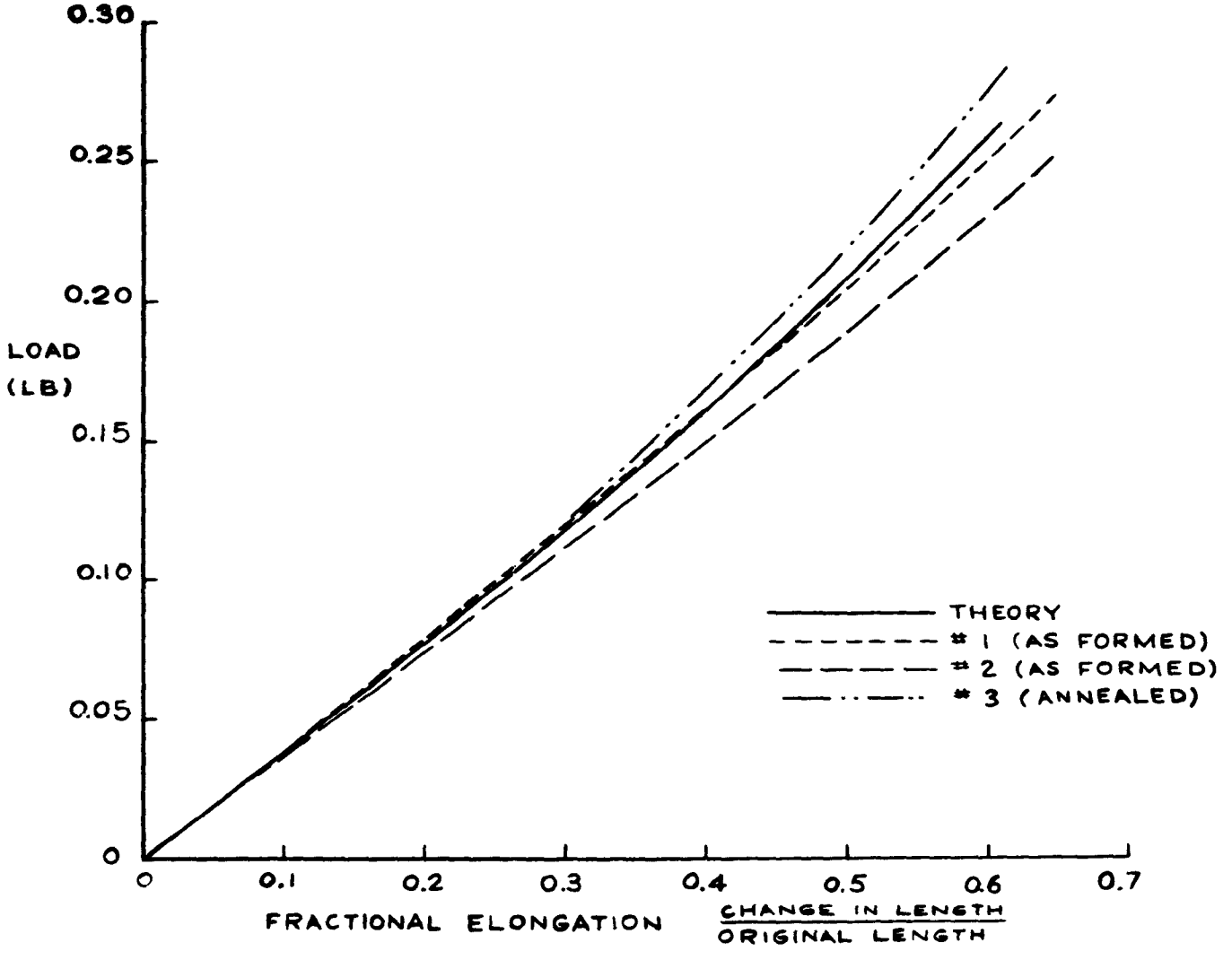

FIG. 36 LOAD-DEFLECTION CURVES FOR 0.003-INCH U-SHAPED SPECIMENS

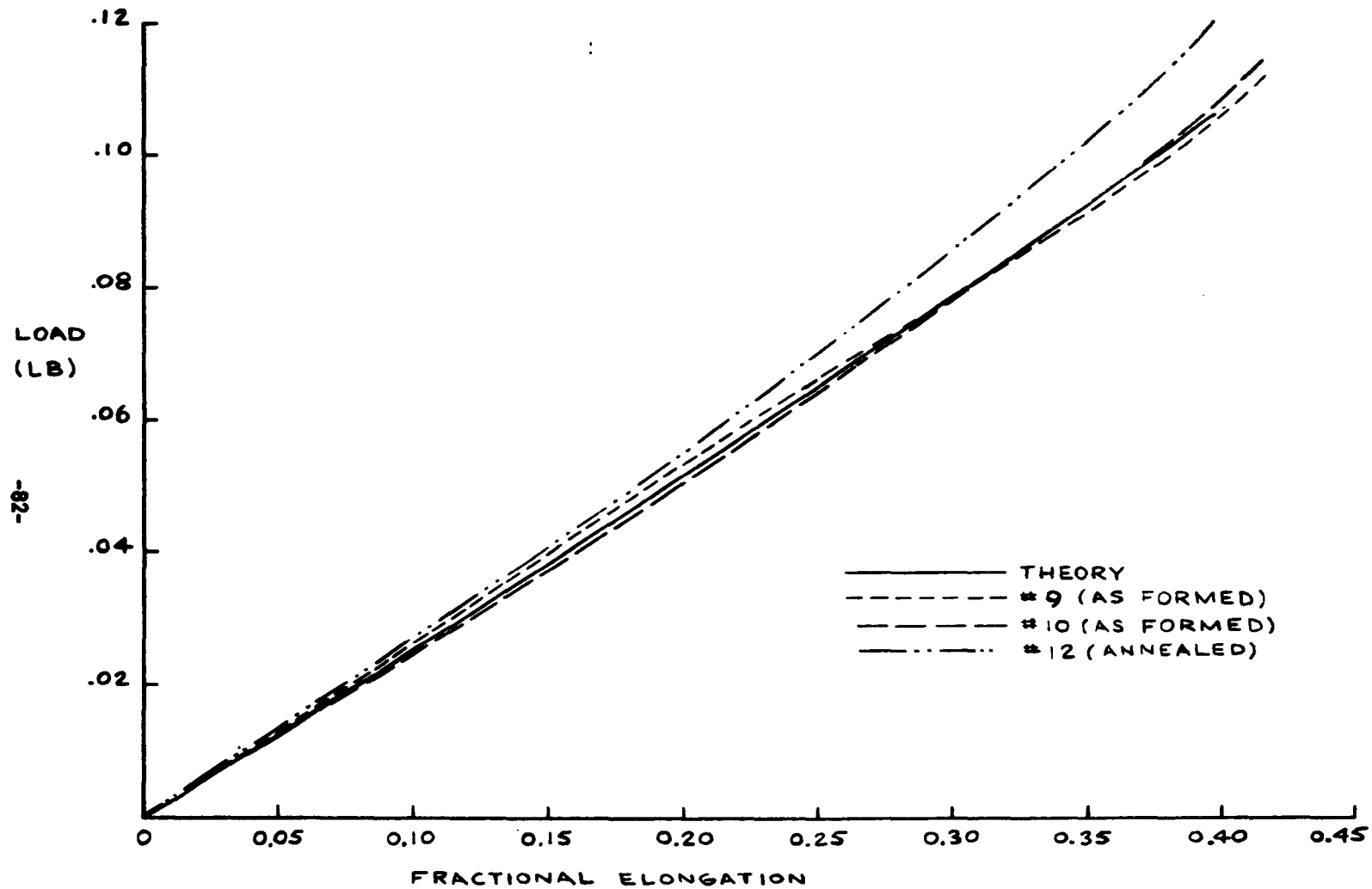

FIG. 37 LOAD-DEFLECTION CURVES FOR 0.002-INCH U-SHAPED SPECIMENS

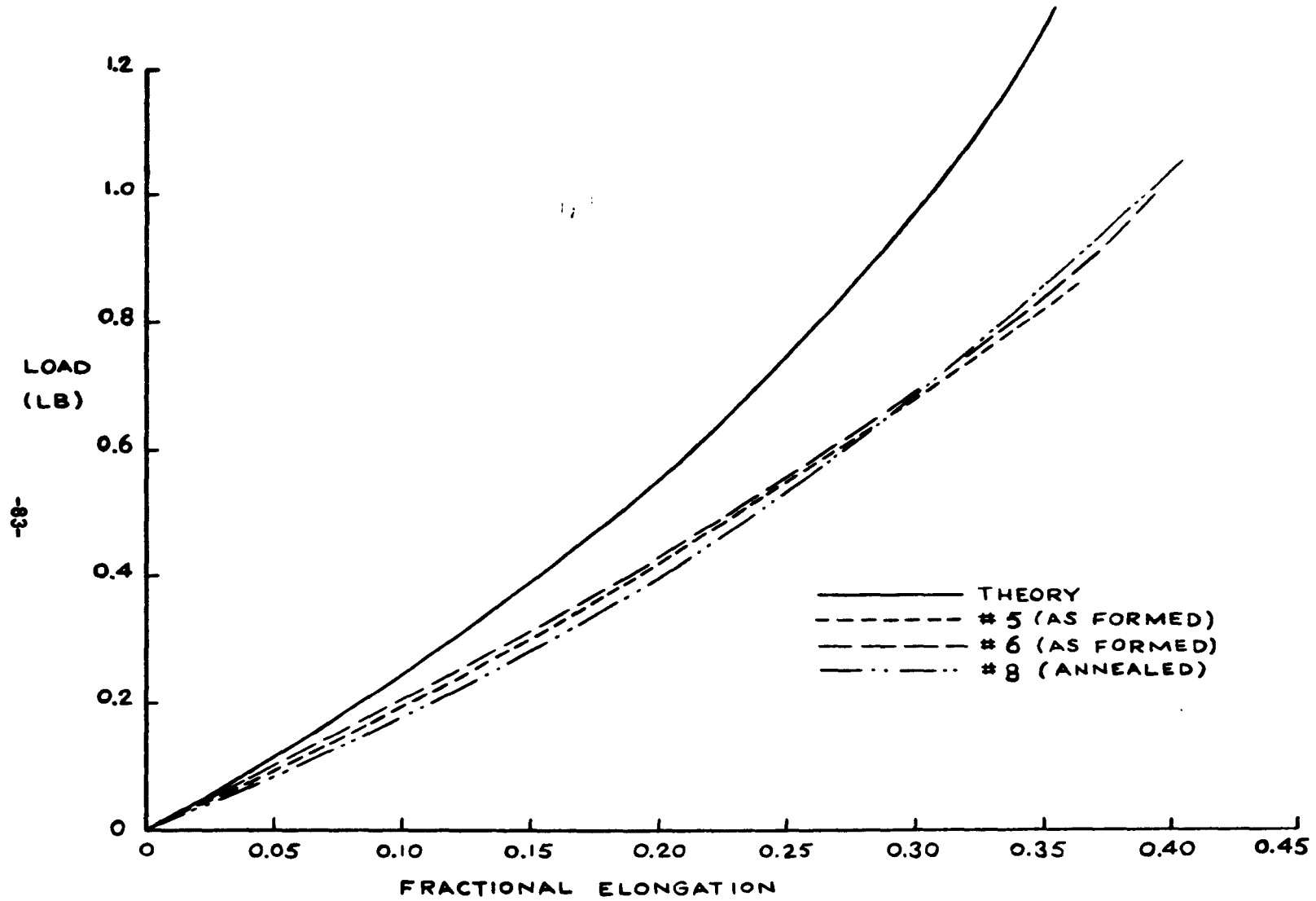

FIG. 38 LOAD-DEFLECTION CURVES FOR 0.003-INCH SEMI-CIRCULAR-ARC SPECIMENS

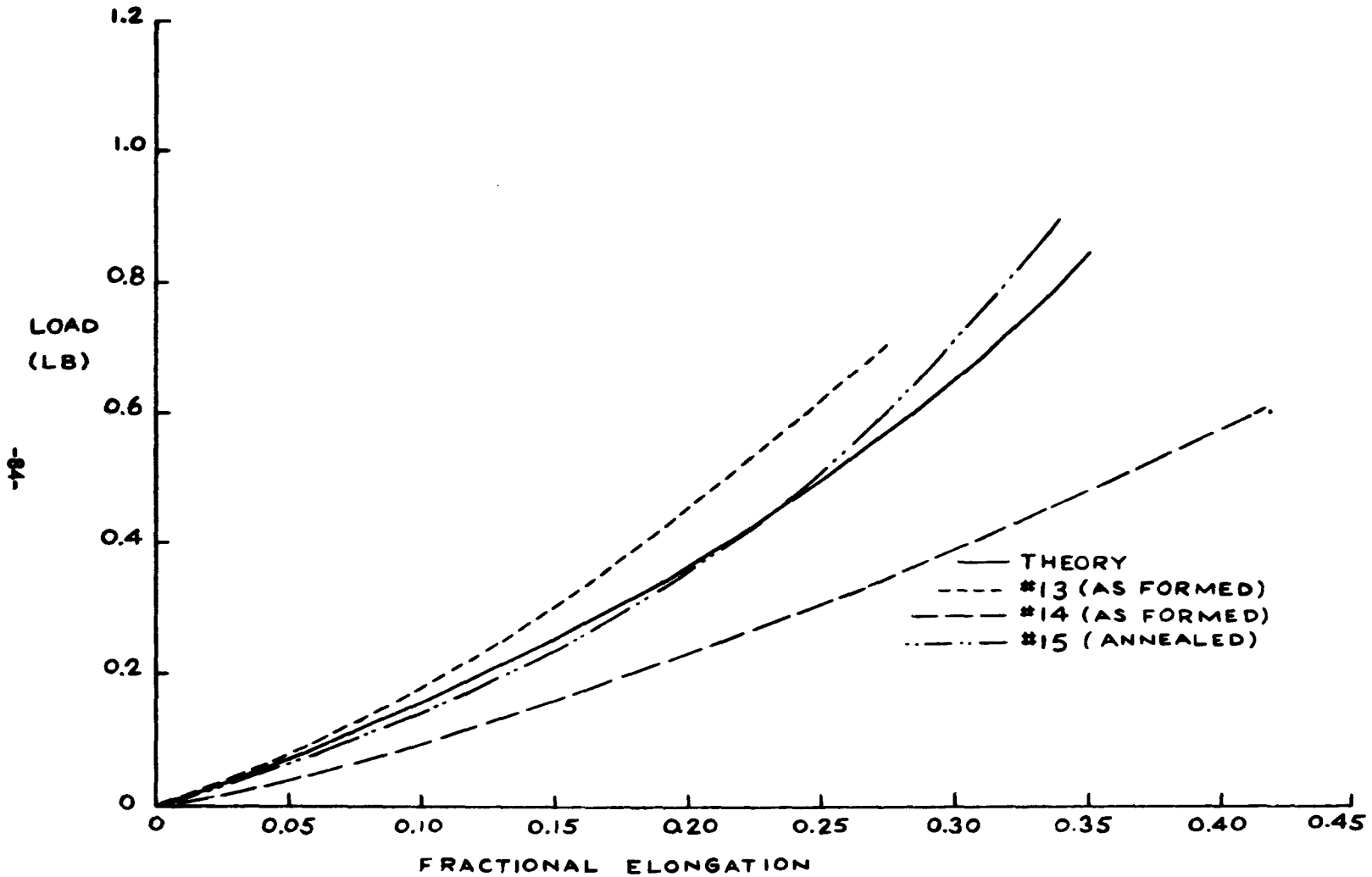

FIG. 39 LOAD-DEFLECTION CURVES FOR 0.002-INCH SEMI-CIRCULAR-ARC SPECIMENS

FIG. 40 NONDIMENSIONAL LOAD-DEFLECTION CURVES FOR 0.003-INCH U-SHAPED SPECIMENS

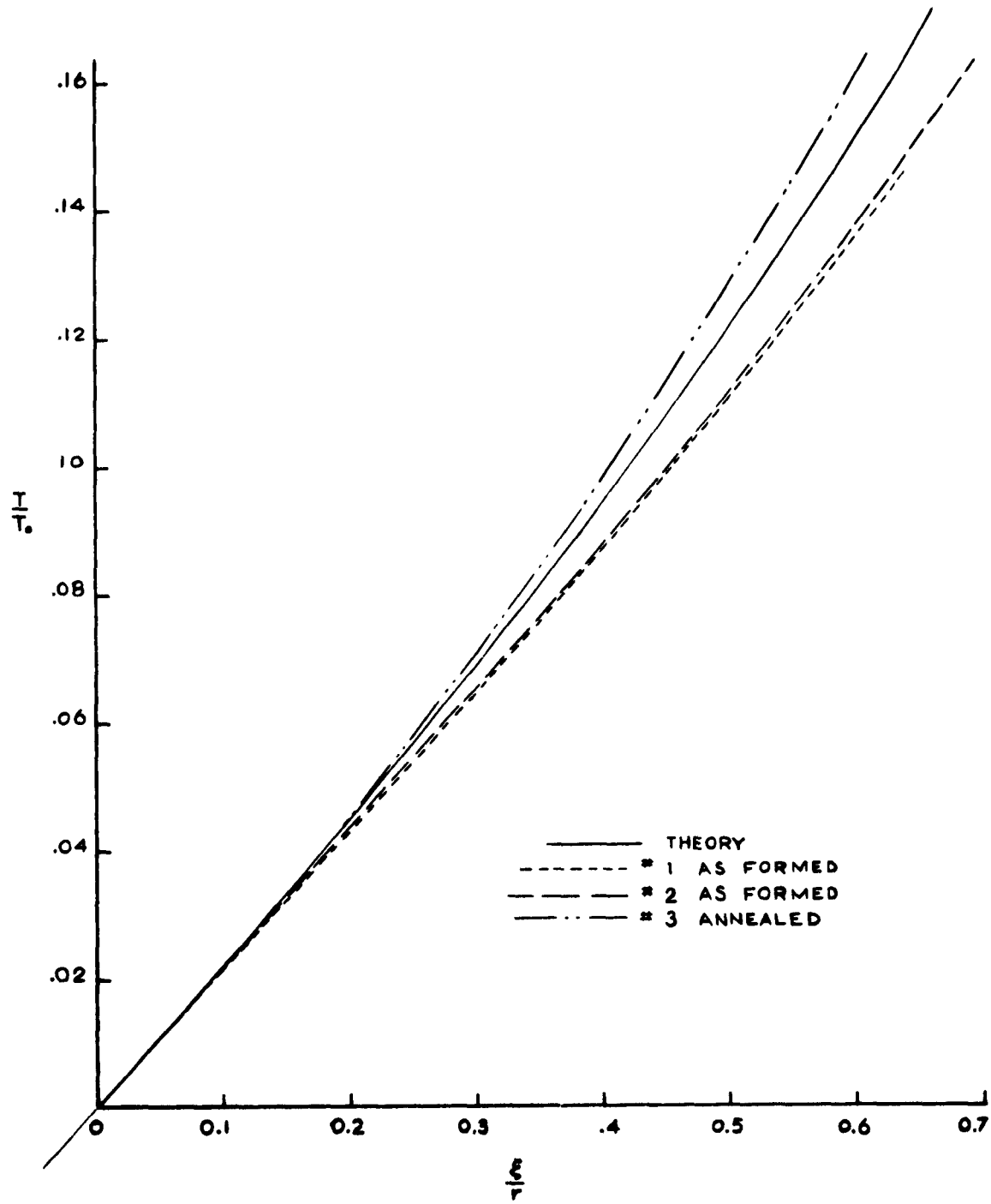

FIG. 41 NONDIMENSIONAL LOAD-DEFLECTION CURVES FOR 0.003-INCH CIRCULAR ARC SPECIMENS

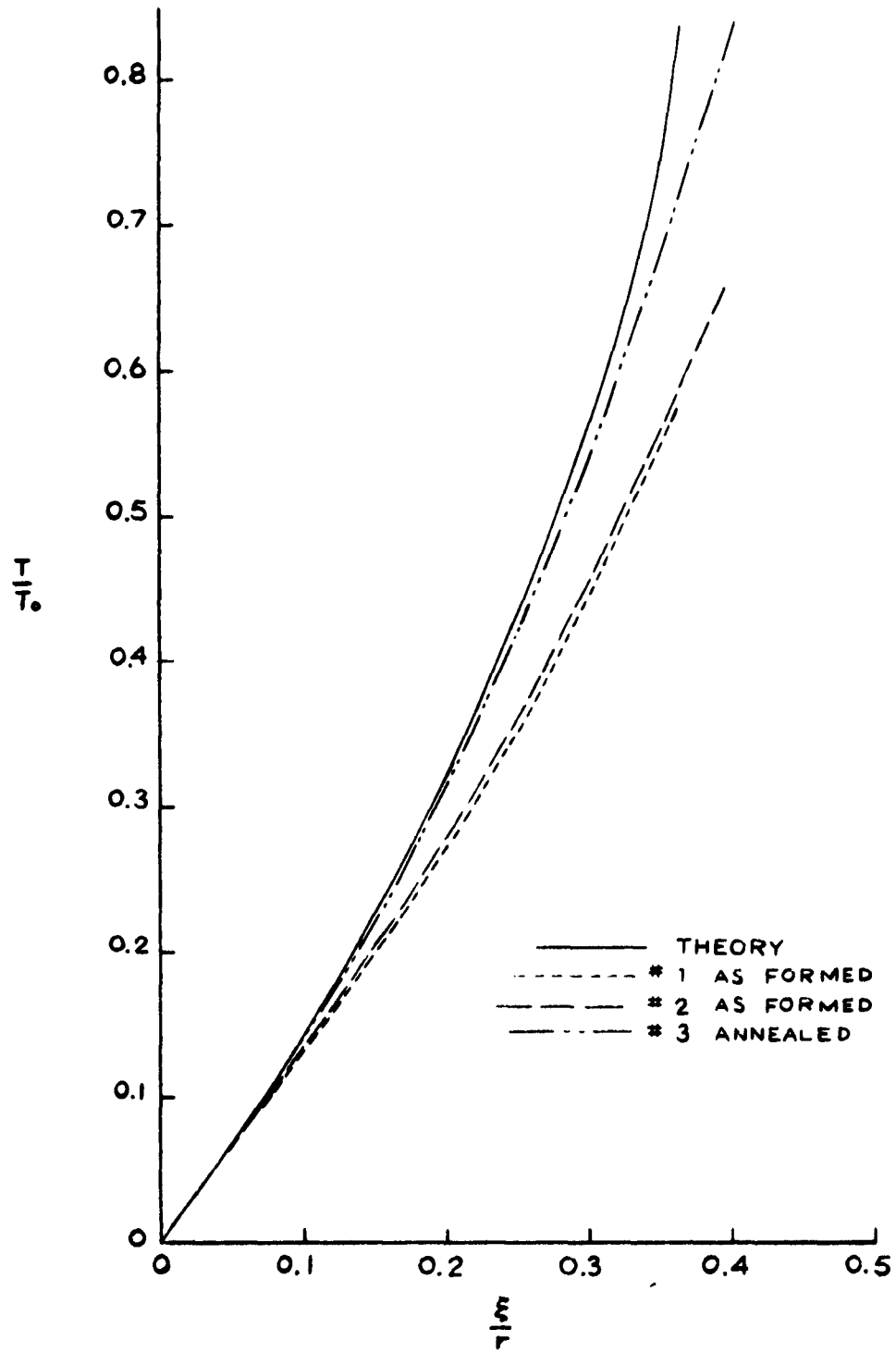

FIG. 42 NONDIMENSIONAL LOAD-DEFLECTION CURVES FOR 0.002-INCH U-SHAPED SPECIMENS

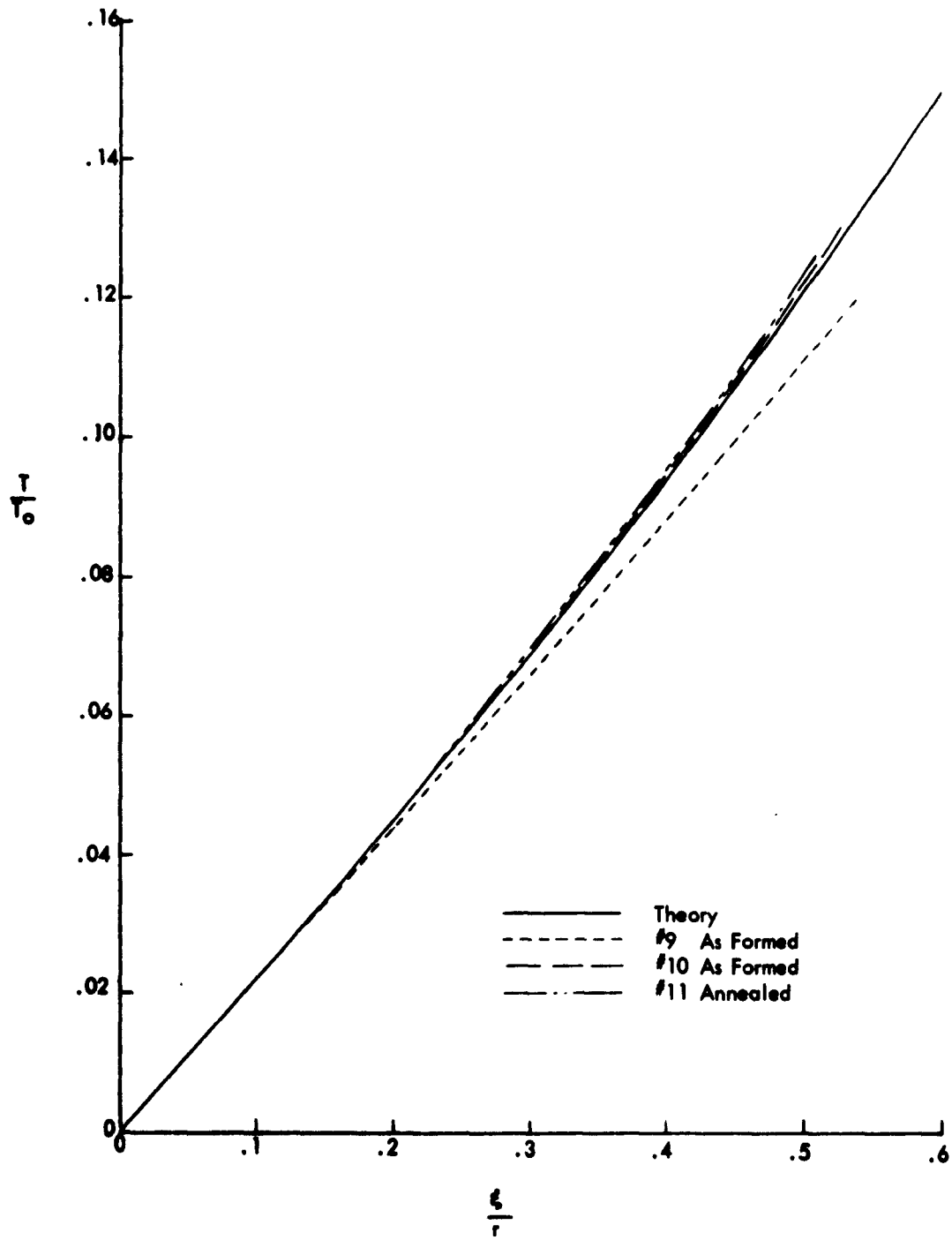

FIG. 43 NONDIMENSIONAL LOAD-DEFLECTION CURVES
FOR 0.002-INCH SEMI-CIRCULAR ARC SPECIMENS

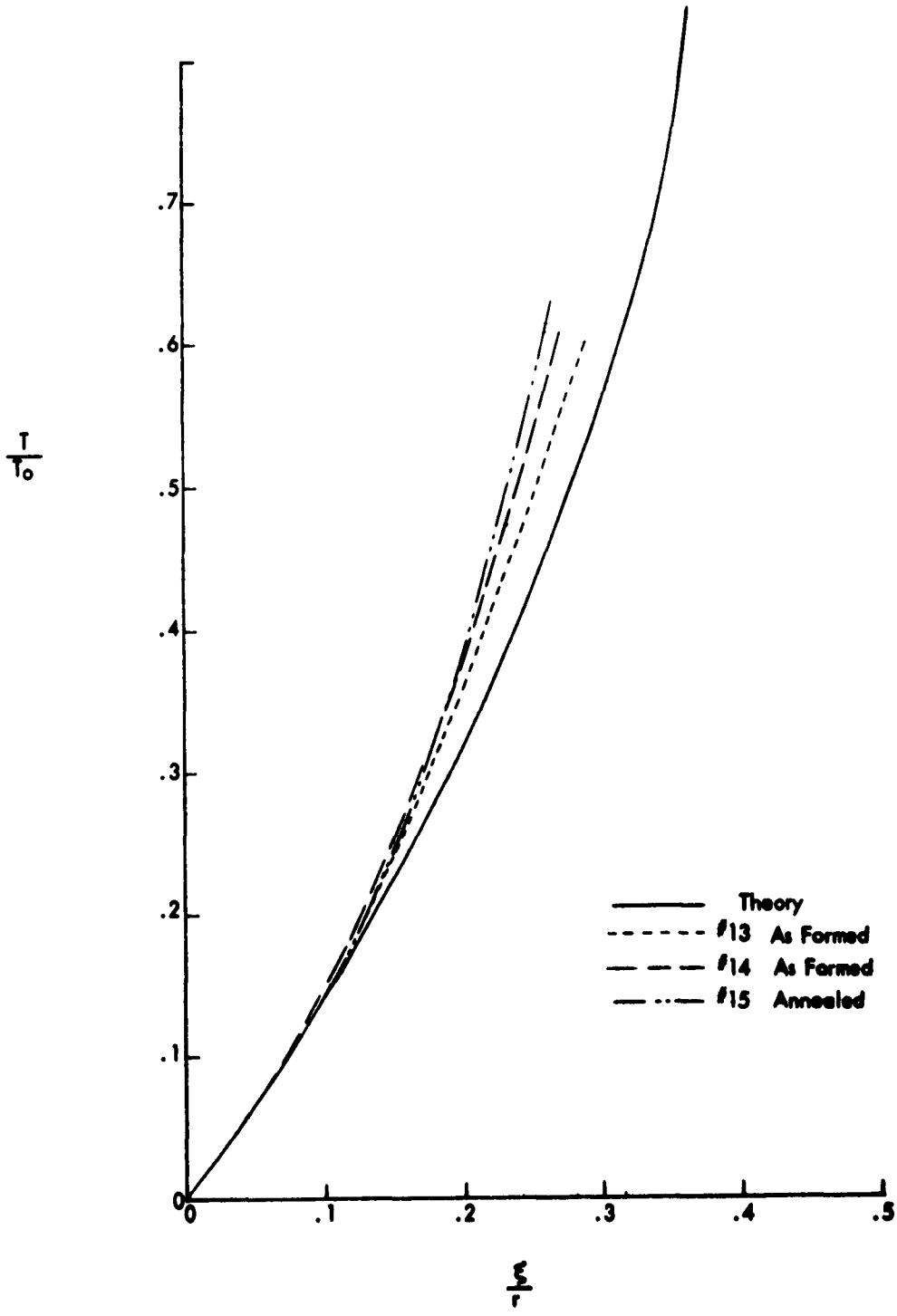

FIG. 44 ENERGY-DEFORMATION CURVE FOR CONVOLUTED CYLINDRICAL STRUCTURE

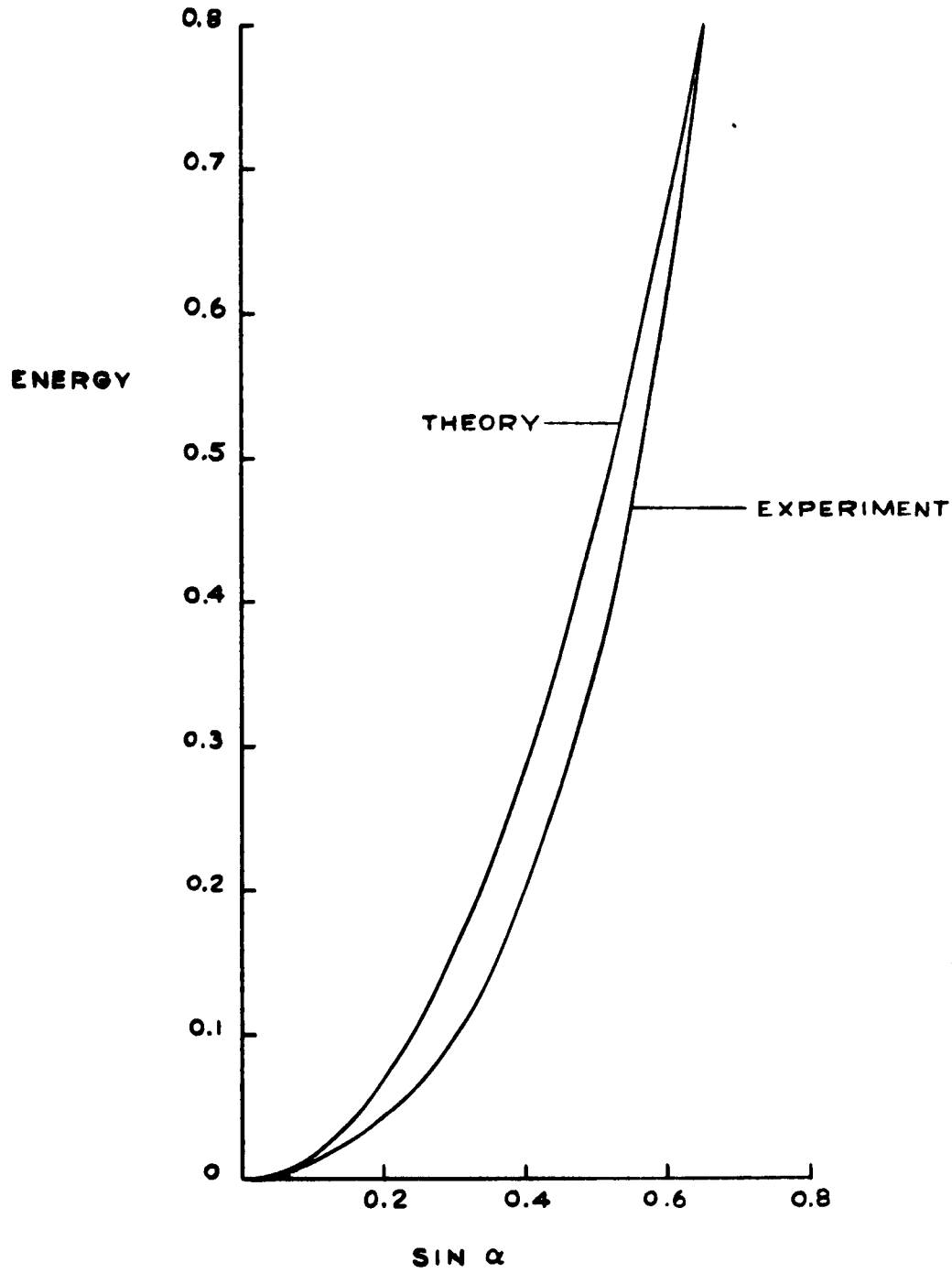

variation in radius can produce over 20% variation in load, and the 0.05 mil variation in thickness can give rise to variations of approximately 5% and 6% in load, respectively, for the 2 and 3 mil specimens. These variations can accumulate and thereby account for most of the scatter in the data.

A considerable improvement results in the "rotated" curves of Figures 40 to 43. It is interesting to note the similarity in the curves for the 3 mil cases and the closer correlation than in the 2 mil cases. This would be expected since the dimensional tolerances that can be attained are about the same for both cases, but a given dimensional error in a 2 mil case has a greater effect than in a 3 mil case.

It is expected that the consistently lower curves for the as-formed specimens, compared with the annealed specimens, are due to the Bauschinger effect. * This effect is related to peculiarities in the stress-strain curve, particularly the earlier yielding and lowering of the curve, when a polycrystalline metal is plastically deformed in one direction and then loaded in the reverse direction. This situation occurs with the convoluted specimens. The forming operation produces plastic bending deformation in one direction, and elongation of the specimens results in bending in the reverse direction. Moreover, a mild annealing is known to remove these effects and restore the metal to its normal behavior.

The disagreement between the theory and experiment that persists in the "rotated" curves of Figures 40 to 43, besides possible Bauschinger effects in the

* See, for example, Reference B, Chapter 12, and Reference E, Section 3.4.

as-formed cases, can probably be attributed to dimensional nonuniformities. E.g., the curves were not truly circular, and variations in curvatures and other dimensions occurred within a single specimen. This is particularly true of the annealed specimens in which considerable distortion resulted from the annealing process. Nevertheless, the overall agreement appears to be quite good so that the theory appears to be substantiated, at least in the elastic range.

It should be mentioned that some plastic yielding occurred over the latter portion of the load-deflection curves. No attempt was made to compute this effect with the exception of the plastic computations on the semi-circular-arc configuration presented in Section IV-F. The lack of adequate stress-strain data for very thin sheet material and the scatter in the data, coupled with the slight effect yielding has in this range, would make correlations quite difficult. The effects of plastic deformation can be evaluated more easily with larger specimens in which dimensions and material properties can be more closely controlled.

B. Convoluted Cylindrical Structure

The curves of Figure 44 disagree considerably over the lower range of expansion but show rather good agreement at the higher range. The maximum error is about 65% and the average error is about 30%. This error can be attributed to the appreciable difference between the inner and outer radii of the cylinder and the consequent inadequacy of the theory in this case. As mentioned in Section V-B, this difference in radii gives rise to additional twisting effects which are not accounted for in the present analysis. A more proper analysis of the deformation should treat the

large-deflection bending and twisting of the circumferentially-convoluted strips simultaneously.

A more quantitative substantiation of the source of error arises from a consideration of Equation (115) with the dimensions of the structure and the basic assumption that the difference in radii is small compared with the average radius. According to Equation (115) the energy is approximately inversely proportional to the square of the average radius, R_1. In the actual structure the inside, outside, and average radii were 2.34 inches, 3.94 inches, and 3.14 inches, respectively. Thus, if the inner and outer radii were used to compute the energy, rather than the average radius, variations of approximately 80% and -37%, respectively, would result. In view of this it appears that the theory gives a fairly good first approximation, particularly for the upper range of expansions. Moreover, it would appear that considerable improvement in the theory would result as the difference in radii were decreased.

VIII. CONCLUSIONS AND RECOMMENDATIONS

Theoretical methods of analysis have been developed for two-dimensional convoluted-type structures subjected to large deformations, with material behavior in both the elastic and plastic ranges. Computations have been carried out for structures of several typical configurations, utilizing numerical techniques suitable for use with a desk calculator. Results of the two-dimensional analysis have been applied to the analysis of a typical three-dimensional convoluted cylindrical structure.

Tests have been performed on two-dimensional specimens and a three-dimensional cylindrical structure similar to that used in the analysis. The tests appear to substantiate the two-dimensional analysis within the elastic range of behavior. The results with the convoluted cylindrical structure indicate that the simplified theory developed can be used for a first-approximation analysis of a considerably more complex structure. They further indicate that a considerably more refined analysis will be required in order to accurately predict the behavior of a three-dimensional structure of the type tested.

In view of the limited experimentation that could be performed under the present study the following investigations are recommended in order to amplify and extend the present findings:

A. Tests with larger two-dimensional specimens so that dimensions and material behavior can be more carefully controlled

B. Tensile tests to determine stress-strain behavior of specimen sheet materials

C. Simple bend tests for independent determinations of plastic bending behavior

D. Compression tests with as-formed specimens to determine initial slopes and evaluate Bauschinger effects

E. Tests with the same specimen in the as-formed and annealed conditions in order to evaluate Basuchinger effects

F. Refined analyses of the convoluted cylindrical structure tested in order to account for the large difference in radii

G. Tests with convoluted cylindrical structures having smaller differences in the radii in order to determine the range of applicability of the simplified theory

In addition to the above investigations it is recommended that future theoretical and experimental studies be carried out on three-dimensional convoluted cylindrical and conical structures in which (a) bending of the structure occurs in the axial as well as in the circumferential directions; and (b) the convolute span height varies axially so as to produce preferential expansions of the structure. In particular, attempts should be made to determine if a simplified theory based on the two-dimensional structure can be developed, as in the present study.

It should be noted that the development of a successful theory for analyzing the structures described by (a) and (b) would constitute a significant step toward understanding the general behavior of convoluted shell structures. As seen from the simplified analysis of the convoluted cylindrical structure in the present study, the general treatment of convoluted shell structures will be extremely difficult. Therefore, if it can be developed, a simplified theory based on an extension of the present study would be quite useful for design purposes.

APPENDIX A

Determination of Parameters for Convoluted Cylindrical Structure from Two-Dimensional Analysis

The determination of the parameters k_1, a_1, b_1, a_2, and b_2, defined in Equations (92), (97), and (101), is described below. The parameter k_1 is a measure of the distribution of rotation over the cross section of a typical longitudinal strip of the cylinder and is determined from the changes in slopes of the two-dimensional structure, as illustrated in Figures 1 and 27. The parameters a_1 and b_1 relate the maximum rotation of the strip to the fractional elongation, and a_2 and b_2 describe the two-dimensional load-deflection curve.

It was assumed in Section V-B that k_1, as defined in Equation (92) is, in effect, independent of the circumferential elongation of the structure. The validity of this assumption for the U-shaped configuration used in the numerical example and in the experiment is demonstrated by Figures 45 and 46. Figure 45 shows distributions of the changes in slope, φ, over the cross-section of the typical section for several elongations, as determined from the two-dimensional analysis. Figure 46 shows the corresponding distributions of the incremental changes in slopes, normalized on the basis of the maximum values. The slight variation in the curves of Figure 46 over the range of expansion shown justifies the initial assumption. The value for k_1 was obtained from the data of Figure 46 and Equation (92), which can be approximated as follows:

$$k_1 = \int_{\frac{s}{\ell}=0}^{1} \left(\frac{d\varphi/dx}{d\varphi_m/dx} \right)^2 d\left(\frac{s}{\ell}\right) \simeq \int_{0}^{1} \left[\frac{\delta\varphi(s/\ell)}{\delta\varphi_m} \right]^2 d\left(\frac{s}{\ell}\right) . \qquad \text{(A-1)}$$

FIG. 45 DISTRIBUTION OF CHANGE IN SLOPE FOR U-SHAPED CONFIGURATION, a/r = 1

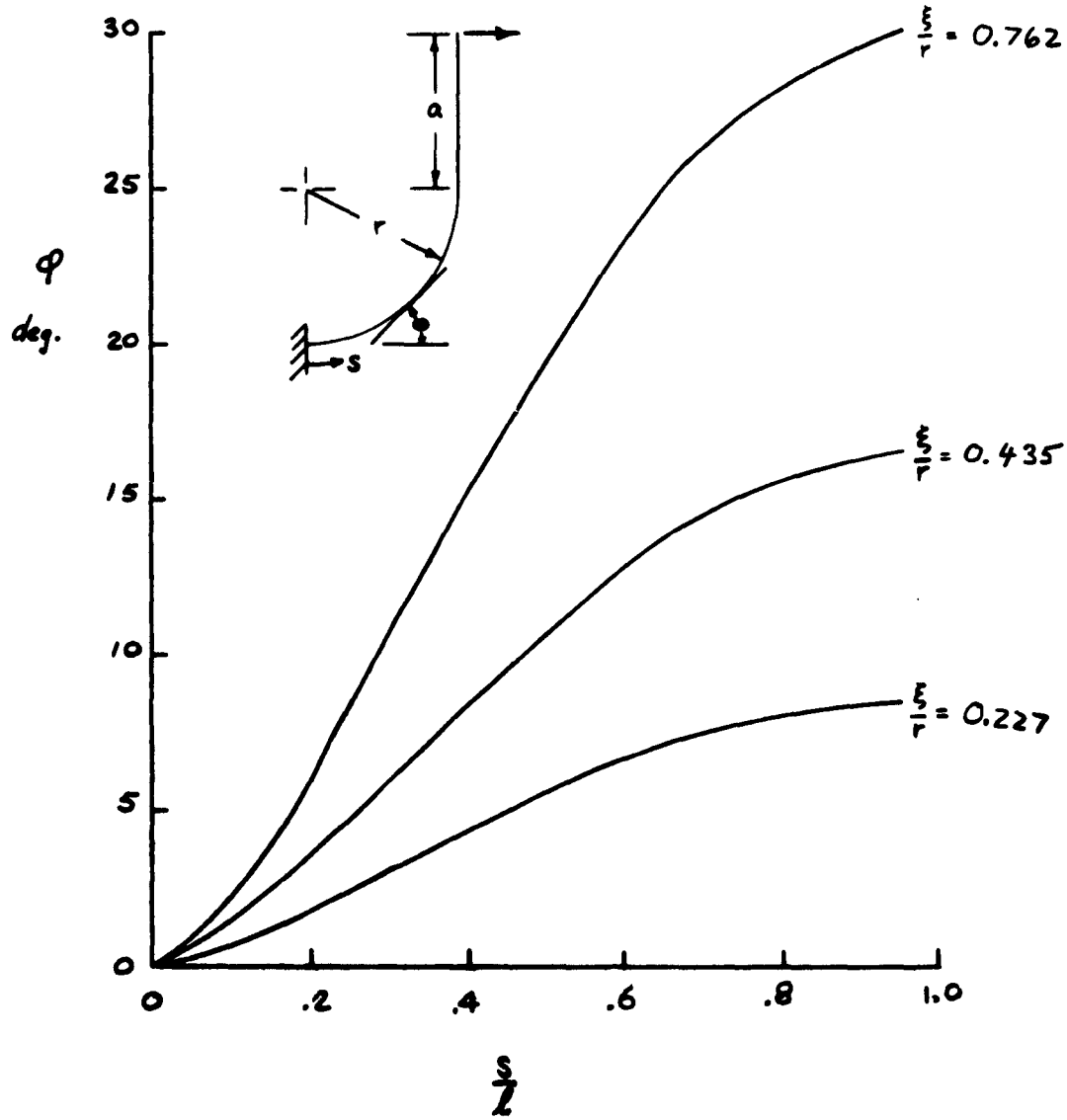

FIG. 46. NORMALIZED DISTRIBUTIONS OF INCREMENTAL CHANGES IN SLOPE FOR U-SHAPED CONFIGURATION, $a/r = 1$

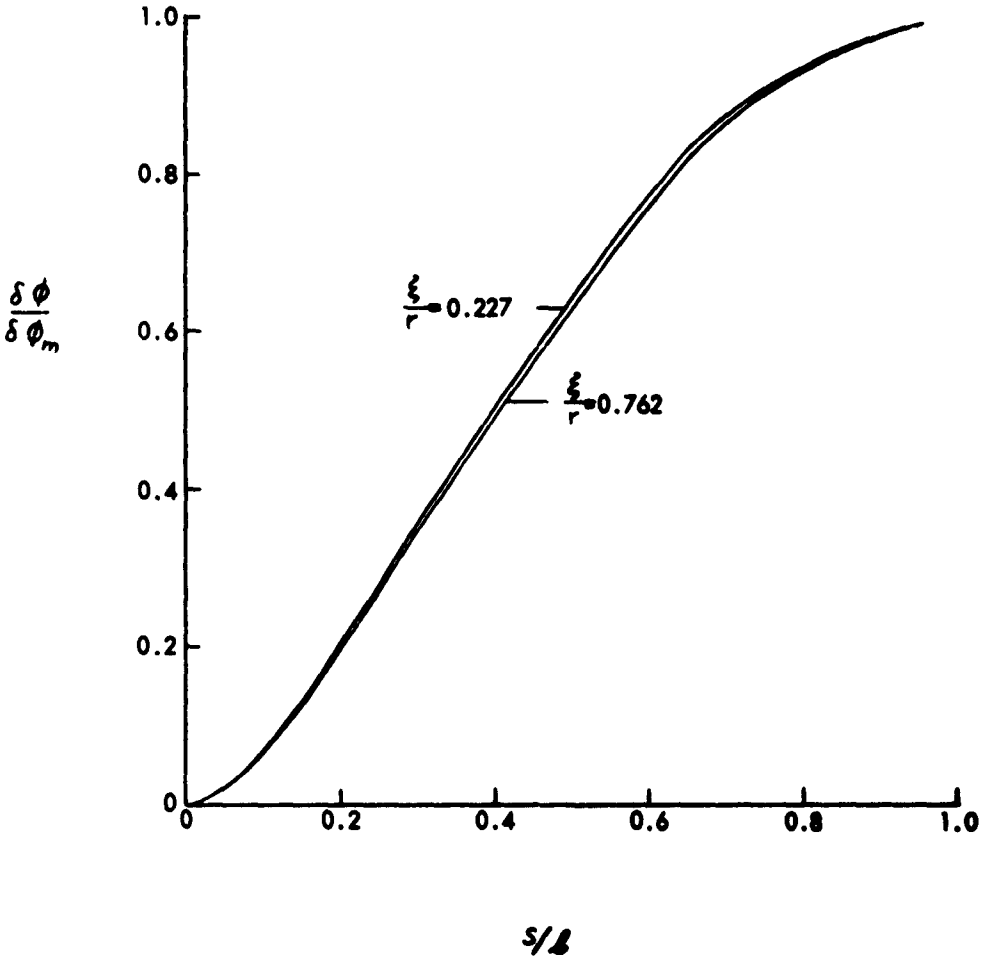

The average values of $\delta\varphi/\delta\varphi_m$ were used in Equation (A-1) and k_1 was determined by numerical integration.

The parameters a_1, b_1, and a_2, b_2 were obtained by fitting the curves of φ_m vs. ξ/h and T/T_o vs. ξ/h, determined from the two-dimensional analysis, to Equations (97) and (101), respectively. The original curves and fitted expressions are shown in Figures 47 and 48.

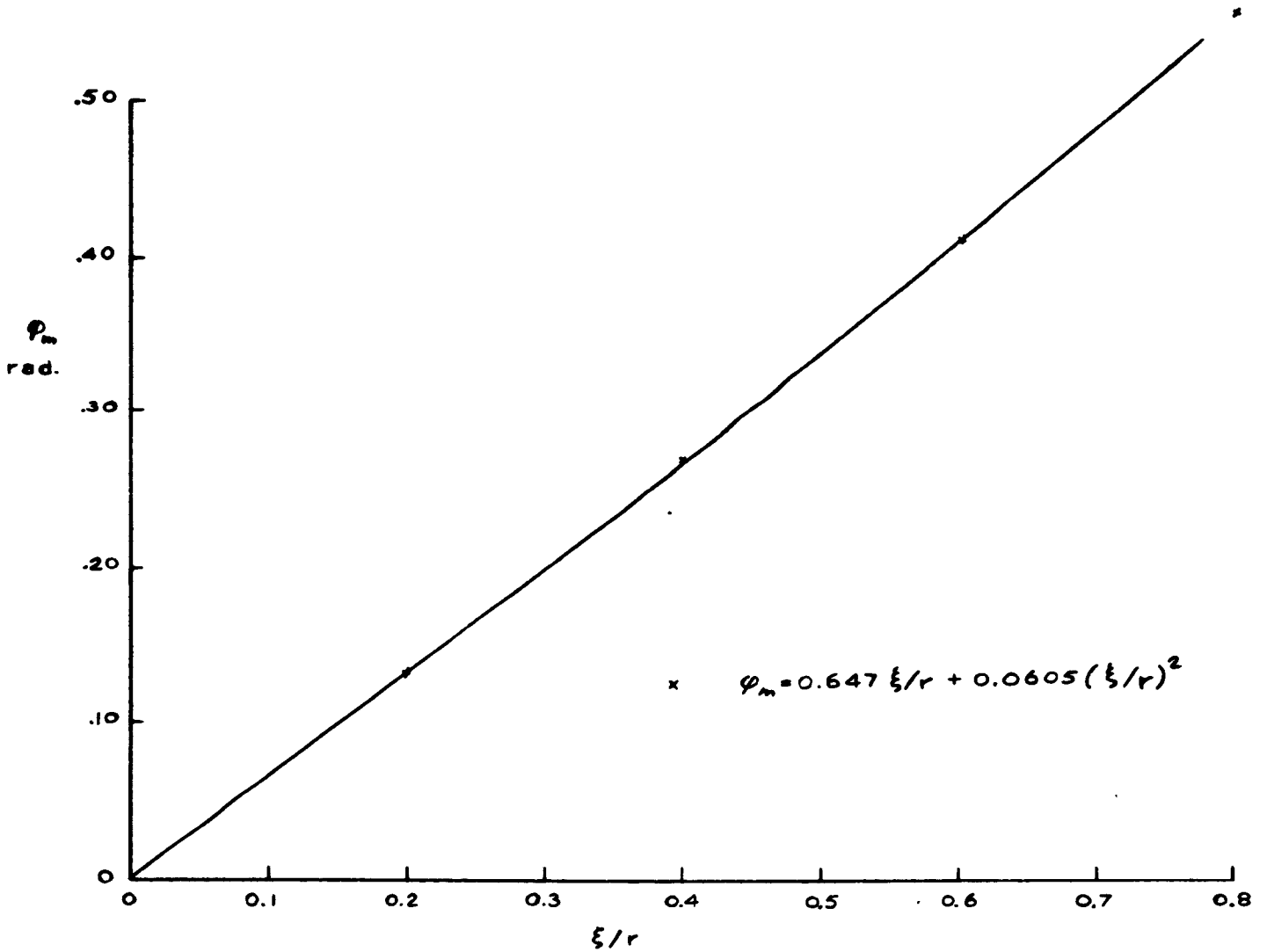

FIG. 47 φ_m VS ξ/r FOR U-SHAPED CONFIGURATION, $\frac{a}{r} = 1$

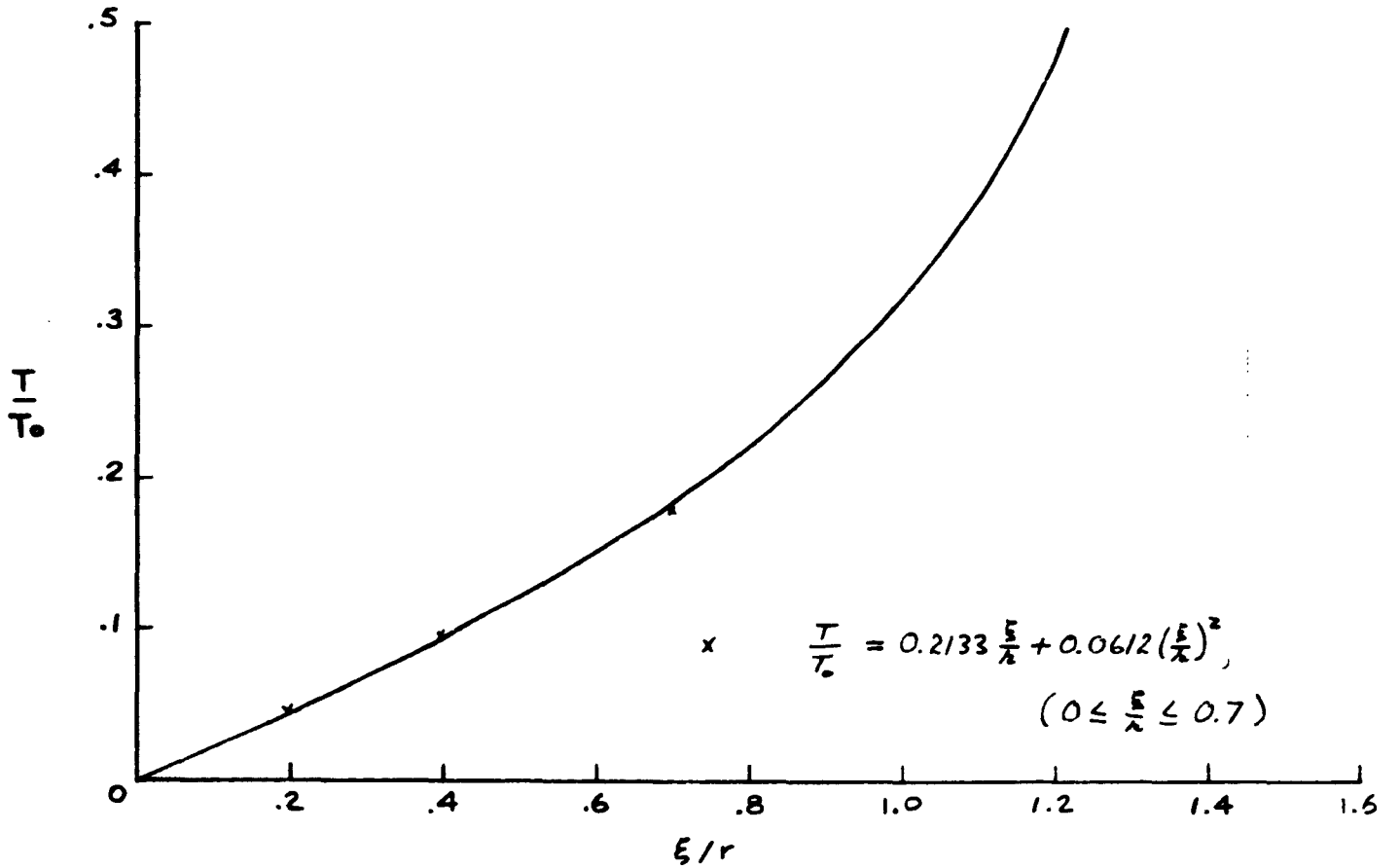

FIG. 48 ELASTIC LOAD - DEFLECTION CURVE FOR U-SHAPED CONFIGURATION

a/r = 1

REFERENCES

A. R. Hill, The Mathematical Theory of Plasticity. London: Oxford University Press, 1950, Ch. IV, Sec. 5, 6.

B. J. D. Lubahn and R. P. Felgar, Plasticity and Creep of Metals. New York: John Wiley & Sons, Inc., 1961.

C. W. Ramberg and W. R. Osgood, "Description of Stress-Strain Curves by Three Parameters," NACA TN 902, July 1943.

D. S. Timoshenko and J. N. Goodier, Theory of Elasticity, 2nd Ed. New York: McGraw-Hill Book Company, Inc., 1951, Sec. 94.

E. A. Nadai, Theory of Flow and Fracture of Solids, Vol. One, 2nd Ed. New York: McGraw-Hill Book Company, Inc., 1950.